BONE TARGETED PHOTODYNAMIC THERAPY

by

Gönül DEMİRCİ

B.S., Chemistry Education, Middle East Technical University, 2008

Submitted to the Institute for Graduate Studies in
Science and Engineering in partial fulfillment of
the requirements for the degree of
Master of Science

Graduate Program in Chemistry
Boğaziçi University

2010

To my mother and my family

ACKNOWLEDGMENTS

First of all, I would like to express my most sincere gratitude to my thesis supervisor Assist. Prof. Rana SANYAL for all the support she has given me throughout my research and master education life. I really appreciate her endless guidance and friendship.

I wish to express my thanks to Assist. Prof. Amitav SANYAL for his patience and care during my study and also for review of the final manuscript.

I would like to thank Prof. Güniz KÜÇÜKGÜZEL for her serving in my committee. I would like to extend my thanks to Burcu Selen Çağlayan and Ayla Türkekul for their patience and help in running NMR analysis supporting my laboratory work.

I would like to extend my gratitude to all of the former and present SANYAL lab members for making laboratory enjoyable for me with their endless friendship.

I would like to thank all my other friends and all the members of the faculty in the Chemistry Department.

Finally, my deepest thanks go to my whole family for their great support, encouragement throughout my master education life and for their endless love.

This research has been supported by Boğaziçi University BAP 09S107 and TÜBITAK 107T623 and 108T898.

LIST OF SYMBOLS/ ABBREVIATIONS

J	Coupling constant
υ	Frequency
ATRP	Atom transfer radical polymerization
PDT	Photodynamic therapy
PS	Photosensitizer
ISC	Intersystem crossing
ROS	Reactive singlet oxygen
HAP	Hydroxyapatite
BP	Biphosphonate
EPR	Enhanced permeability and retention effect
BODIPY	4-bora-3a,4a-diaza-s-indacene
FITC	Fluorescein isothiocyanate
ALD	Alendronate
PEG	Poly(ethylene glycol)
PEGMA	Poly(ethylene glycol) monomethyl ether methacrylate
NHS	N-hydroxy succinimide
HPMA	Hydroxypropyl methacrylate
TEA	Triethyl amine
NBS	N-bromosuccinic imide
AIBN	Azo bis isobutyronitrile
FT-IR	Fourier Transform Infrared
GPC	Gel Permeation Chromotography
MHz	Mega hertz
NMR	Nuclear Magnetic Resonance
NIR	Near-infrared
THF	Tetrahydrofuran
CH_2Cl_2	Dichloromethane
D_2O	Deuterium oxide
$CDCl_3$	Deuterated chloroform

ABSTRACT

BONE TARGETED PHOTODYNAMIC THERAPY

Photodynamic therapy (PDT) is a method for treatment of cancerous tumors and many other diseases. PDT is the preferential delivery of a photosensitizer (PS) to tumor tissue which is followed by irradiation of light of specific wavelength. After irradiation, the generation of reactive singlet oxygen (ROS) species on tumor, where photosensitizer has been localized specifically, results in cell death due to interaction of ROS with vital cellular components. Bone targeting is an alternative to apply in photodynamic therapy. No BP-based targeting has been designed for photodynamic therapy at bones to date. BP-mediated PS targeting improves therapeutic effects on bone tissue by concentrating PS at bones.

In this work, PEG based copolymers containing a potosensitizer and a targeting group was prepared to accomplish bone targeting in photodynamic therapy. As a carrier, a biocompatible polymer was chosen primarily because of its ease of processing and the ability to control the chemical and physical behaviour.

ÖZET

KEMİKLERDE BİRİKİME DAYALI FOTODİNAMİK TERAPİ

Fotodinamik terapi (PDT) noninvasiv oluşu, yan etkilerinin yok denecek kadar az olması sebebiyle kemoterapi, radyoterapi ve cerrahiye alternatif bir tedavi şeklidir. PDT kanserli hücrelerin tedavisinde ve diğer birçok hastalığın tedavisinde kullanılan etkili bir yöntemdir.

PDT ışığa duyarlı ilacın (photosensitizer) vücudun istenilen kısımlarına gönderilerek, bu ilacın tümörlü dokuda birikmesinin ardından, yoğunlaşan ilacın belli dalga boyundaki ışık ile uyarılarak, reaktif oksijen molekülleri oluşturulmasına dayanmaktadır. Oluşan reaktif oksijenin hayati hücresel bileşenler ile etkileşimi, hücrenin ölümüne yol açmaktadır. Kemiklerde birikime eğilimli maddelerin ışığa duyarlı ilaçlara bağlanması fotodinamik terapinin uygulanabilirliğini olumlu yöde etkiler.

Bu çalışma ışığa duyarlı ilacın ve kemiklerdeki fosfat yapılara duyarlı hedef moleküllerin belirli ağırlıktaki polimer zincirlerine bağlanarak, fotodinamik tedavide kullanılabilecek yapıların sentezlenmesine dayanmaktadır. Polimer taşıyıcılarının kullanılma sebebi, polimerik yapıların ilaçların farmakokinetiğini arttırması ve normal hücrelere oranla tumörlü hücreler üzerinde daha çok yoğunlaşarak vücuttaki ilacın yan etkilerini azaltmasından dolayıdır.

TABLE OF CONTENTS

LIST OF FIGURES

LIST OF TABLES

1. INTRODUCTION

1.1. PHOTODYNAMIC THERAPY

Photodynamic therapy (PDT) is a non-invasive alternative methodology for treatment of malignant tumors [1] and age related macular degeneration [2] along with several other diseases like psoriasis and scleroderma. It can be used alone or in combination with chemotherapy, surgery or radiotherapy by the help of low systemic toxicity of photodynamic therapy. PDT combines the use of a photosensitizer (PS) and light in presence of oxygen as a three main components to selectively destroy abnormal tissue. Figure 1.1 demostrates the steps in therapy simply. After diagnosis, the preferential delivery of a photosensitizing drug to tumor is followed by irradiation with light to destruct tumors [3], [4].

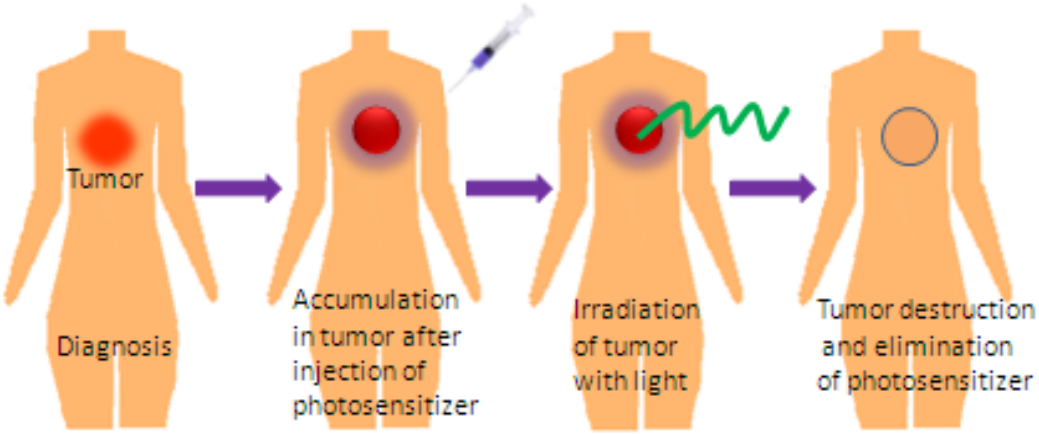

.

Figure 1.1 Schematic representation of photodynamic therapy [3]

The selectivity of PDT is based on the enrichment of the photosensitizer in the target tissue through an appropriate carrier system and giving light directly into that tissue. For the therapy, photosensitizer localized on targeted tissue is subjected to light of specific wavelenght (preferably red light due to its higher tissue permeability) which excites the photosensitizer from its ground state (S_0) to the first excited singlet state (S_1) or to higher excited singlet states (S_2-S_n) which is usually followed with an immediate relaxation to the first excited state (blue circles)**.** Because of too short lifetime of S_1 state, it instantly decays to first excited triplet state (T_1) through intersystem crossing [3], [4].

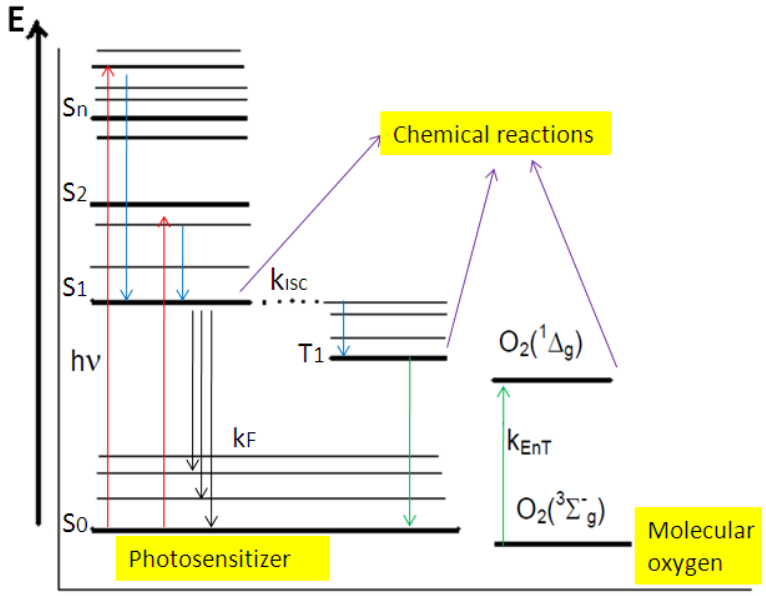

Figure 1.2. Jablonski diagram of the primary photophysical processes for PDT

The energy transfer from T_1 state to ground state oxygen (molecular O_2) produces reactive singlet oxygen (ROS) species which cause the cell death as a result of singlet oxygen interaction with cellular components such as lipids, amino acid residues, and nucleic acids. The process is outlined in Figure 1.3. The mechanism of cell apoptosis or necrosis depends on the positioning of photosensitizer drug within the cell and the amount of singlet oxygen produced [4].

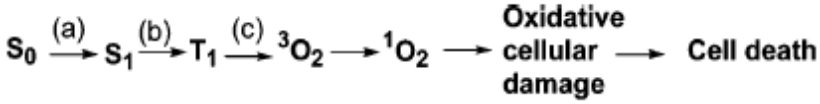

Figure 1.3. Photophysical pathway for the PDT process: (a) absorbance, (b) intersystem crossing, (c) energy transfer

Because of the short lifetime of highly reactive singlet oxygen, the close proximity of the photosensitizer to the target site is essential to cause maximum damage on tumor cell. The non-specific accumulation of photosensitizers causes phototoxicity, e.g. skin phototoxicity [3].

1.2. Photosensitizer

The photosensitizer causes tumor cell death by inhibiting oxygen supply to cell and by preventing its function via damaging celllular components. The properties for an efficient photosensitizer are summarized in Table 1.1. Photodynamic therapy agents with an extended π-electron system for a number of PDT relevant electronic properties exhibit a high intersystem crossing and singlet oxygen quantum yield as well as long triplet lifetimes. PS should have high absorbance in body's therapeutic window for good cell permeability and should disintegrate metabolically without giving toxic byproducts [5]. Easy synthesis without isomeric product and water solubility also for circulation in the body are essential. Photostability of the photosensitizer is another important parameter to prevent degradation of the molecule under illumination (photobleaching). In absence of illumination, low dark toxicity of PS makes them convenient in PDT [3], [6].

Photosensitizers emiting in the nearinfrared (NIR) region are also applied for vivo imaging in addition to singlet oxygen generation. A fluorescently detectable photosensitizer can be useful to see PDT progress in respect of photosensitizer localization and degree of photosensitizer uptake by abnormal tissue.

Table 1.1. Requirements for ideal photodynamic therapy agent

Ideal photosensitizer properties	**Carrier system demands**
High extinction coefficient beyond 630nm	Good intracellular uptake
Low dark toxicity	Low immunogenicity
Good singlet oxygen yield	Non toxicity
Appropriate solution behavior	High loading capacity
Biodegradability	Selective accumulation in tumor tissue
Photostability	Good water solubility
Straightforward synthesis	Macromolecularity
Accumulation in subcellular structures of tumor cells	

1.3. Macromolecular Carrier Systems for PDT

Clinically delivery of a photosensitizer to target tissue is limited to some cancer type because of toxicity coming from PS accumulation on healthy tissue. As a macromolecular carrier, different size of delivery constructs can be used without changing the function of the drug by chemical modification. For becoming ideal agent, biocompatible carriers should be in nanometer size to allow necessary penetrations and transportation in blood stream. Basic demands for a carrier are listed in Table 1.1. Carrier non-immunogenicity which minimizes the systemic side effects [7], [8] and high loading capacity of a carrier to localized desire PS drug amount on target tissue are very important.

According to their mechanism of targeting; macromolecular carrier systems for PDT can be categorized as active and passive targeting systems. Active targeting is a mechanism that enhances the delivery of the photosensitizer to target tissues by using specific interactions with target sites that is based on antigen receptor binding interactions [9]. Peptide-based delivery vehicles [10], amino acid photosensitizer conjugates [11], glucose-based transporters [12] and photosensitizer immunoconjugates (PICs) employing antibodies as targeting units [13], [14], [15] involve this kind of interaction.

By passive targeting, the physical and chemical properties of carrier are used to make a physiological difference between target and non-target tissues. Drug loaded carriers can be carried to tumor cells by selectively using the unique pathophysiology of tumors, such as their enhanced permeability and retention (EPR) effect mediated by leaky vascular structures of tumors and the tumor microenvironment [16]. EPR effect is the property by which certain sizes of molecules, typically macromolecular drugs, have a tendency to localize on tumor tissues much more than normal tissues. Liposomes [17], protein nanoparticles [18] and polymeric micelles [19] are carriers giving drug to tumor tissue by passive targeting.

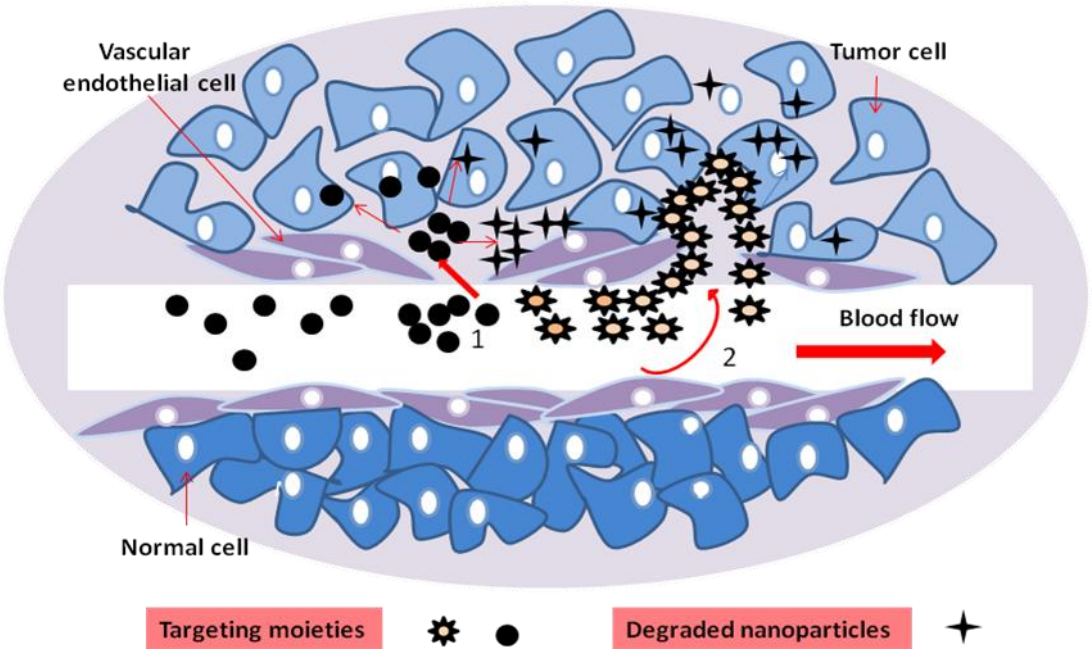

Figure 1.4. Targeting strategies for cancer therapy; (1) Passive targeting by EPR effect via degradation of drug carriers at extracellular space or inside cells after endocytosis. (2) Due to the ligands, drug release primarily inside cells after endocytosis by active targeting [20].

1.4. Bone Structure

Bone is a complex and highly organised connective tissue with very rigid and strong structure. Bone tissue involves relatively few cells and much intercellular integredients involving collagen fibres and stiffening substances. All bones serve as a reservoir of calcium and actively participate in calcium homeostasis of the body. There are many other function of bone in the body. All bones provide attachment to various muscle groups and do a protective function to many vital organs such as brain, lungs, heart, pelvis and bladder. Bones, skeletal muscles, tendons, ligaments and joints function together to give a three-dimensional shape to the body. Bone tissues can also store heavy metals and other foreign elements, to reduce their effects on other tissues. They arrange excessive pH changes by absorbing or releasing alkaline salts [21].

1.4.1. Cellular Structure

In the bone tissue, there are three cell types which are osteoblasts, osteocytes, osteoclasts. Osteoblasts are bone forming cells, located on the surfaces of bone. These cells are responsible for making a protein mixture known as osteoid which is primarily composed of Type I collagen and mineralizes to make bone. Osteoblasts show high alkaline phosphatase activity. Osteocytes are the cells occupying the lacunae in the calcified bone matrix. They maintain the exchange of nutrients and waste with the blood for daily metabolism of bone tissue. Osteoclasts lie in shallow depressions on the bone surface. They are the cells responsible for bone resorption and breaking down the bone [21].

1.4.2. Molecular Structure

The bone matrix consists of organic and inorganic part. The organic part is mainly composed of Type I collagen which is synthesized intracellularly. It provides bone flexibility and tensile strength. The inorganic matrix of bone is made up of crystalline mineral salts and calcium, which is present in the form of hydroxyapatite (HAP) with the formula $Ca_{10}(PO_4)_6(OH)_2$. The association of hydroxyapatite with collagen fibres make bone hard and rigid. The inorganic mineral hydroxyapatite (HAP) forms the seventy percent of bone and gives the opportunity for some molecules to bind to bone tissue. One of the most important molecules which can bind to HAP is bisphosphonate.

1.5. Bone Diseases

An imbalance in the activity of osteoblasts that form bone and osteoclasts that break it down causes many disorders such as osteoporosis, osteoarthritis, rheumatoid arthritis and bone cancer [22]. Osteoporosis is a disease with an increased risk of fracture. In osteoporosis, the bone mineral density is decreased and disruption in bone arctitecture occurs. The another disease is osteoartitis which means bone inflammation resulting in pain in the joints. In rheumatoid arthritis condition, the attack by immune system to joints leads to loss of mobility due to pain and joint destruction.

Bone cancer is another important disease. Cancer is a disease in which abnormal cells divide without control and invade other tissues. Bone cancer may form in the cells of the bone and may emerge from spreading to bone from any other part of the body. Benign (noncancerous) bone tumors are more common than malignant ones. For many kind of bone diseases, wide range of drug applications are possible. However in all cancer types like bone cancer there is no real efficient treatment that make scientist concentrate on mainly cancer.

1.6. Bisphosphonates

Bisphosphonates (BP) are clinically stable derivatives of pyrophosphate compound. Bisphosphonates are also called as diphosphonates which is a kind of drug that have been used to treat bone disorders since the 1960s. Because of the inefficiency of pyrophosphate compound on normal mineralization and on bone resorption in vivo, bisphosphonate analogs were applied as a drug candidate for treatment of bone diseases [23]. Unlike pyrophosphate, BP are resistant to enzymatic hydrolysis and they inhibit bone resorption by interfering with the action of the bone-resorbing osteoclasts which make bisphosphonate favorable with respect to pyrophosphate.

Bisphosphonate **Inorganic pyrophosphate**

Figure 1.5. Structure of bisphosphonate and inorganic pyrophosphate

Figure 1.5 shows the structures of pyrophosphate and its non-hydrolyzable bisphosphonate derivative. Several BPs are established for treatment of various diseases of excessive bone resorption, including Paget's disease, myeloma, bone metastases, and osteoporosis.

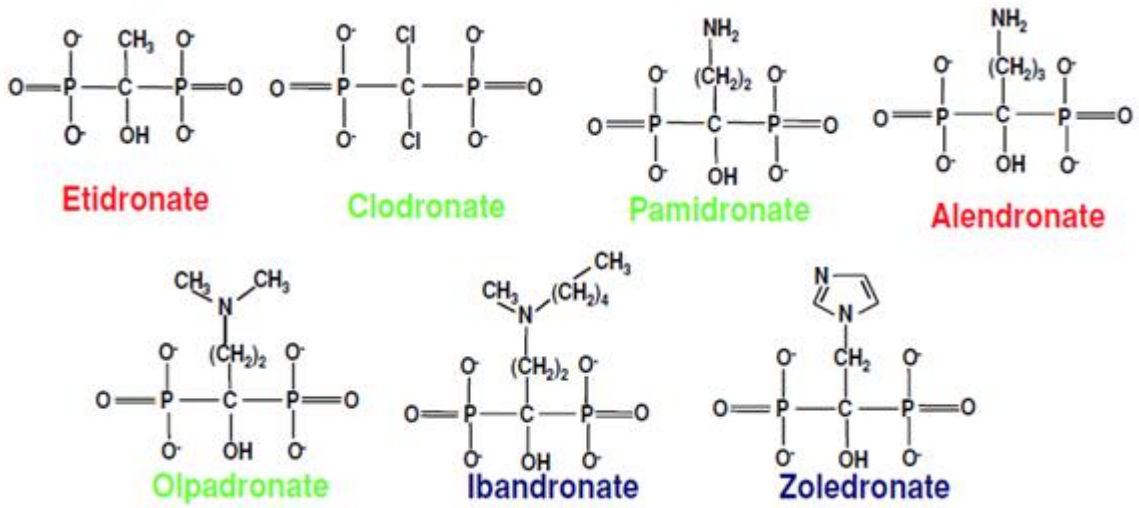

Figure 1.6. Structures of the bisphosphonates used clinically [24]

1.6.1. Chemistry of bisphosphonates

To explain the function of the substituent on bisphosphonate, the P-C-P moiety is responsible for the affinity of the BP's for hydroxyapatite (HAP) and also for chelation to Ca^{+2} ions. To give an example, pentane monophosphonate, or P-C-C-P or P-N-P compounds cannot be used as an inhibitors for bone resorption due to absence of P-C-P moiety.

When R_1 group is a hydroxy group (as in etidronate) rather than halogen atom (as in clodronate), it enhances binding to HAP crystals and inhibit crystal growth and dissolution. Hydroxy group as R_1 substituent increases the affinity for calcium with the possibility of chelating calcium ions by tridentate rather than bidentate binding [24].

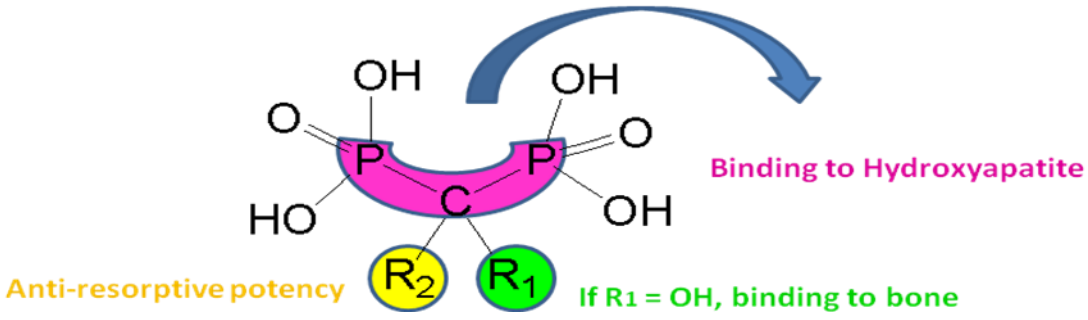

Figure 1.7. The structural explanation of bisphosphonate

R_2 group gives the antiresorptive property tending to slow or block the resorption of bone. The most potent antiresorptive BPs were those containing a nitrogen atom within a heterocyclic ring (as in risedronate). The compounds containing a tertiary nitrogen, (as in ibandronate) and (as in olpadronate), were even more effective in inhibiting bone resorption. The spatial configuration of nitrogen atom in the R_2 side chain and its distance away from the P-C-P group are very critical for maximal potency.

Bisphosphonates can be categorized as non-nitrogen-containing bisphosphonates (such as clodronate and etidronate) and nitrogen-containing bisphosphonates (such as pamidronate, alendronate, risedronate, ibandronate, and zoledronate). The non-nitrogen-containing bisphosphonates may inhibit ATP-dependent intracellular enzymes. However, nitrogen-containing bisphosphonates can inhibit enzymes of the mevalonate pathway which blocks synthesis of some vital protein for osteoclast activity and thereby induce apoptosis [24].

1.6.2. The mechanisms of Action of BP's at A Cellular Level

Because of their preferential uptake in bone and adsorption to mineral surfaces, BPs specifically get close to osteoclasts. Studies have shown that BPs play a role in osteoclast-mediated bone resorption. They have an effect on osteoclast recruitment, differentiation, and resorptive activity. During bone resorption, the acidic environments of the subcellular space beneath the osteoclast bring about dissolution of the HAP bone mineral. Due to affinity of BPs to bone mineral at bone resorption region where the mineral is highly abundant the osteoclast exposure to free, non-mineral-bound bisphosphonate is inevitable as a result of getting off the bisphosphonate from bone mineral in the low pH environment around osteoclast. Furthermore, BPs may prevent osteoclast formation and so block bone resorption also. It was shown that, in long-term cultures of human bone marrow BPs inhibited the formation of osteoclast-like cells [24].

1.7. TARGETED PHOTODYNAMIC THERAPY

The major problem of traditional drug delivery is the toxicity depending on the dose when the the difference between the maximum tolerated dose (MTD) and the minimum

effective dose is very close to each other. Targeted drug delivery is the delivery of a therapeutic agent to a specific target site in the body where the agent has greatest pharmacological effects without diffusing to other sites or tissue where they may cause damage or trigger side effects.

Targeted photodynamic therapy (PDT) gives the chance of enhancing photodynamic efficiency by directly targeting tumor cells and tissues. According to their mechanism of interaction, there are mainly two kind of targeted drug deliveries which are passively targeted drug delivery and active targeted drug delivery. For the passive targeting some properties such as EPR effect of tumor tissues with leaky blood vessels and imperfect lymph drainage, the pH or the presence of certain enzymes can be used to achieve targeting to a certain site. For the active targeting the expression of certain disease specific markers such as antigens or receptors can be targeted using corresponding antibodies or ligands. Active targeting minimize the possible side effects of drugs by making drug molecules mainly accumulate on a certain tissue or organ instead of distribution of it over the entire body [3].

The tumor cells have some properties to target the drug carriers to tumor tissue. The over expression of some certain receptors for enhanced uptake of nutrients, including folic acid, vitamins, and sugars on tumor tissue, increased levels of specific cell surface membrane lipids and proteins and changes in the cellular microenvironment give the opportunity of targeting the carriers covered with ligands ready to interact with these receptors to tumor cells. These strategies have been applied to increase the efficacy of PDT to increase the uptake of the dye by the target cells and tissues or to improve subcellular localization of dye.

In literature, many drug targeting conjugates involving macromolecular carriers have been illustrated for tissues like colon [25], liver [26] and lung [27] or specific inflammation sites [28] with the ligand-receptor interactions. Several kind of macromolecular carriers such as polymers, lipids, self-assembling amphiphilic molecules, micelles, dendrimers, metal, and inorganic semiconductor nanocrystals (quantum dots) have been demonstrated for drug delivery systems [29].

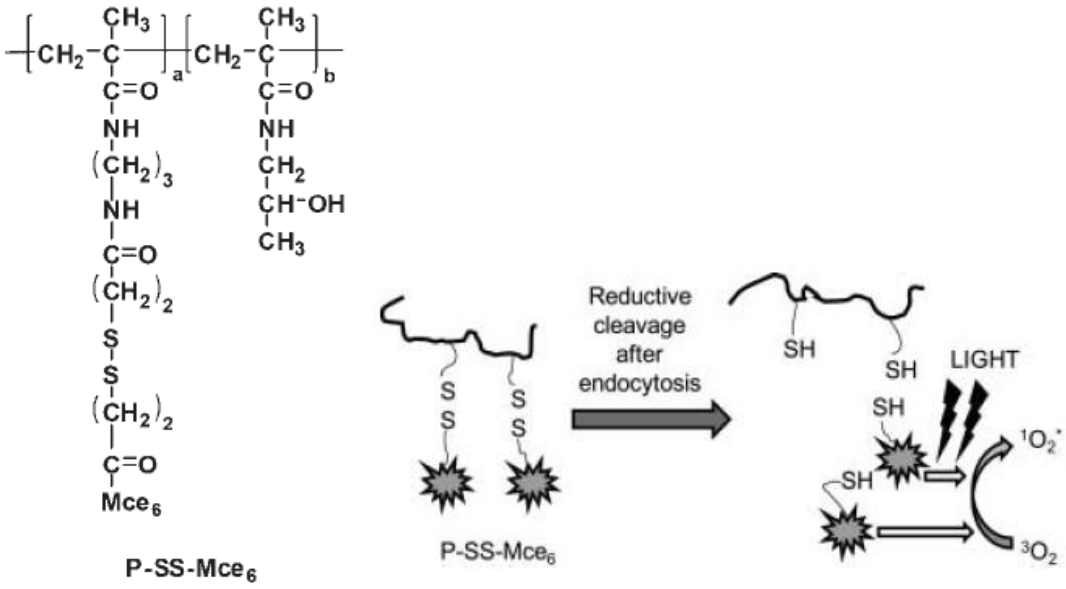

Figure 1.8. The structure of P-SS-Mce6 conjugate

In 2008, Kopecek and coworkers synthesized disulfide linked HPMA copolymer-drug conjugates involving mesochlorin e_6 (Mce_6) as a photosensitizer drug. The passive targeting of Mce_6 drug by helping of EPR effect via polimeric delivery made this conjugates potential vehicle for PDT. Figure 1.8 shows the P-SS-Mce6 conjugate [30].

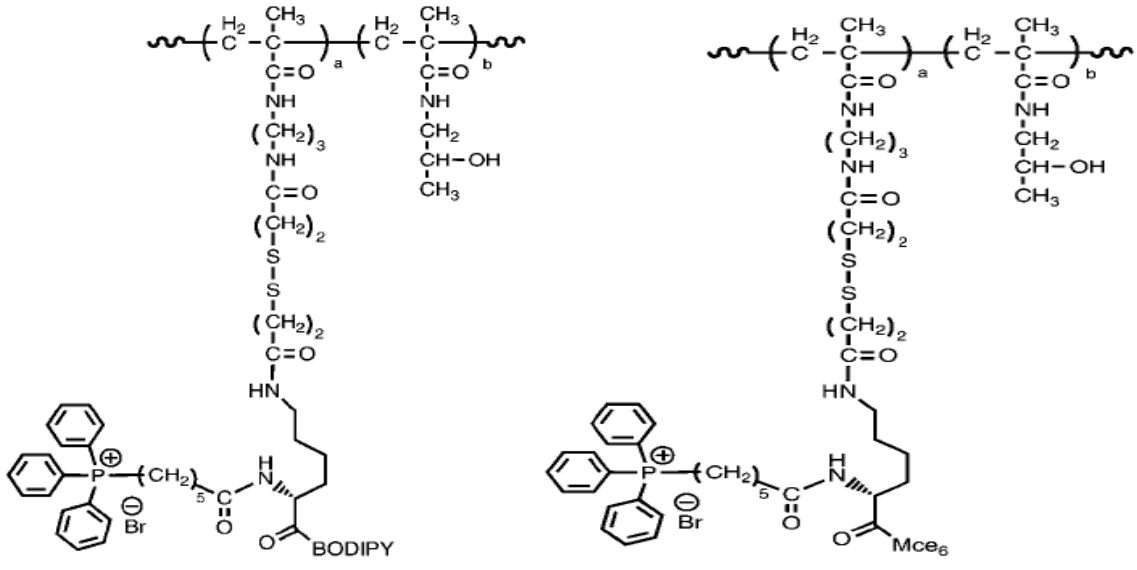

P-SS-TPP-lysine-BODIPY **P-SS-TPP-lysine-Mce_6**

Figure 1.9. The structures of P-SS-TPP-lysine-BODIPY and P-SS-TPP-lysine-Mce_6

In the same year again Kopecek group synthesized HPMA copolymer bound with triphenylphosphonium (TPP) as a mitochondrial targeting drug and mesochlorin e_6 (Mce_6) as a photosensitizer. BODIPY labeled P-SS-TPP-lysine (Figure 1.9) was synthesized to visualize the subcellular distribution and mitochondrial targeting ability of the designed constructs. The conjugation of Mce_6 to HPMA copolymer backbone via a disulfide linkage has improved photodynamic efficacy of the construct for tumor specific mitocondrial targeting [31].

1.7.1. BODIPY as a photosensitizer

While porphyrin based compounds are most known photosensitizer, there are also many other examples in litearture such as BODIPY derivatives, chlorin(e_6), texaphyrins, phthalocyanines, squaraines, and perylenediimide as a photosensitizer drug. Among these photosensitizer, BODIPY derivatives have some fascinating properties to apply it in PDT. High wavelenght capacity with extended π conjugation and bromination at 2 and 6 position give BODIPY dye some special properties. Bromination of BODIPY increases the intersystem crossing via heavy atom effect and the conjugation at 3 and 5 position by condensation reaction with aldehydes improves the higher wavelenght absorbing capacity which allow BODIPY use in PDT in an efficient way. Also photostable BODIPY agents has environment independent fluorescence and good cellular uptake for therapeutic treatment with respect to other photosensitizer [5], [32].

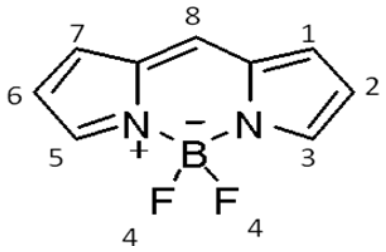

Figure 1.10. The structure of 4-bora-3a,4a-diaza-s-indacene

In literature, there are several BODIPY based photosensitizers with different properties. In 2006, Nagano and coworkers synthesized a hydrophobically activatable

photosensitizer (Figure 1.11) involving a protein targeting unit (blue) for chromophore-assisted light inactivation. Inositol 1,4,5- triphosphate ligand (blue) with a photoinduced electron transfer quencher (pink) was attached to red BODIPY core to address the photosensitizer to its protein target. The quenching ability of drug conjugate depends on the hydrophobicity of medium where singlet oxygen formation can damage specifically targeted protein, after specific binding of triphosphate ligand [33].

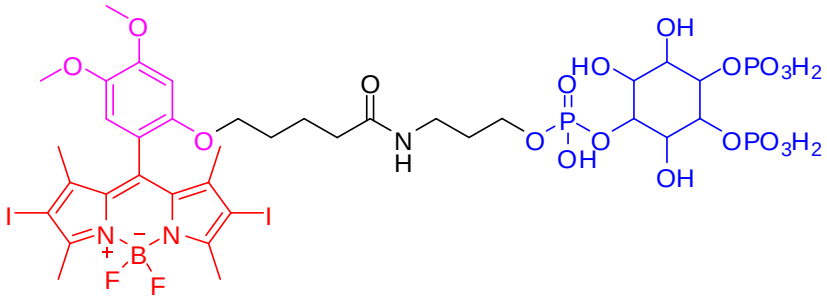

Figure 1.11. The structure of protein targeted BODIPY conjugate

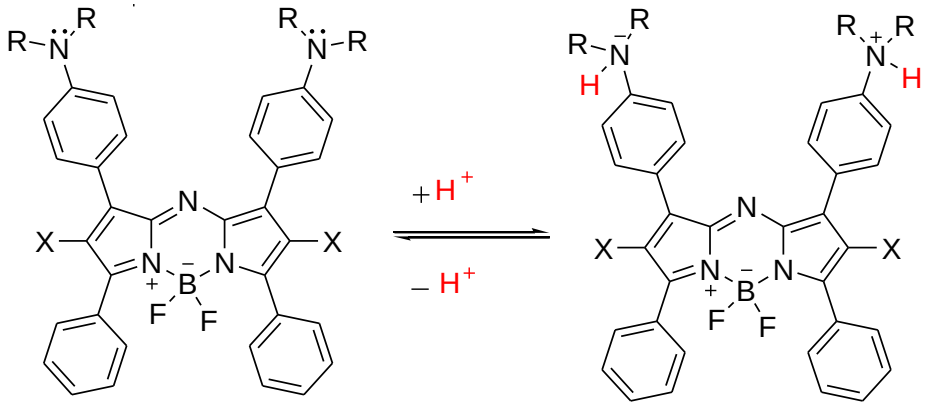

Figure 1.12. The structure of pH dependent activable BODIPY photosensitizer

Another activatable photosensitizer based on electron transfer by depending on pH was synthesized by O'Shea group. In a acidic medium, extended BODIPY derivatives with different R (the photoinduced electron transfer moieties) and X groups increased singlet oxygen formation. This kind of photosensitizers provide highly regioselective ROS generation at the target tissue, with little or no nonspecific phototoxicity elsewhere in the cell [4].

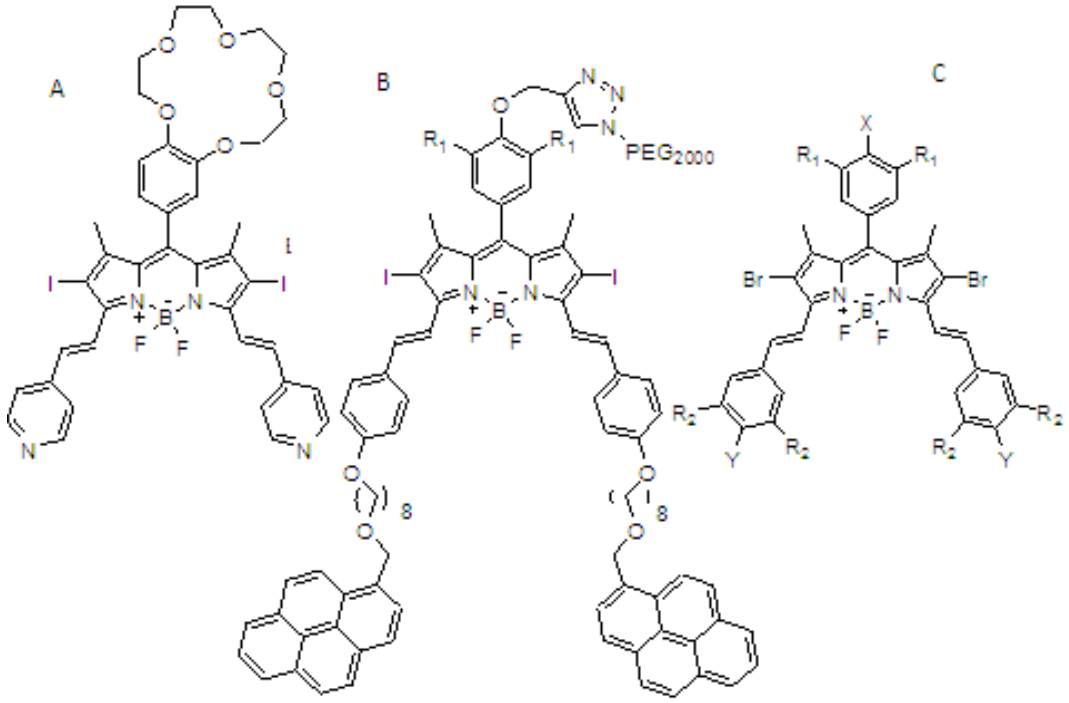

Figure 1.13. The structures of BODIPY based photosensitizers for PDT

Some other efficient photosensitizers (Figure 1.13) synthesized by Akkaya group. Activable photosensitizer (A) generate high amount of ROS in presence of both high salt and high [H^+] conditions together but not either separately which takes the advantage of highly acidic tumor tissues with high intracellular sodium ion concentration. The conjugation of pyrenyl group in compound B gives the chance of non covalent attachment of carbon nanotubes as a carrier and conjugation of PEG molecule also improves the solubility of photodynamic therapy agent. Another photosensitizer C also synthesized in the same group by conjugation of different water soluble R group to BODIPY unit to improve solubility of dye [5], [32], [34].

1.7.2. Bisphosphonates as Targeting Group

Because of their affinity for HAP, bisphosphonates are potential candidate to use as a targeting agent in bone targeted drug delivery systems. In literature, there are many different designed constructs involving BP as a targeting unit. BPs can be simply categorized depending on their attachment to the drug molecules. They may attach directly or via a linker designed according to the required release profile.

In 2006, gemcitabine (Gemzar) - bisphosphonate drug conjugate (Figure 1.14) was shown by Amal A. El-Mabhouh and coworkers to treat metastatic bone cancer. Even though gemcitabine drug itself does not have affinity for bone, its conjugate with bisphosphonate has been directly targeted to bone via binding affinity with HAP [35].

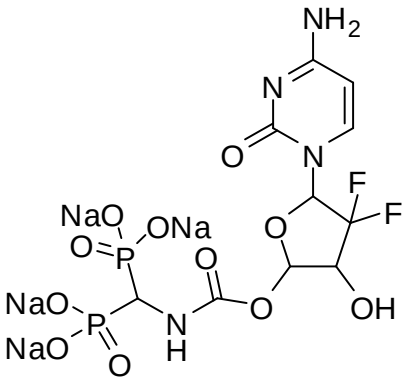

Figure 1.14. The structure of Gemcitabine - bisphosphonate conjugate

Zaheer and coworkers have synthesized a near-infrared (NIR) fluorescent bisphosphonate drug. The specific binding of this drug to HAP *in vitro* and *in vivo* was studied. The attachment of flourescent dye gave the opportunity for detection of osteoblastic activity in mice [36].

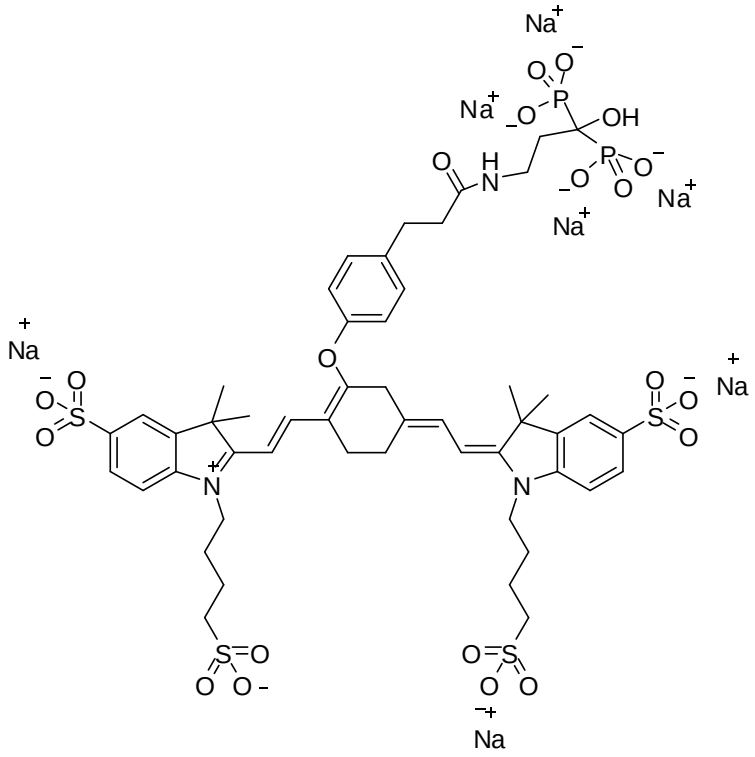

Figure 1.15. The structure of NIR fluorescent diagnostic agent for bone diseases

Wang and coworkers have demonstrated another bone targeting constructs. They used two different polymers as poly(ethylene glycol) (PEG) and poly[N-(2-hydroxypropyl) methacrylamide] (PHPMA) with two different bone targeting moieties, namely alendronate and aspartic acid peptide. Fluorescein isothiocyanate (FITC) has been conjugated for detection or imaging purposes via fluorescence technique. Polymeric carriers which have targeting moieties and FITC at the end of chain and on the side chain of backbone have been demonstrated both in Figure 1.16 and 1.17. The results obtained in vitro with hydroxyapatite (HAP) and results from mice have verified specific accumulation of this drug conjugates in the bone tissue. Dual targeting has been achieved by passive accumulation due to the EPR effect and active targeting by ALN's affinity to bone mineral [37].

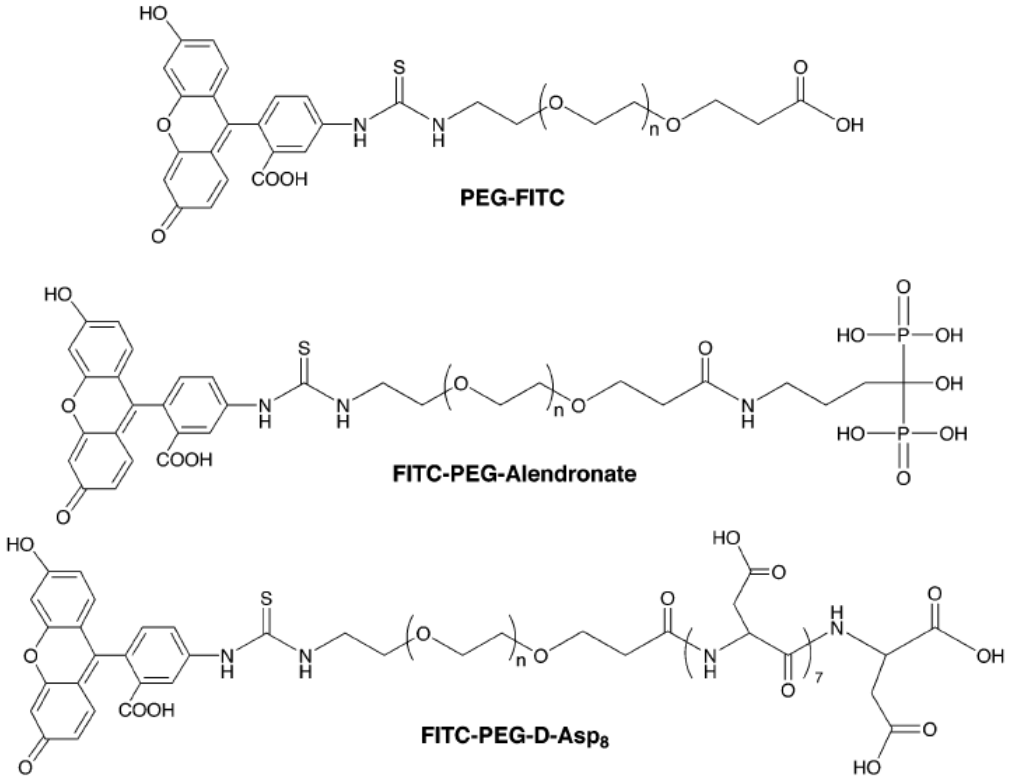

Figure 1.16. Structures of bone-targeting PEG conjugates

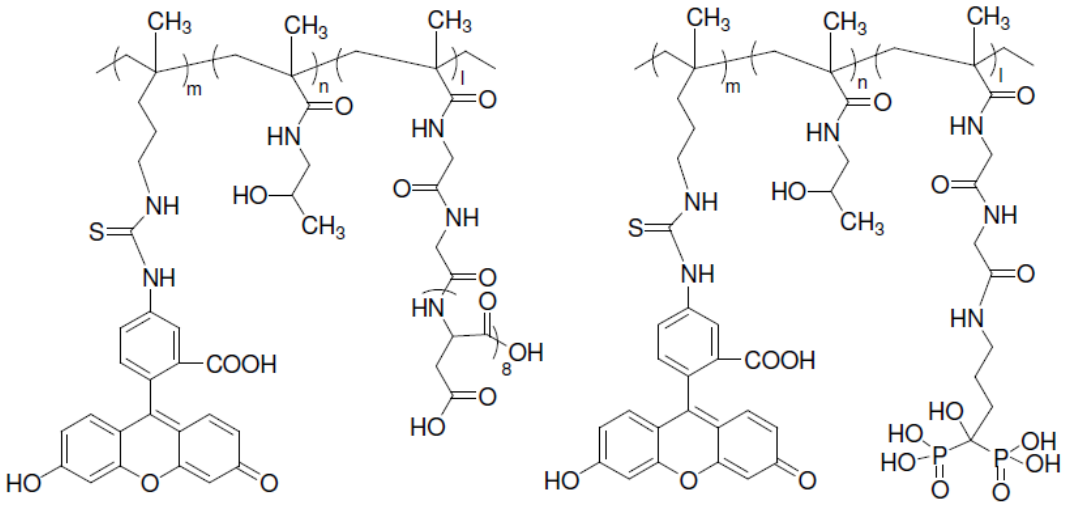

Figure 1.17. Structures of bone-targeting HPMA conjugates

2. AIM OF THE STUDY

The study involves three main parts: the functionalizable polymer synthesis, a photosensitizer dye synthesis and the conjugation of photosensitizer and a targeting moiety to that polymer for bone affinity.

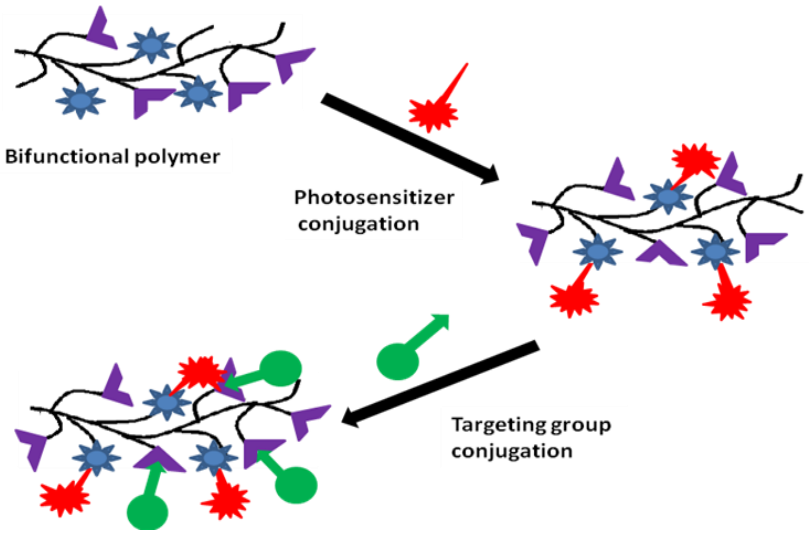

Figure 2.1 Schematic approach for the main focus of thesis study

Due to having tendency for binding to bone tissue, Alendronate, bisphosphonate drug was conjugated to the polymeric carrier. As a carrier, a PEG based polymer was chosen because of its excellent properties in biological application. It is known that polymer-conjugates enhance drug solubility, decrease toxicity and side effects of the conjugated drug, and increase tumor accumulation via EPR effect. For photonic treatment, long range BODIPY photosensitizer was conjugated to the polymer. BODIPY was preferred owing to its fascinating features for PDT. Photostable BODIPY dye has good singlet oxygen generation with high intersystem crossing value that makes it indispensable for photodynamic therapy applications.

3. RESULTS AND DISCUSSION

3.1. Reactive Polymers

In this study, PEG based macromoleculas were chosen because of excellent advantages of pegylated compounds such as nontoxicity, high water solubility, non-immunogenicity, a decreased degradation by metabolic enzymes and prolonged blood circulation time. It was also shown that macromolecular pegylated photosensitizer conjugates has demonstrated increased tumor retention and improved therapeutic profile [38], [39].

To solve the problem of low loading capacity of PEG polymers which hold only one or two hydroxyl terminal groups that can be activated, Polyethylene glycol monomethyl ether methacrylate (PEGMA) monomer was copolymerized with N-hydroxy succinimidyl methacrylate (NHSMA) monomer by atom transfer radical polymerization (ATRP). In adddition to NHS functional copolymers, alkyne and both alkyne and NHS bifunctional polymers were obtained by adding different equivalence of propargyl amine to PEG-NHS copolymer.

ATRP method was used to synthesize polymers with low poly dispersity indeces. Typically ATRP reaction requires an ATRP initiator, a metal ion complexed with some ligand(s), and monomers of course. As an advantage, molecular weight and functionality can be controlled by ATRP which are essential for biological purposes. PEG based polymers will enhance cell permeability and tumor targeting ability (via EPR effect) on photosensitizers.

3.1.1. NHS Funtionalized Reactive Polymer (4) Synthesis

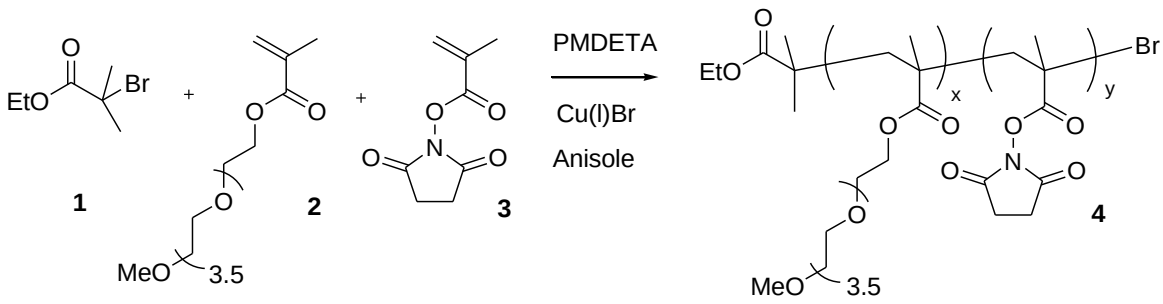

Figure 3.1. The synthesis of NHS functionalized copolymer

PEGMA, **2** and NHSMA, **3** monomers were copolymerized in presence of an alkyl halide (ethyl 2-bromoisobuthyrate, **1**) as an initiator and PMDETA (N,n,n',n',n-Pentamethyldiethylenetriamine) and Cu(I)Br as a transition metal complex. Copolymers with 23K was obtained in a desired way. Conversion to PEG-NHS copolymer was monitored by GPC and also characterized by ^{1}H NMR. Figure 3.2 shows the proton NMR of the copolymer in $CDCl_3$. The peak at 2.77 ppm (s, 4H, CH_2-CH_2) from NHS and other intense peaks between 4.04 ppm and 3.34 ppm from PEG chain confirms the formation of the copolymer. Peak (c) from methoxy group of PEG chains at 3.34 ppm and peak (a) from NHS at 2.77 ppm give the information about the ratio of PEG to NHS which is 4.7 by integration. However, for the reaction we used 6 fold higher amount of PEGMA monomer than NHSMA monomer.

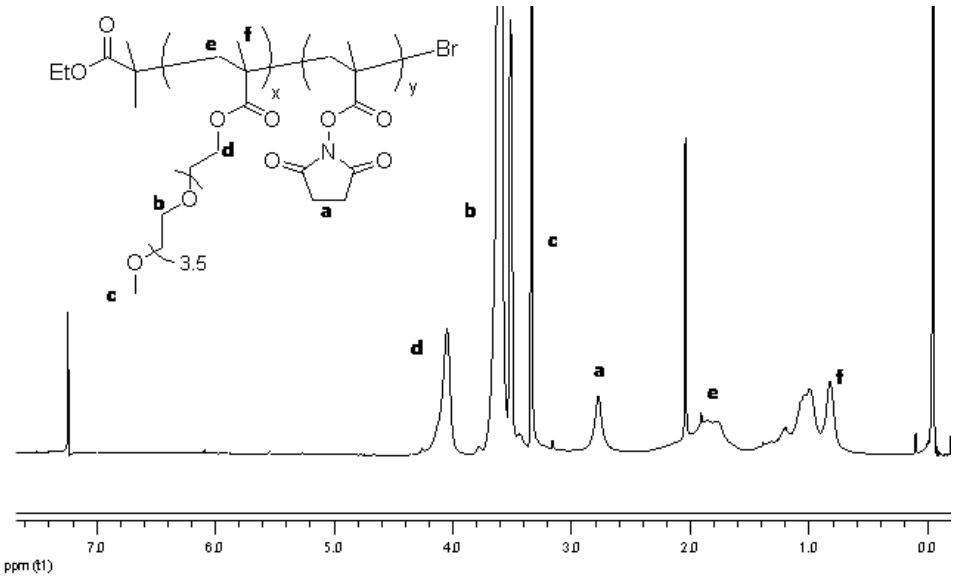

Figure 3.2. ^{1}H NMR spectra of PEG-NHS copolymer (**4**)

3.1.2. Alkyne Funtionalized Reactive Polymer (6) Synthesis

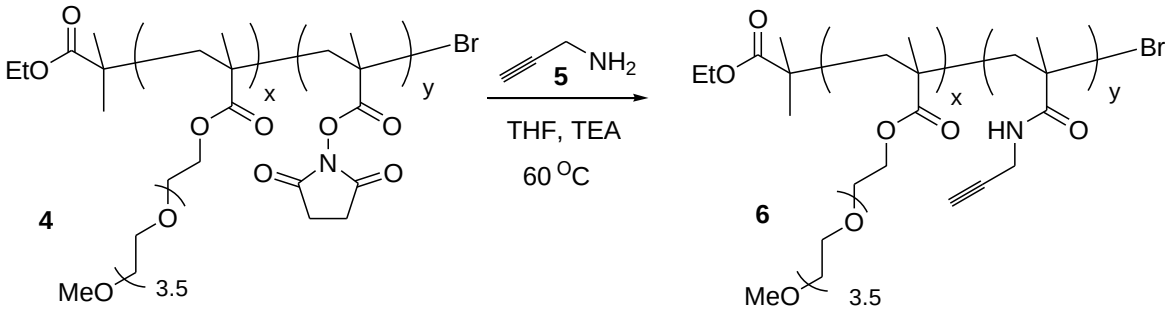

Figure 3.3. The synthesis of Alkyne functionalized copolymer

Propargyl amine, **5** and TEA were added to PEG-NHS copolymer, **4** (Mn: 23K, PDI: 1.39) in dry THF. The excess equivalence of propargyl amine, **5** was used for total conversion of NHS groups to the alkyne groups. Compound **6** was characterized via ^{1}H NMR. The disapperance of the peak at 2.8 ppm and the appearance of the new peak (a) at 2.18 ppm (s, 1H, CH≡C) has demonstrated the replacing of all NHS units with alkynes by attacking of amine group to ester group of NHS. The extra peak at 5.25 ppm comes from CH_2Cl_2 solvent.

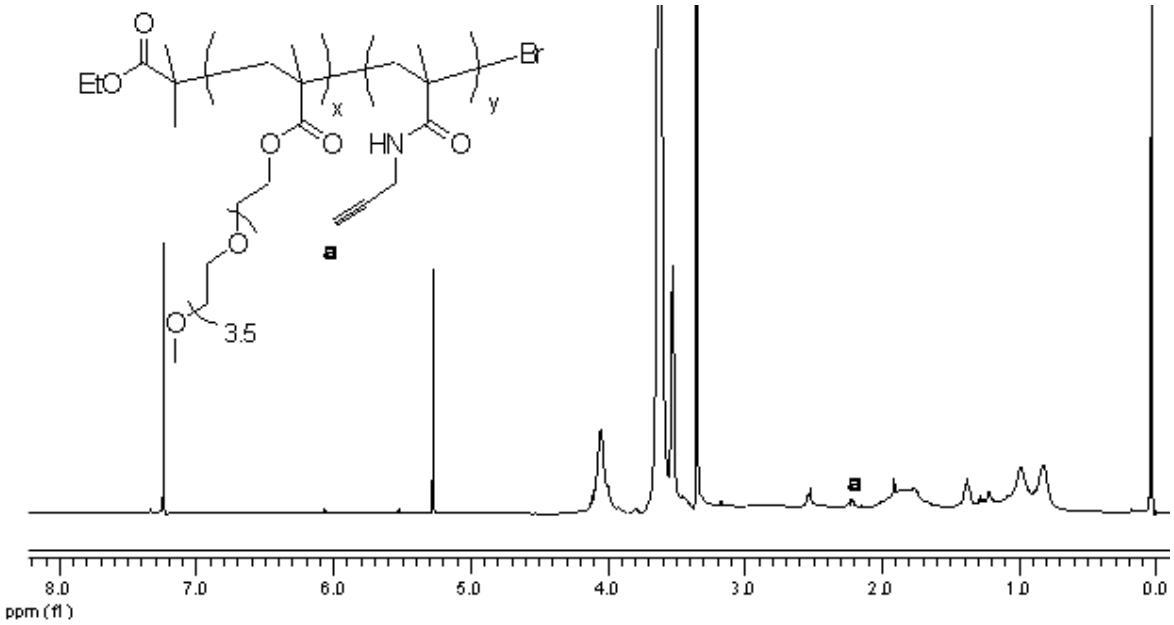

Figure 3.4. ^{1}H NMR spectra of Alkyne functionalized copolymer (**6**)

3.1.3. Alkyne and NHS Funtionalized Reactive Polymer (7) Synthesis

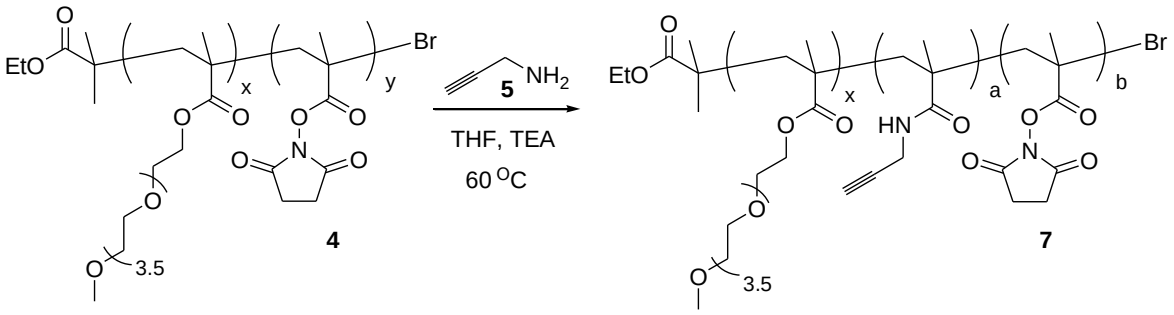

Figure 3.5. The synthesis of Alkyne and NHS functionalized copolymer

PEG-NHS copolymer, **4** (Mn: 23K, PDI: 1.39) was dissolved in dry THF and propargyl amine and TEA were added. Partial conversion of NHS to alkyne depending on the equivalence of the propargyl amine used was monitored by ^{1}H NMR. The appearance of the new peak (a) at 2.29 ppm coming from triple bond has indicated the partial conversion of NHS to alkyne on polymer side chain which gave the copolymer with two different reactive groups that can be activated.

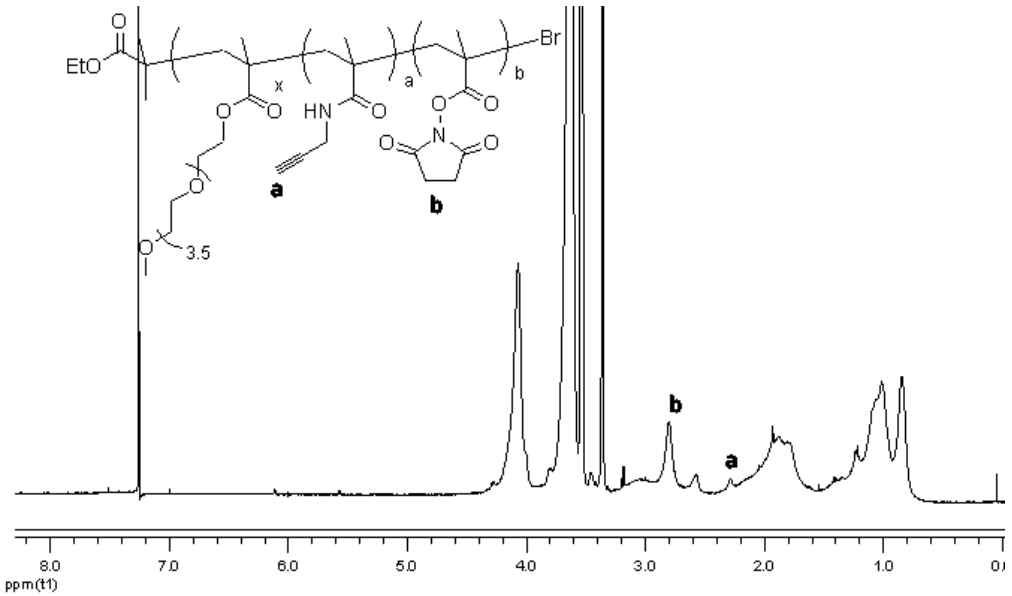

Figure 3.6. ^{1}H NMR spectra of PEG-NHS-alkyne functionalized copolymer (**7**)

The ratio of NHS to alkyne was determined from proton NMR by the peak (c) at 3.34 ppm coming from methoxy group of PEG chains and peak (b) at 2.7 ppm coming from –CH_2-CH_2- group of NHS. Because of overlapping of alkyne peak with the peaks of

polymer backbone, we used methoxy peak again instead of alkyne peak to determine ratio. Despite of using one to one equivalence of NHS and propargly amine, only 23.8 percentage of NHS was converted to alkynes. It means that there are 3.4 alkynes groups together with 11 NHS groups on the copolymer.

3.2. Reactive Dye Synthesis

A good photosensitizer essentially requires singlet oxygen generation capacity, good solubility in water and long wavelength excitability in body's therapeutic window. As a PDT agent, BODIPY derivative was synthesized with an extended conjugation. To improve intersystem crossing via heavy atom effect, bromine substituents were located at 2 and 6 position of BODIPY unit and to increase wavelenght absorbing capacity, p-anisaldehyde was modified to the BODIPY agent by conjugation to methyl group at 3 and 5 position. Then these longer wavelength absorbing dyes incorporated into the polymer side chains which overcame the problem of the hydrophobicity of dye and made it water soluble as a favorable photodynamic therapy agent.

3.2.1. BODIPY$(CH_2)_{10}$Br (10) synthesis

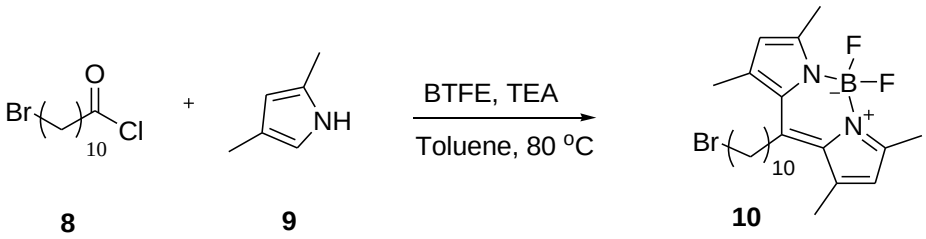

8 **9** **10**

Figure 3.7. BODIPY$(CH_2)_{10}$Br synthesis

BODIPY$(CH_2)_{10}$Br was synthesized by starting with 2,4-dimethylpyrrole, **9**. Figure 3.7 shows the detail of the reaction according to literature [40]. Oil like compound **10** was obtained with a yield of 43 % . Product was characterized by ^{1}H NMR. In ^{1}H NMR spectra, appearance of the proton peaks at 6.03 ppm (b), at 2.49 ppm (c), at 2.39 ppm (a) proved the formation of BODIPY core. The peak (f) at 3.38 ppm and the peak (d) at 2.91 ppm with other high field peaks have indicated presence of alkane chain on molecule.

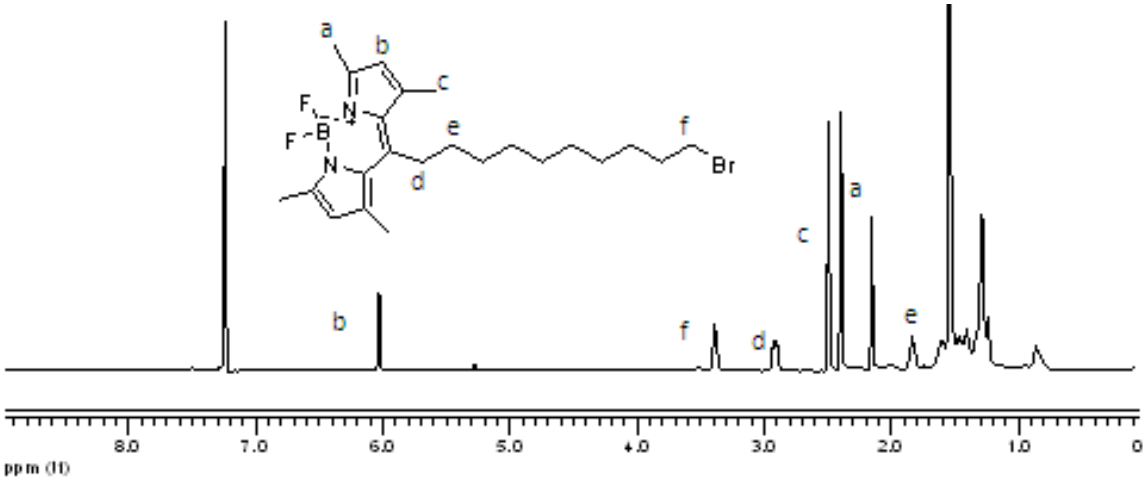

Figure 3.8. ^{1}H NMR spectra of BODIPY$(CH_2)_{10}$Br **(10)**

3.2.2. BODIPY$(CH_2)_{10}N_3$ (11) synthesis

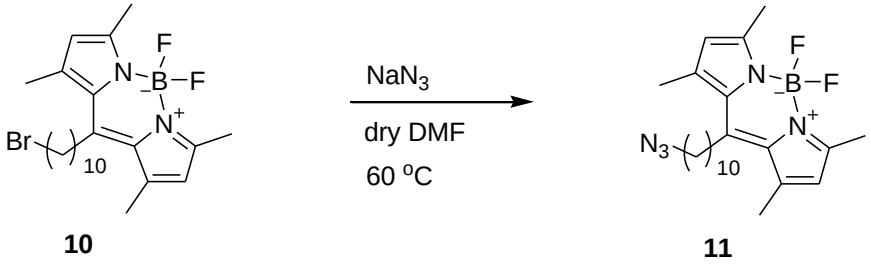

10 **11**

Figure 3.9. BODIPY$(CH_2)_{10}N_3$ synthesis

In order to funtionalize BODIPY$(CH_2)_{10}$Br, excess NaN_3 was added to the compound **10** in DMF. Figure 3.9 shows the synthesis of BODIPY$(CH_2)_{10}N_3$ to give a yield of 77 %. Compound was verified by ^{1}H-NMR and FTIR. The shift of the peak (f) at 3.38 ppm (Figure 3.8) to 3.24 ppm (Figure 3.10, peak a) has exhibited the replacing of bromine atom with azide group on molecule. The other peaks coming from compound has remained nearly same. In addition to ^{1}H NMR analysis, the apperance of the azide stretch at 2091 cm^{-1} in FTIR spectra has verified presence of azide functional group on BODIPY dye.

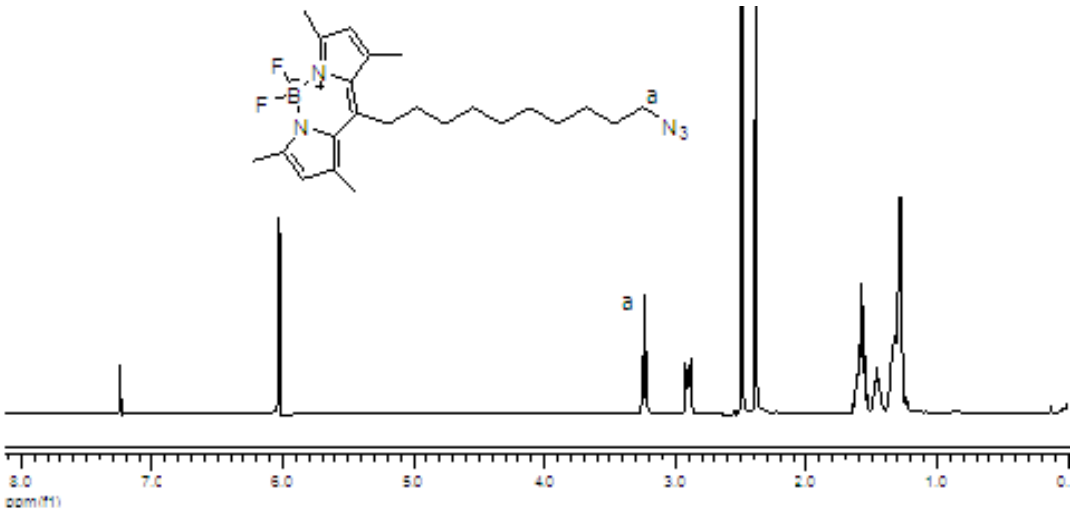

Figure 3.10. ^{1}H NMR spectra of BODIPY$(CH_2)_{10}N_3$ **(11)**

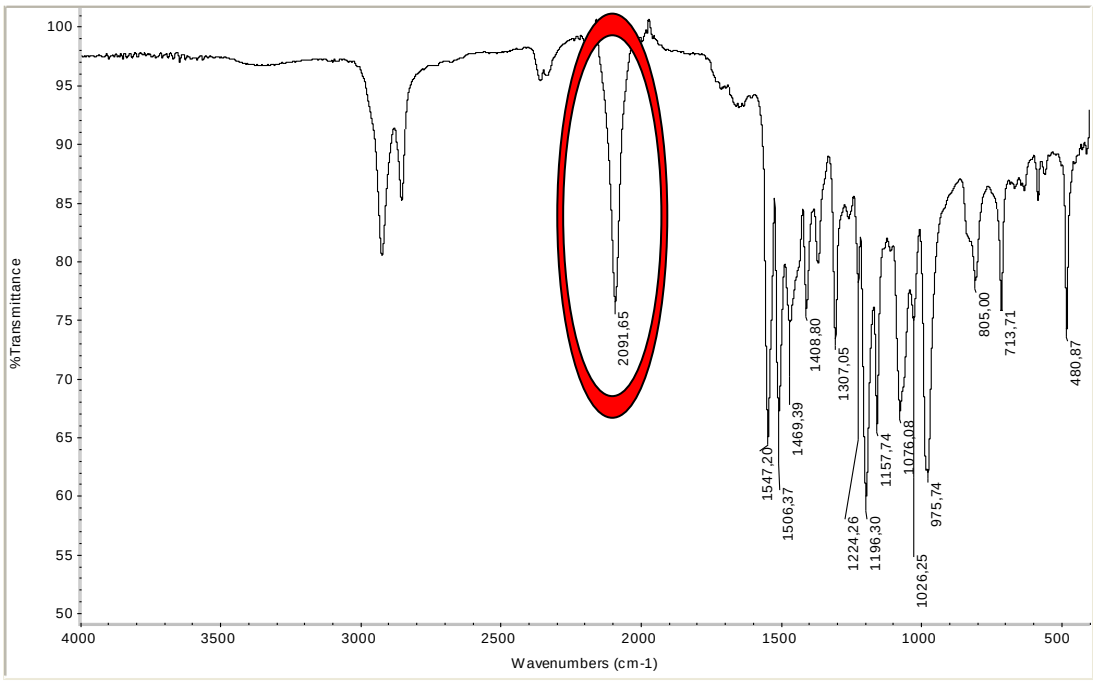

Figure 3.11. IR spectra of BODIPY$(CH_2)_{10}N_3$ **(11)**

3.2.3. BODIPY$Br_2(CH_2)_{10}N_3$ (12) synthesis

The conjugation of bromine substituents to BODIPY results in the heavy atom effect that facilitates the intersystem crossing (ISC) from photosensitizer to produce reactive singlet oxygen during photodynamic therapy. The substitution has also changed the color of the dye.

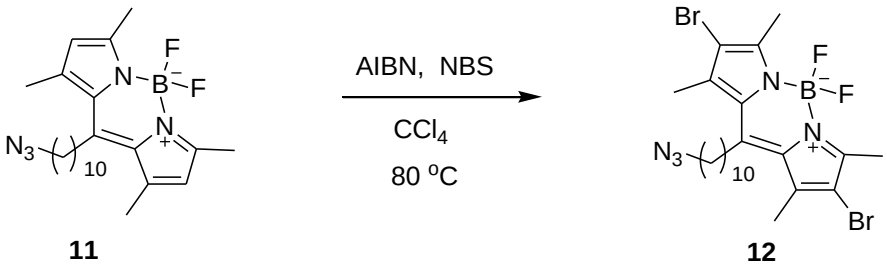

Figure 3.12. $BODIPYBr_2(CH_2)_{10}N_3$ synthesis

$BODIPY(CH_2)_{10}N_3$, **11** was treated with N-bromosuccinic imide (NBS) and Azo bis isobutyronitrile (AIBN) in CCl_4 at 80 ^oC (Figure 3.12) to give a product having bromine substituents at 2 and 6 position of BODIPY unit [41]. Compound **12** was characterized by both ^{1}H-NMR and FTIR. The disappearance of the peak (b) at 6.03 ppm (Figure 3.8) has indicated the attachment of bromine atoms to the BODIPY rings. FTIR spectra also have demonstrated that the functional azide group is not damaged during the reaction by the peak at 2091 cm^{-1} (Figure 3.14), it remains intact after exposition to the reaction condition.

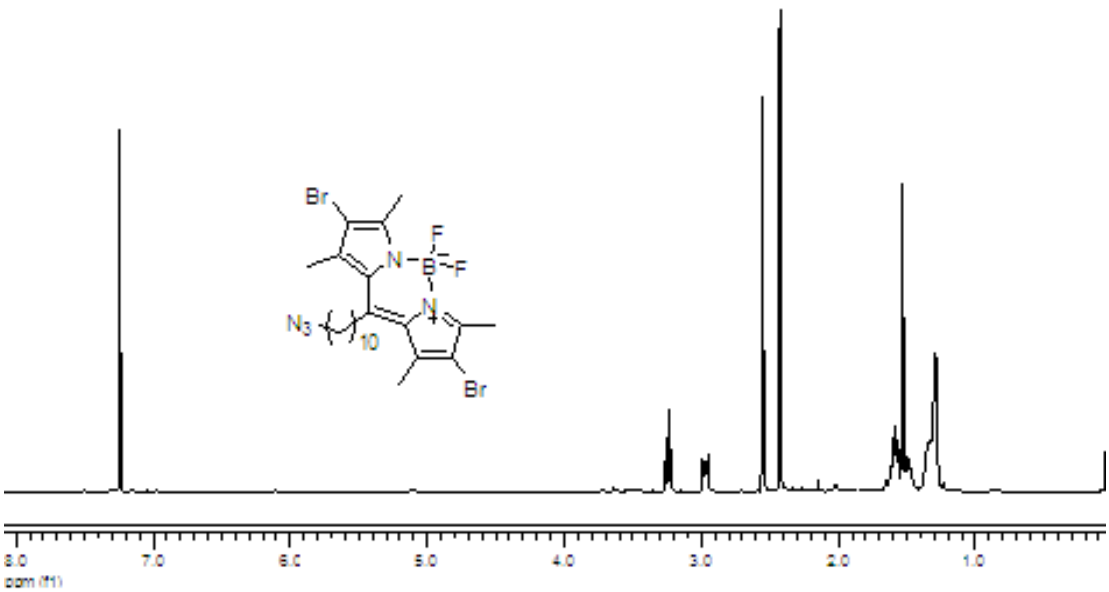

Figure 3.13. ^{1}H NMR spectra of $BODIPYBr_2(CH_2)_{10}N_3$ **(12)**

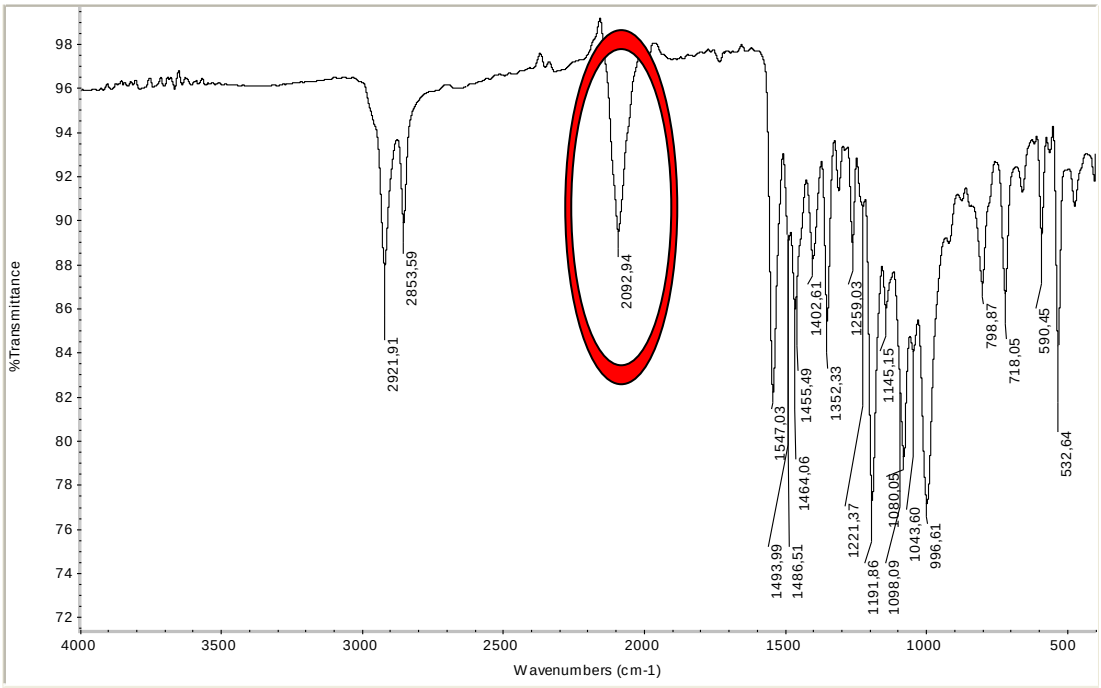

Figure 3.14. IR spectra of $BODIPYBr_2(CH_2)_{10}N_3$ **(12)**

3.2.4. $BODIPYBr_2(C_6H_5OMe)_2(CH_2)_{10}N_3$ (14) synthesis

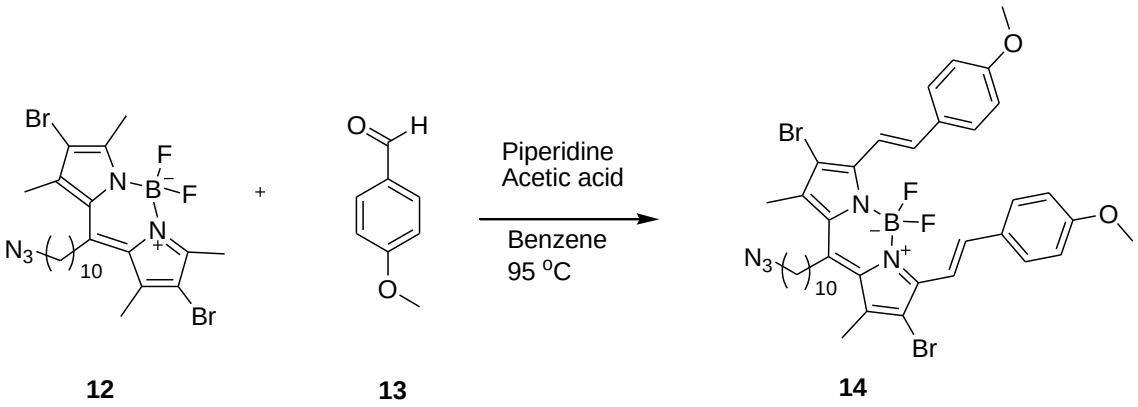

Figure 3.15. $BODIPYBr_2(C_6H_5OMe)_2(CH_2)_{10}N_3$ synthesis

$BODIPYBr_2(CH_2)_{10}N_3$, **12** and p-anisaldehyde, **13** were mixed in a solution of piperidine, acetic acid and benzene. Figure 3.15 shows the details of the reaction process [42]. By applying Dean stark apparatus, a product with a dark blue color has been obtained with a yield of 15 %. The compound was characterized by ^{1}H-NMR, ^{13}C-NMR and FTIR.

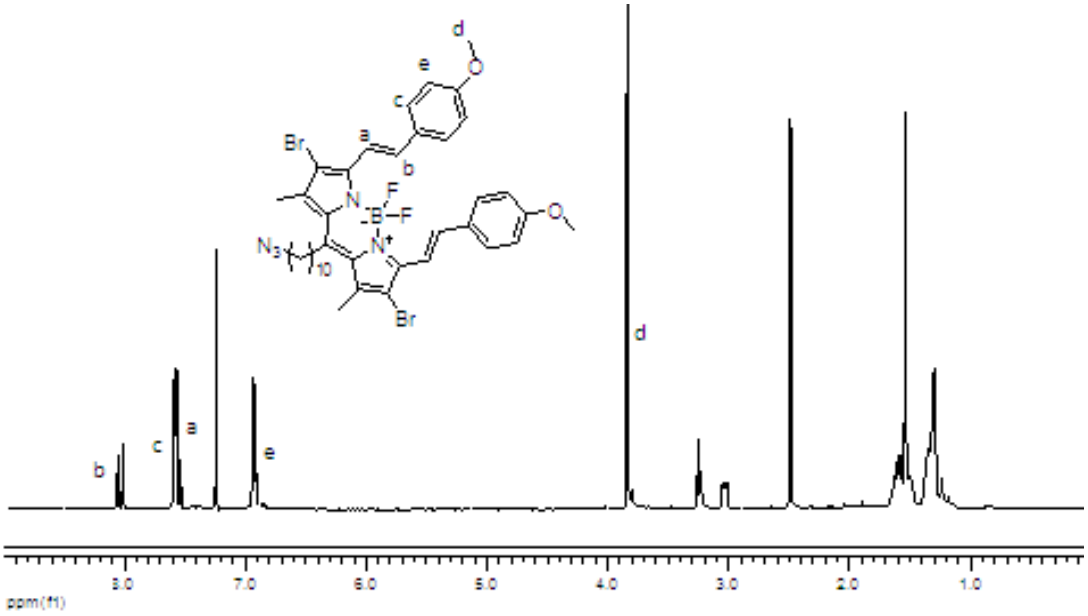

Figure 3.16. ^{1}H NMR spectra of $BODIPYBr_2(C_6H_5OMe)_2(CH_2)_{10}N_3$ **(14)**

Figure 3.16 indicates the proton NMR spectra of compound **14**. The appearance of the aromatic peaks coming from the benzene ring and the double bond proton has shown the conjugation of p- anisaldehyde to the compound **12**. The intense peak (d) at 3.84 ppm is due to the methyl protons of the methoxy group on benzene ring. Again the azide part remained intact after completion of the reaction. It was clear from the peak at 3.24 ppm of proton NMR spectrum and from the peak at 2086 cm^{-1} in the FTIR spectrum. Figure 3.17 shows the FTIR spectra comparision of reactive dyes stepwise and indicates the undamaged azide groups.

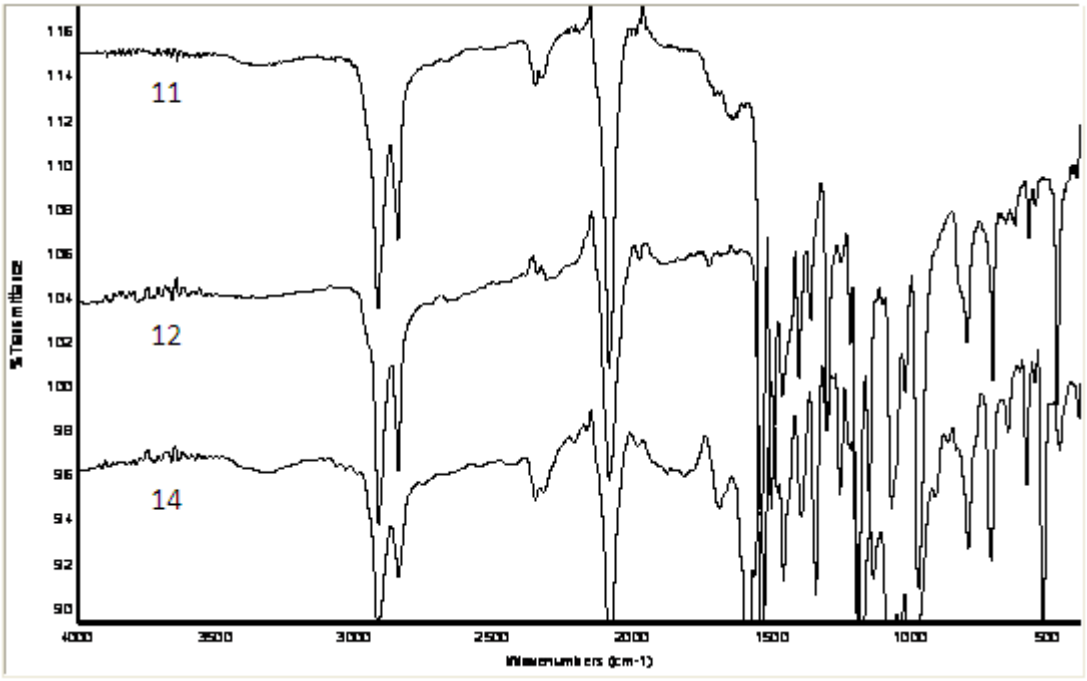

Figure 3.17. FTIR spectra comparision of the compounds **11, 12, 14**

^{13}C-NMR spectra also confirms the formation of BODIPY$Br_2(C_6H_5OMe)_2(CH_2)_{10}N_3$ and shows aromatic carbons peaks at low field and other up field carbons. Carbon NMR results shows that this new compound is unsymmetric with benzene conjugated groups.

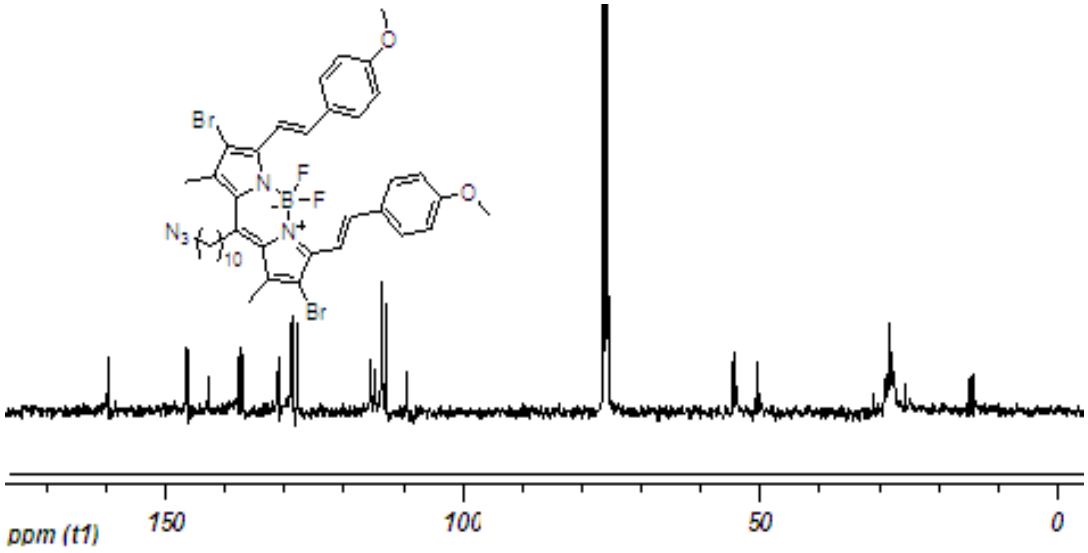

Figure 3.18. ^{13}C-NMR spectra of BODIPY$Br_2(C_6H_5OMe)_2(CH_2)_{10}N_3$ **(14)**

3.3. The Conjugation of Photosensitizer to PEG Based Copolymer

Passive accumulation in tumor tissue can be achieved via the EPR effect which is based upon structural differences between tumor tissue and healthy tissues. By active targeting, the delivery of the photosensitizer to a target tissue is through the use of specific interactions at target sites. In that study we used both high molecular weight polymer to benefit from EPR effect and specific targeting biphosphonates as active targeting unit to direct the photosensitizer to tumor in bone tissues.

The copolymerization of PEGMA and NHSMA monomers gave the biodegradable copolymer with the ester groups between the PEG chains and the polymer backbone.

3.3.1. BODIPY$Br_2(C_6H_5OMe)_2(CH_2)_{10}N_3$ Conjugation to Polymer 6

For the compound **6**, it was planned to attach BODIPY$Br_2(C_6H_5OMe)_2(CH_2)_{10}N_3$, **14** to alkyne polymer **6** with the partial conjugation via Huisgen type ‘click’ reaction. The reaction was performed in the presence of $CuSO_4 .5H_2O$ and NaAsc in $CHCl_3$: EtOH: H_2O (1: 0.75: 0.75) at room temperature. Remaining reactive alkyne groups can be used for further conjugation with chemotherapy agents which could be beneficial in term of delivering a dual modality agent.

The compound **15** was characterized by proton NMR. The presence of aromatic peaks as shown in Figure 3.20 affirms the conjugation of compound **14** to polymer **6**. By the peak at 3.34 ppm from methoxy proton of the PEG chains and the peak at 8.03 ppm coming from double bond protons behind the benzene ring (or any other aromatic peaks from dye **14**) were used to determine functionalization. The functionalization efficiency is 19.3 %. In other words, reactive dye **14** was attached to only 2.46 alkyne unit by leaving 10.24 alkyne group free for further functionalization.

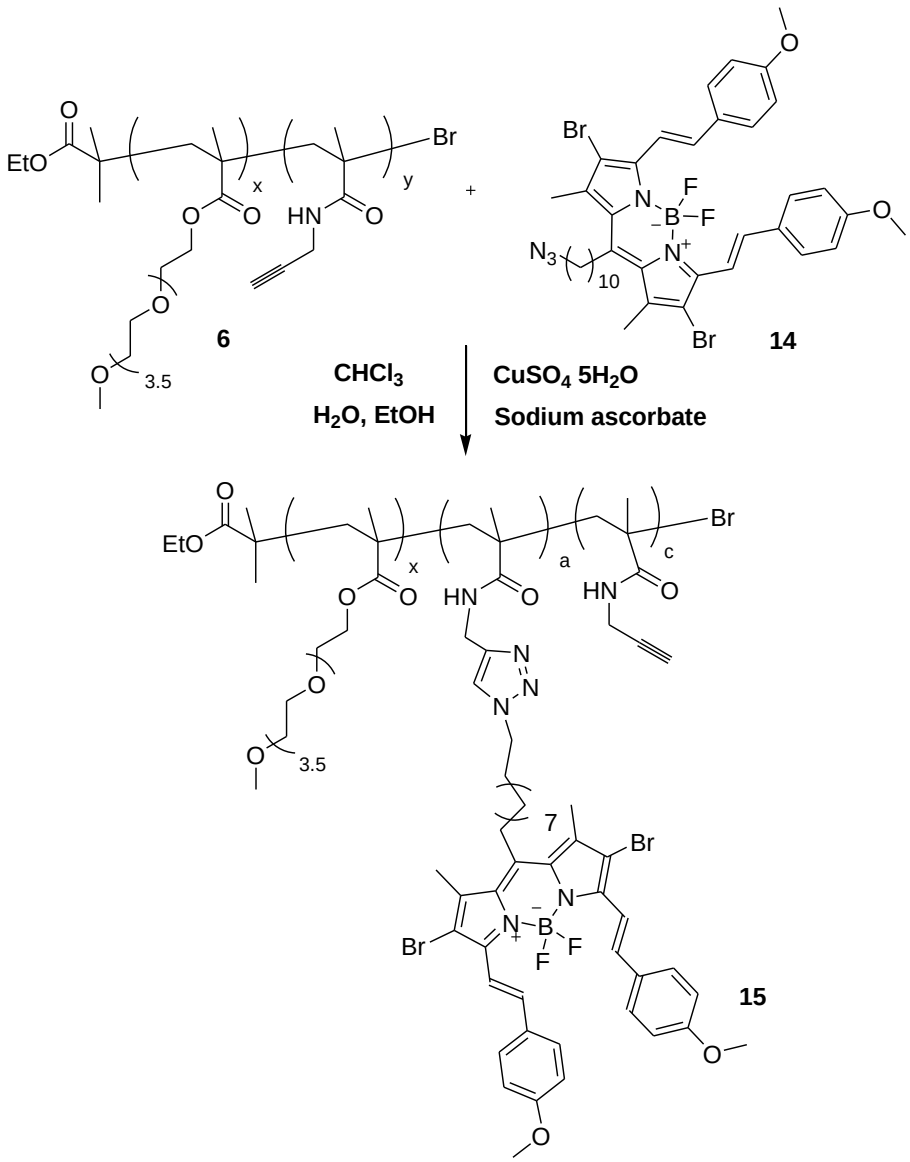

Figure 3.19. $BODIPYBr_2(C_6H_5OMe)_2(CH_2)_{10}N_3$ Conjugation to Polymer **6**

Additionally, FTIR spectra were taken for compound **15** which is shown in Figure 3.21. Infrared spectra shows the C=O strecthing at 1725 cm^{-1} and C-O strecthing at 1096 cm^{-1} coming from polymer itself. Since FTIR spectra didn't show clearly the specific peak for dye conjugation like amide streching, Ultraviolet- visible spectroscopy (UV) was used to be sure about the attachment of dye to the copolymer. Figure 3.23 demonstrates the comparison of Alkyne reactive polymer **6** with compound **15**. In red line, sharp absorbance peak at 641 nm from conjugated long range dye **14,** explains the attachment of dye to polymer **6**.

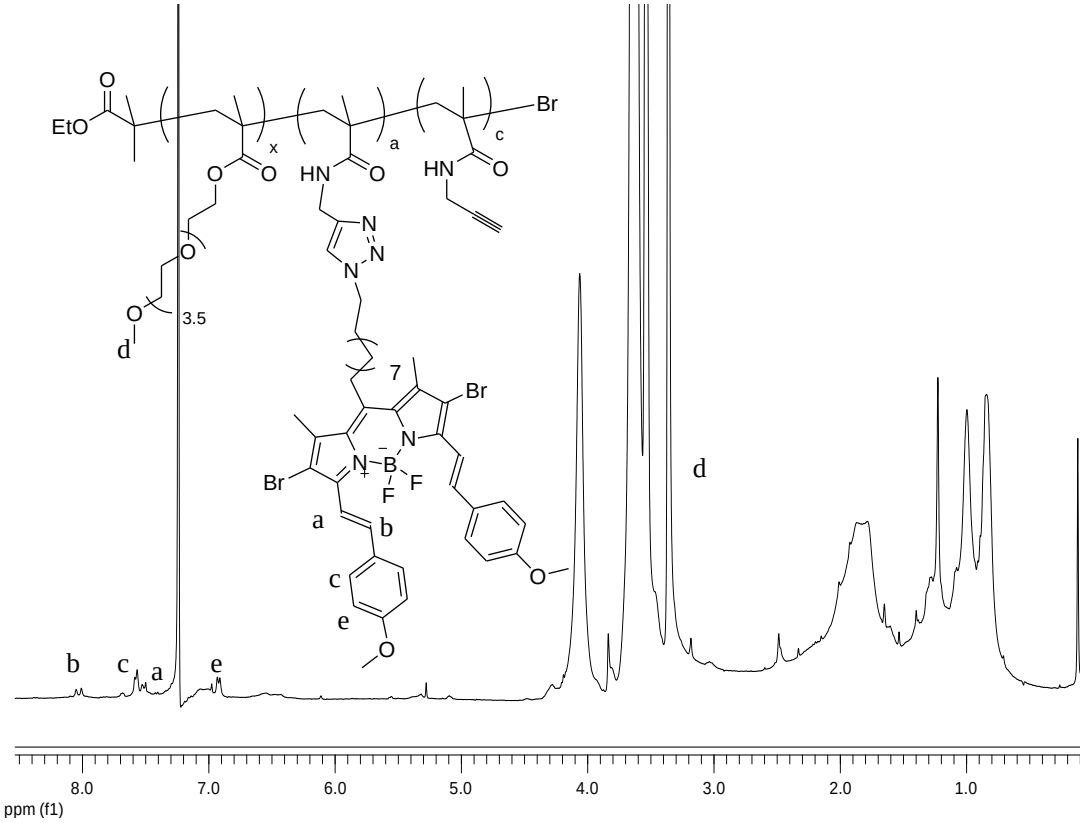

Figure 3.20 ^{1}H NMR spectra of polymer conjugate **15**

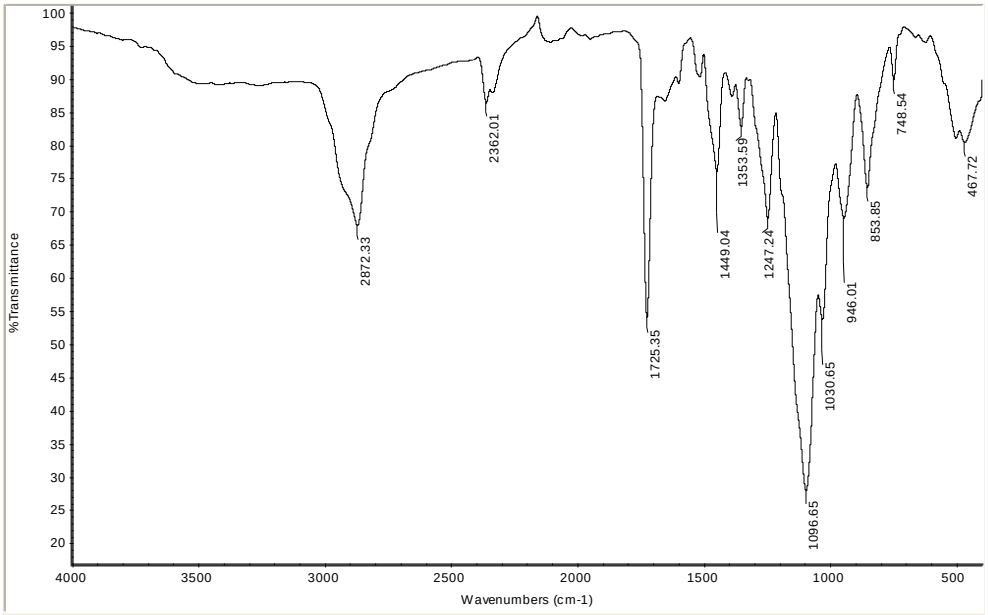

Figure 3.21 IR spectra of the polymer conjugate **15**

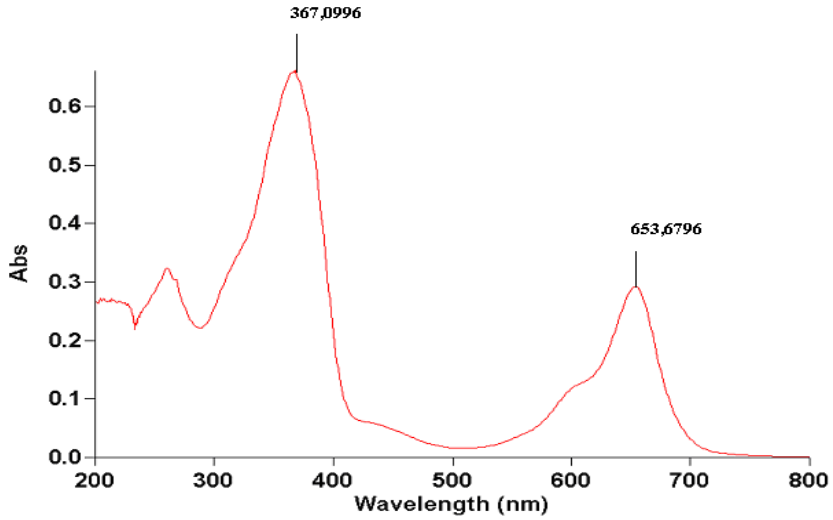

Figure 3.22 UV spectrum of $BODIPYBr_2(C_6H_5OMe)_2(CH_2)_{10}N_3$

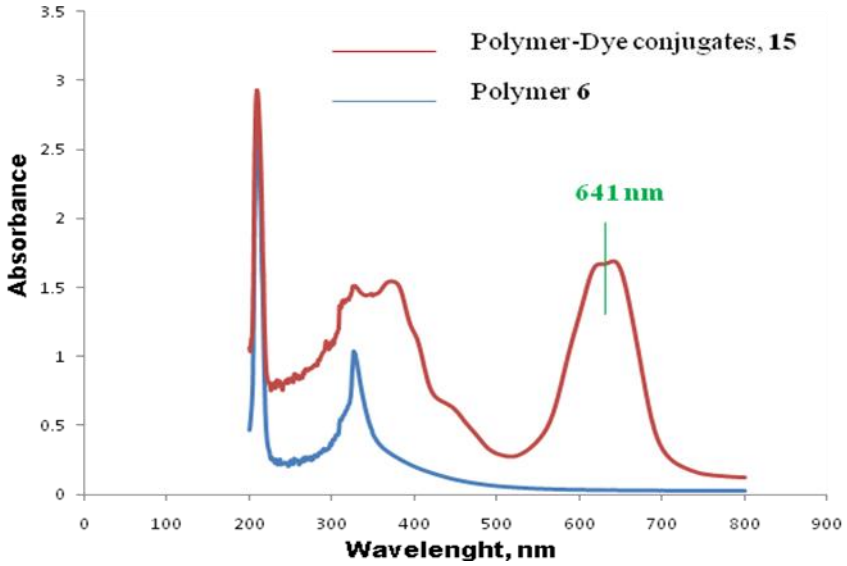

Figure 3.23 UV spectrum of polymer **6** and polymer dye conjugate **15**

3.3.1. $BODIPYBr_2(C_6H_5OMe)_2(CH_2)_{10}N_3$ Conjugation to Polymer 7

The aim was to react all of the alkyne side chains on polymer **7** with compound **14** via Huisgen type ‘click’ reaction and leave the NHS groups for further functionalization.

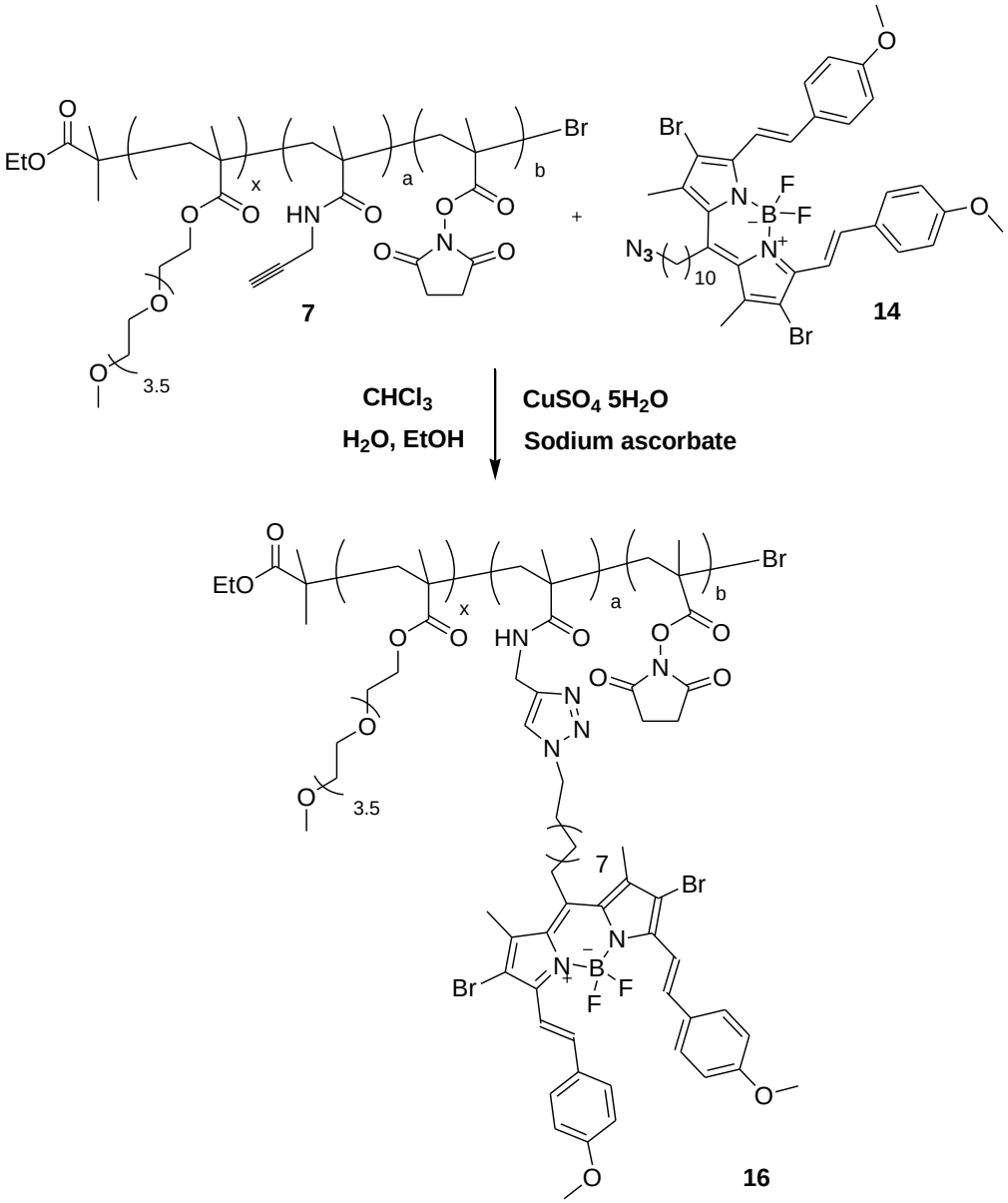

Figure 3.24. BODIPYBr$_2$(C_6H_5OMe)$_2$(CH_2)$_{10}$$N_3$ conjugation to Polymer **7**

To bind the BODIPYBr$_2$(C_6H_5OMe)$_2$(CH_2)$_{10}$$N_3$ dye to copolymer **7**, click reaction was performed in the presence of $CuSO_4$.$5H_2O$ and NaAsc in $CHCl_3$: EtOH: H_2O again. After purification, attachment of the dye to the polymer was checked by ^{1}H-NMR. The disappearance of alkyne peak at 2.26 ppm and appearance of the aromatic peaks at 8.03 ppm, 7.51 ppm and 7.41 ppm coming from dye show the conjugation of the dye to the polymer. Unfortunately, peaks from dye are not really visible and the integration of aromatic peaks of dye is not easy to understand functionalization efficieny.

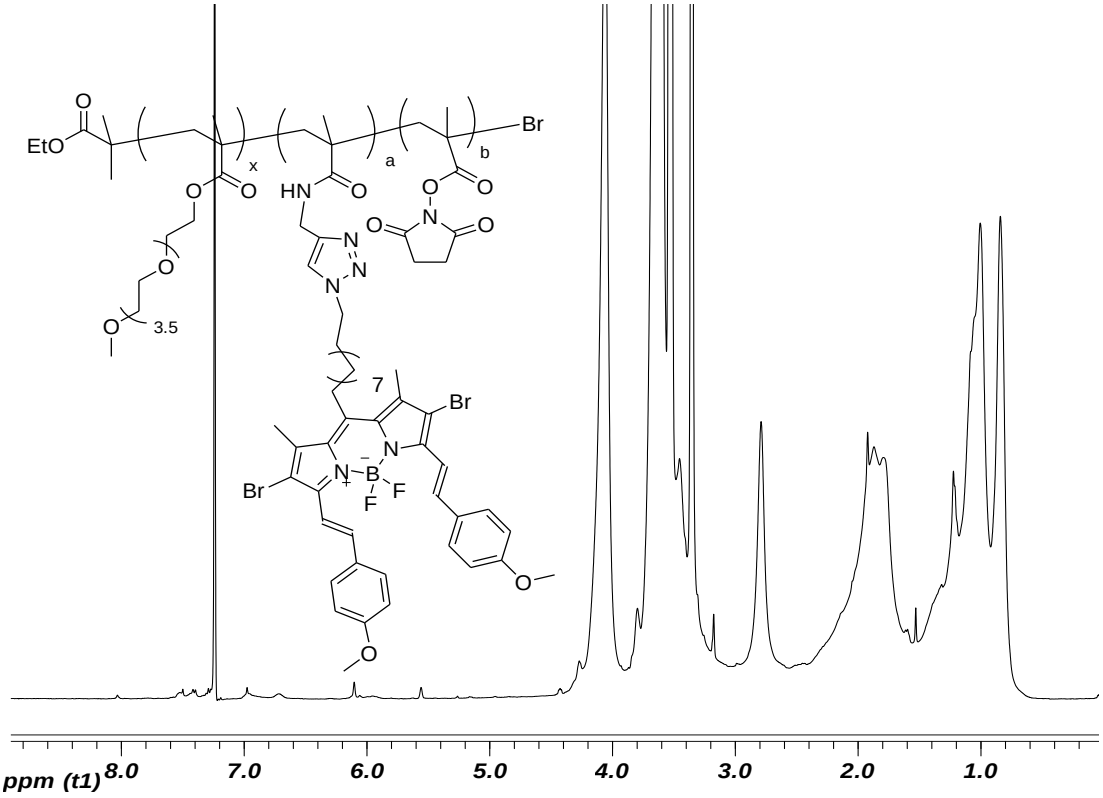

Figure 3.25. ^{1}H NMR spectra of the polymer conjugate **16**

Remaining reactive NHS groups can be used for the conjugation of alendronate biphosphonate drug to the polymer which will be a potential candidate to become a photodynamic therapy agent for active targeting to bone tissues. The problem with the characterization of polymer conjugate **16** is that the dye **14** was aimed to be attached to only 2 alkyne group on polymer **7** behind approximately 12 NHS group. However, because of high molecular weight of the polymer and unsatisfactory amount of the alkyne, it is not so easy to make integration to understand the attached amount of dye **14** to the polymer. To understand the conjugation of akyne groups we can use integration again. Aromatic peaks from dye and methoxy peak from PEG can be used to understand the consumption of all alkyne reactive groups. However because of the small amount of conjugated dye, integration didn't help to understand the conjugation proportion of alkyne groups. Additionally FTIR spectra were obtained but it didn't help for precise characterization like previous compound **15**. Then UV absorbance analysis was applied. UV analysis was done for both polymer **7** and polymer dye conjugate **16** to see the difference in absorbance range. The sharp absorbance peak at 646 nm appears after the conjugation of dye to polymer **7** via click reaction that means the reaction worked.

Furthermore, the peaks at 6.10 ppm and 5.56 ppm result from the elimination of HBr from the end of polymer backbone.

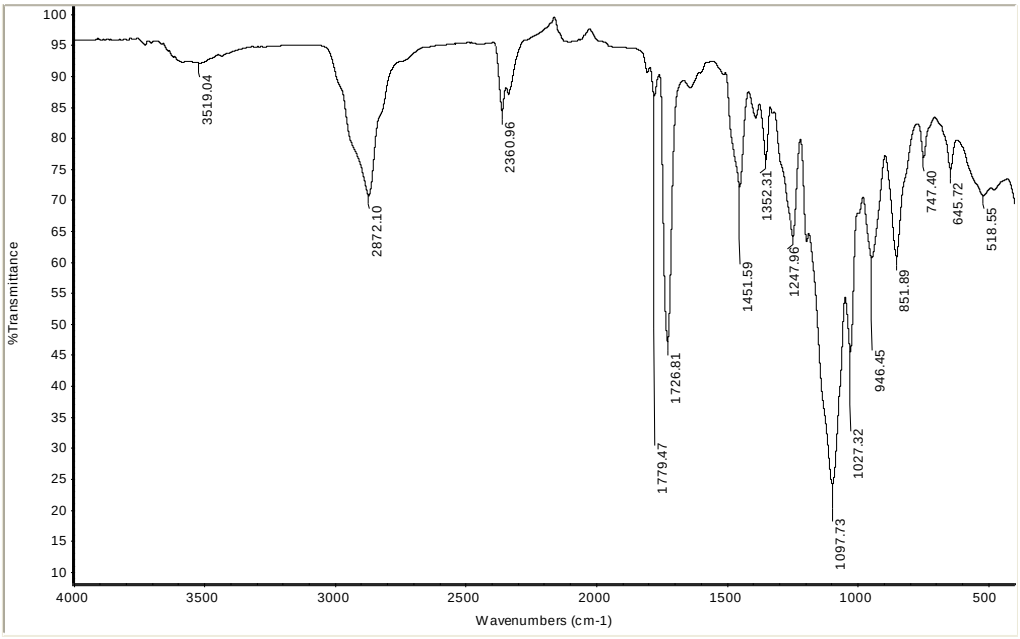

Figure 3.26. IR spectra of the polymer conjugate **16**

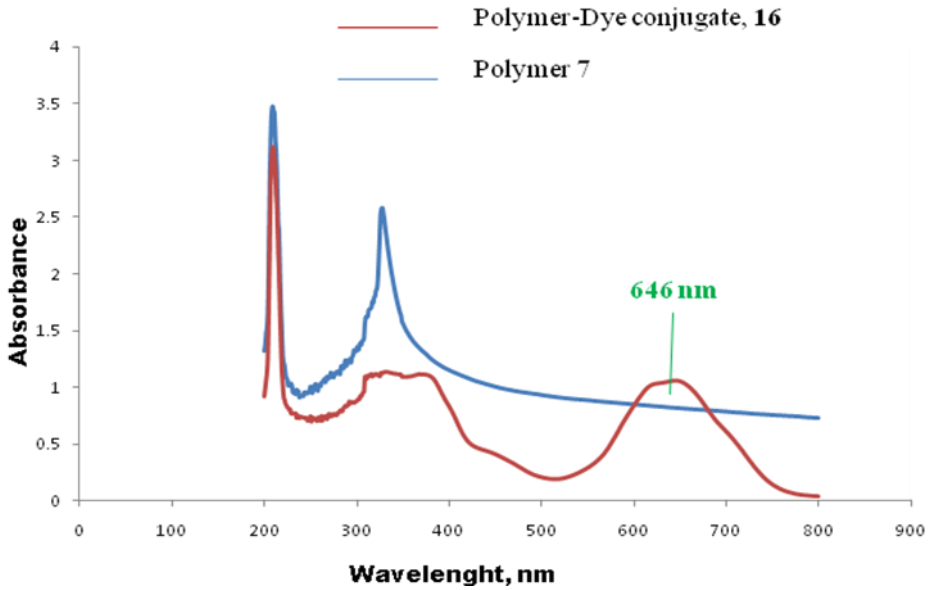

Figure 3.27. UV specrum of polymer **7** and polymer dye conjugate **16**

3.4. The Attachment of Targeting Moiety to Polymer

3.4.1. The conjugation of Alendronate amine (ALD) to polymer 16

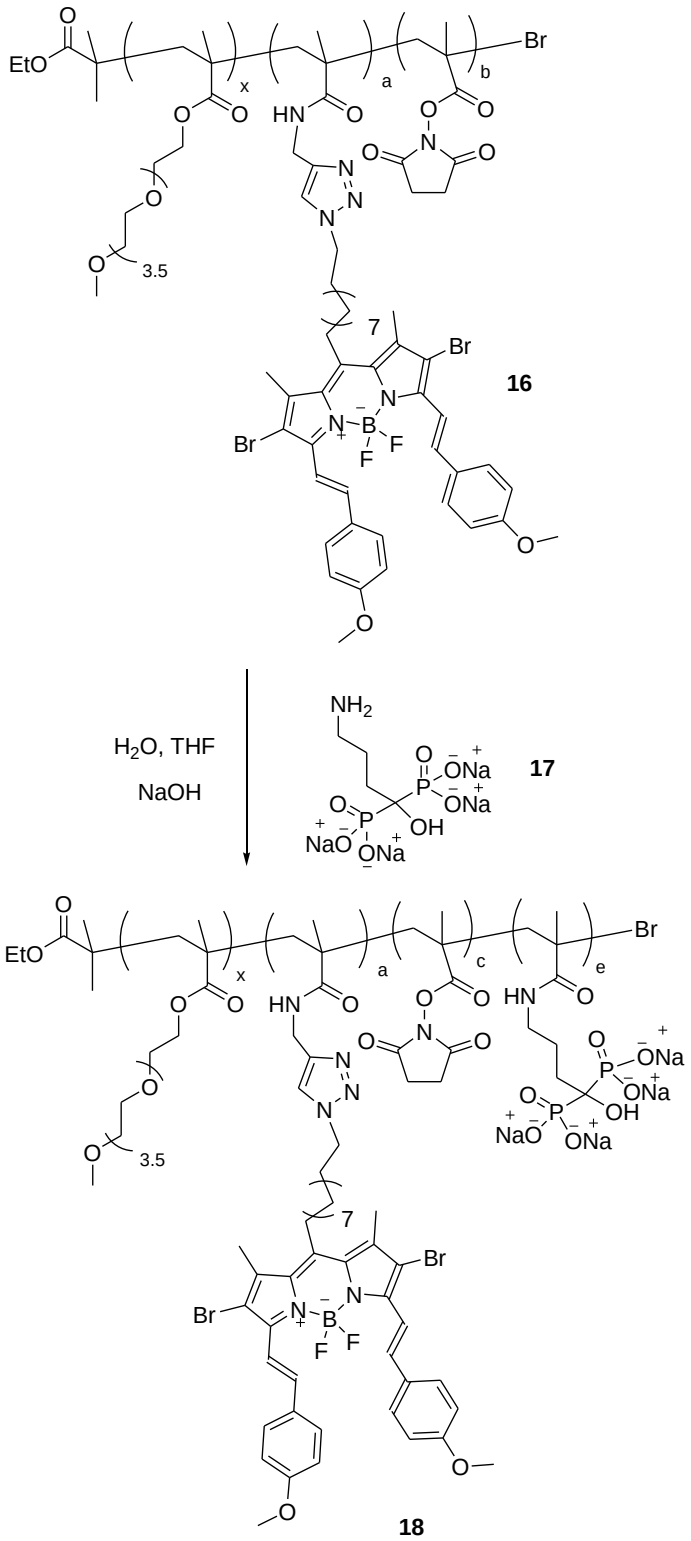

Figure 3.28. The synthesis of compound **18**

To direct the polymer-photosensitizer conjugate specifically to tumor in bone tissue, Alendronate amine as a targeting group was attached to the polymer dye conjugate, **16**. Due to affinity of bisphosphonate alendronate for HAP in bone matrix, polymer-photosensitizer conjugate preferably can be localized on bone sites in the body. For the synthesis, NHS functionalized $BODIPYBr_2(C_6H_5OMe)_2(CH_2)_{10}N_3$ photosensitizer conjugated polymer **16** was dissolved in THF and added to alendronate amine, **17** solution in water. The pH of mixing solution was arranged by addition of NaOH during reaction. By leaving of NHS group, alendronate amine has been conjugated to polymer backbone via amidation reaction.

Compound **(18)** was characterized by ^{1}H NMR in D_2O. The appearance of new peaks at 2.62 - 2.53 ppm has showed the conjugation of targeting bisphosphonate moiety to polymer **16.** Further purification and characterization via ^{31}P NMR spectrum is necessary to unequivocally ascertain the attachment of alendronate to the polymer construct. In proton NMR spectrum, there is an extra peak at 5.35 ppm due to an unknown impurity.

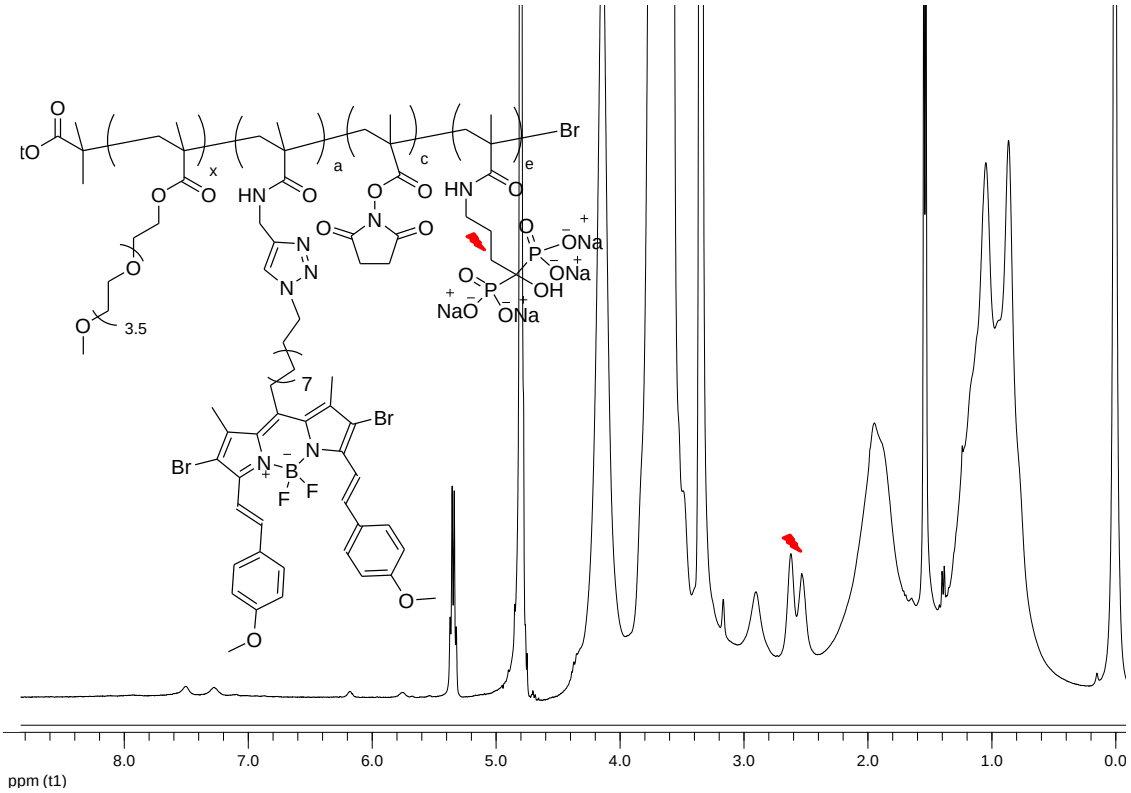

Figure 3.29. ^{1}H NMR spectra of polymer conjugate **18**

In addition to NMR, the compound **18** was also characterized by FTIR. Figure 3.30 shows the infrared spectra of it. Unfortunately, both ^{1}H NMR and FTIR spectrums didn't provide precise identification for the attachment of alendronate amine. Even though we observed some new peaks and decreased intensity of NHS in NMR, the amide formation by attacking of amine group to carbonyl carbon of NHS was not clear. However the integration of remain reactive NHS groups showed that the ratio of NHS to PEG reduced with a 45 % after the reaction with respect to polymer **16**.

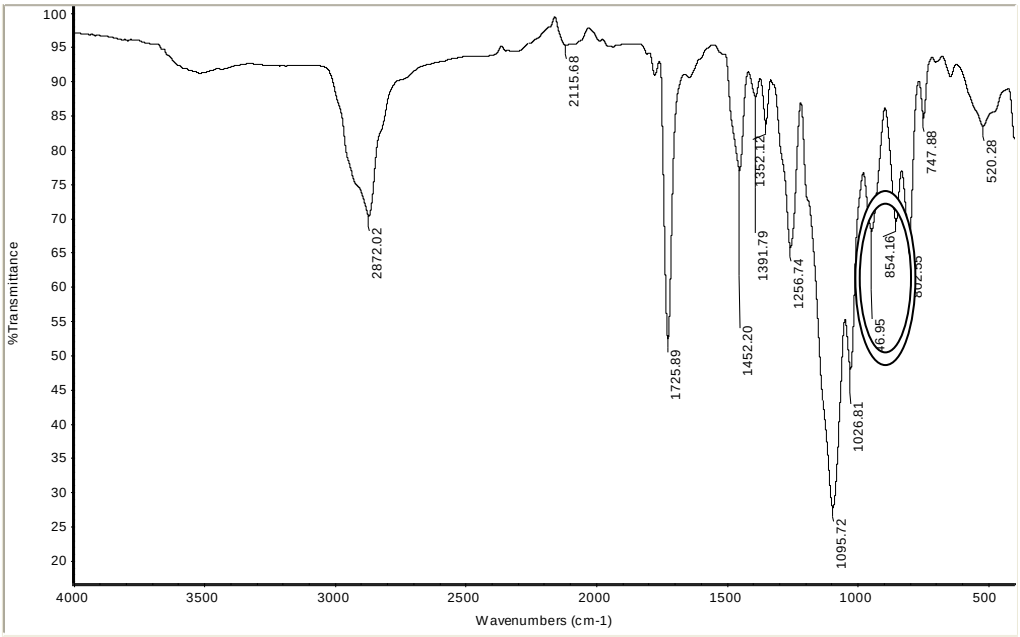

Figure 3.30. IR spectra of polymer conjugate **18**

In FTIR spectrum, due to presence of many carbonyl groups on copolymer, precise identification of the amide linkage wasn't possible but appearance of some new peaks coming from alendronate structure has verified the conjugation of alendronate amine. The peak at 802 cm^{-1} due to P-O-C strecthing from alendronate amine has shown the conjugation of alendronate to polymer **16**.

4. EXPERIMENTAL PART

4.1. Materials and Methods

All chemicals were received from company (Merck, Aldrich, Alfa Aesar, and Riedel de Haen). Dry solvents (CH_2Cl_2, THF, and Toluene) were obtained from ScimatCo Purification System. DMF was dried over molecular sieves. Column chromatography was performed using silicagel-60 (43-60 nm). Thin layer chromatography was applied using silica gel plates (Kiesel gel 60 F254, 0.2mm, Merck). Plates were viewed under 254 and 360 nm UV lamp. Infrared spectroscopy was carried out on Thermo Scientific Nicolet 380 FT-IR spectrophotometer. ^{1}H NMR (operating at 400 MHz) was recorded on Varian Mercury-MX in $CDCl_3$ and D_2O as solvent at the Advanced Technologies Research and Development Center at Boğaziçi University.

Poly(ethylene glycol) methyl ether metacrylate (Mw = 300) (PEGMA, 99%, Aldrich) and *N, N, N', N'', N''*-pentamethyldiethylenetriamine (PMDETA, Aldrich) were passed through basic alumina column to get rid of inhibitor inside them. The polymers were characterized with ^{1}H NMR spectroscopy (Varian 400 MHz and and Bruker 260 MHz), and Fourier transform infrared (FTIR) spectroscopy (Perkin Elmer 1600 Series). The molecular weights were determined by gel permeation chromatography (GPC) analysis using a Viscotek GPCmax VE-2001 analysis system. PLgel (length/ID 300 mm 3 7.5 mm, 5 lm particle size) Mixed-C column was caliberated with polystyrene standards. The refractive index detector was used via THF as elutent at a flow rate of 1 mL/min.

4.2. Synthesis of Reactive Polymers

4.2.1. NHS funtionalized reactive polymer synthesis (4)

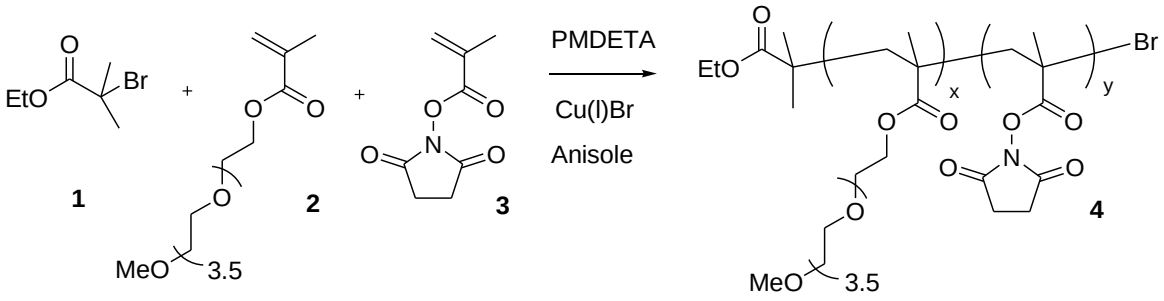

Figure 4.1 The synthesis of NHS functionalized copolymer

Cu(I)Br (11.7 mg, 0.082 mmol) and NHSMA (0.36 g, 1.96 mmol) was taken in a 10 mL round bottom flask equipped with a septum, magnetic bar and gas inlet/outlet. The flask was degassed with nitrogen gas for 10 min. Then, degassed PEGMA (3.44 mL, 12.04 mmol) and *N,N,N',N''*-pentamethyl diethylene triamine (PMDETA) (17.1μL, 0.082 mmol) were added and stirred for 5 more minutes. This reaction mixture was diluted with degassed anisole (6 mL) and it was stirred for another 5 minutes. Then the flask was immersed into a preheated oil bath at 80 °C. To this homogeneous mixture, ethyl 2-bromoisobuthyrate (11.775 μL, 0.082 mmol) was added fast. The polymerization was carried out at the same temperature under argon atmosphere for 1h with a magnetic bar in the reaction flask stirred the reaction mixture. After that, the reaction was stopped and the polymer solution was precipitated in cold diethyl ether for 2 times. After decanting ether solution, the polymerization mixture was diluted with THF and passed through a neutral alumina column to remove the catalyst, and precipitated in hexane. The polymer was concentrated and dried for 24 h in a vacuum oven at 25 °C. $[M]_0/[I]_0$= 171; $[I]_0$:[CuBr]:[PMDETA]=1:1;1, conversion = 53 %. $M_{n,GPC}$= 23K, M_w/M_n= 1.39, relative to PS. ^{1}H NMR ($CDCl_3$, δ, ppm); 4.05 (br s, 4H, COO-CH_2), 3.61 (br s, 14H, -CH_2CH_2O-), 3.34 (s, 3H, O-CH_3), 2.77 (br s, 4H, CH_2CH_2C=ON), 1.90-0.83 (m, 6H, CH_2 and CH_3 along polymer backbone).

4.2.2. Alkyne Funtionalized Reactive Polymer Synthesis (6)

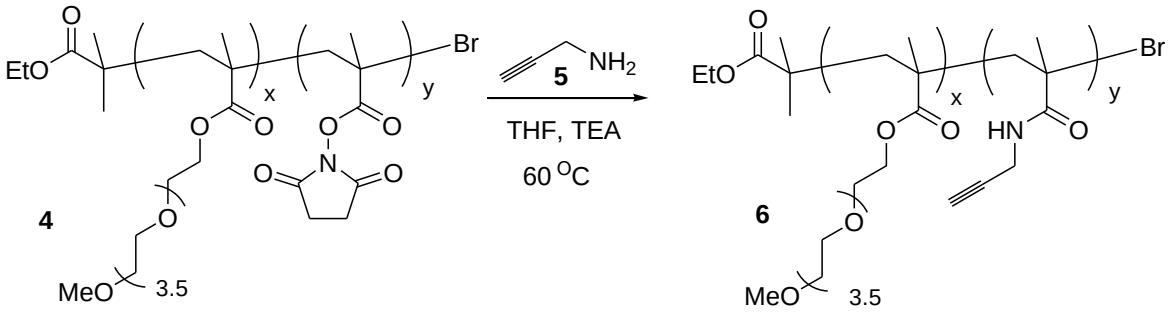

Figure 4.2. Synthesis of Alkyne functionalized copolymer

Polymer **4** (1.91 g, 1.075 mmol (total NHS)), propargyl amine, **5** (0.68 mL, 0.011 mol) and TEA (1.5 mL, 0.011 mol) were put in a round bottom flask and mixture was dissolved in dry THF (7 mL). The flask was degassed with nitrogen gas for 15 min. to remove air. The solution was refluxed on stirrer at 60 ^{o}C for 24h. Then polymer was concentrated in *vacuo* and purified by washing or precipitating in diethyl ether. Polymer was dried in vacuum for 24 h at 25 °C. ^{1}H NMR ($CDCl_3$, δ, ppm); 4.09 (br s, 4H, COO-CH_2), 3.65 (br s, 14H, -CH_2CH_2O-), 3.37 (s, 3H, O-CH_3), 2.29 (br s, 1H, ≡CH), 1.72-0.86 (m, 6H, CH_2 and CH_3 along polymer backbone).

4.2.3. Alkyne and NHS Funtionalized Reactive Polymer Synthesis (7)

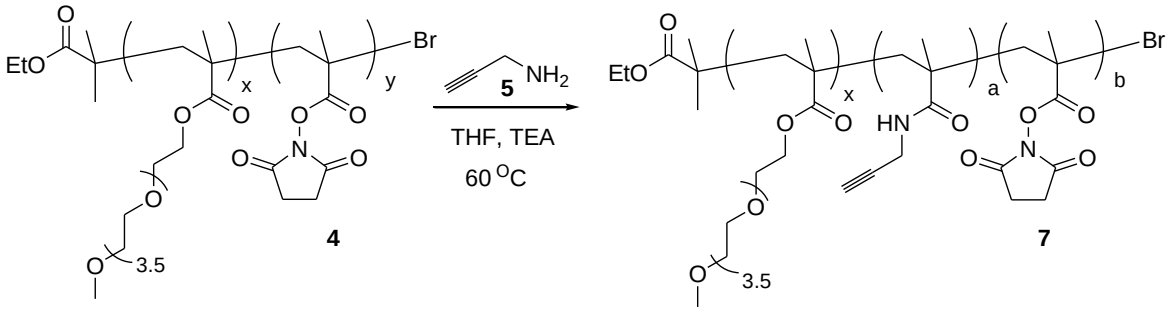

Figure 4.3. Synthesis of Alkyne and NHS functionalized copolymer

Polymer **4** (0.62 g, 0,389 mmol (total NHS)), propargyl amine, **5** (25 μL, 0,389 mmol) and TEA (54.15 μL, 0,389 mmol) were put in a round bottom flask and mixture was dissolved in dry THF (5 mL). The flask was degassed with nitrogen gas for 15 min. to remove all oxygen. Then solution was refluxed on stirrer at 60 ^{o}C for 24h. The polymer

was concentrated in *vacuo* and purified by washing or precipitating in diethyl ether. Polymer was dried in vacuum for 24 h at 25 °C. ^{1}H NMR ($CDCl_3$, δ, ppm); 4.05 (br s, 4H, COO-C*H*$_2$), 3.62 (br s, 14H, -CH_2CH_2O-), 3.34 (s, 3H, O-C*H*$_3$), 2.78 (br s, 4H, CH_2CH_2C=ON), 2.27 (br s, 1H, ≡CH), 1.91-0.83 (m, 6H, CH_2 and CH_3 along polymer backbone).

4.3. Synthesis of Reactive Dye

4.3.1. The Synthesis of BODIPY$(CH_2)_{10}$Br (10)

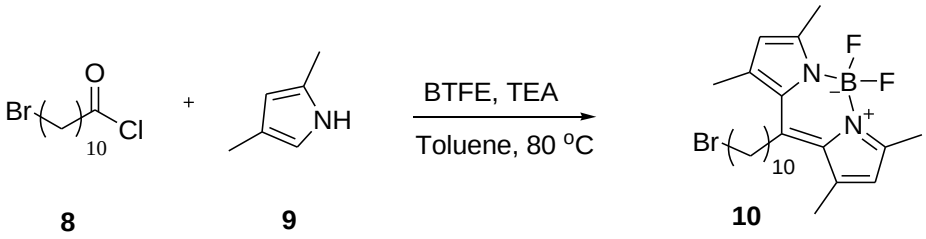

8 **9** **10**

Figure 4.4. BODIPY$(CH_2)_{10}$Br synthesis

To a solution of dry CH_2Cl_2 (40 mL) and dry DMF (2 drop), 11-bromo undecanoic acid (2.0 g, 7.5 mmol) and oxalyl chloride (0.69 mL, 7.9 mmol) were added. The mixture was stirred at room temperature for 1 hour and then residue was concentrated in *vacuo* to remove excess oxalyl chloride.

The compound obtained was dissolved in CH_2Cl_2 (50 mL) and 2,4-dimethylpyrrole (1.54 mL, 15 mmol) was added drop by drop. Mixture was refluxed for 3 hours at 40 °C and concentrated in *vacuo*. The solution was kept in freezer (-20 °C) overnight after adding hexane (200 mL) to resulting solution and mixture was decanted. The resulting precipitates was dissolved in dry toluene (75 mL) and solution was heated up to 80 °C. At this temperature TEA (1.04 mL, 7.5 mmol) was slowly added and mixture was stirred for 10 minutes. Then solution was treated with boron trifluoride dimethyl etherate (BTFE) (1 mL, 7.8 mmol) and stirred for 30 min at 80 °C. After cooling, red solution was washed with saturated NaCl solution (3 x 50 mL), dried by sodium sulfate and concentrated in *vacuo*. Oil like compound **10** was purifed by column chromatography with CH_2Cl_2:Hexane

(25:75), to give 1.48 g compound (43 % yield) . ^{1}H NMR ($CDCl_3$, δ, ppm); 6.03 (s, 2H), 3.38 (t, 2H, *J* = 6.8 Hz), 2.93- 2.89 (m, 2H), 2.49 (s, 6H), 2.39 (s, 6H), 1.79 - 1.86 (m, 2H), 1.58 - 1.63 (m, 2H), 1.43 - 1.38 (overlapping multiplets, 4H), 1.28- 1.32 (m, 8H).

4.3.2. The Synthesis of BODIPY$(CH_2)_{10}N_3$ (11)

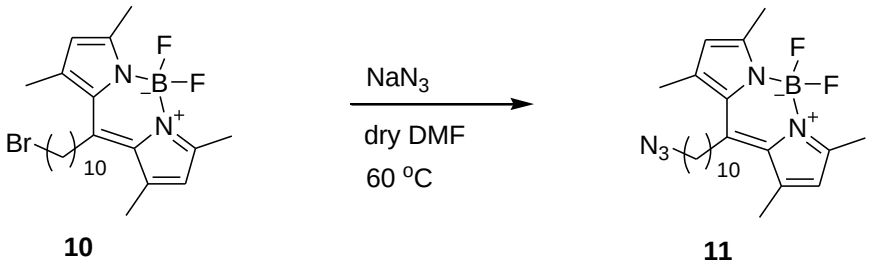

10 **11**

Figure 4.5. BODIPY$(CH_2)_{10}N_3$ synthesis

Bodipy$(CH_2)_{10}$Br (0.2 g, 0.428 mmol) and NaN_3 (0.278 g, 4.28 mmol) were dissolved in dry DMF (5 mL). Solution was stirred at 60 ^{o}C for 48 hours. After reaction completion, solution was diluted with water (50mL) followed by extracting with hegzane and ethyl acetate (50:50). Combined organic layers was dried with Na_2SO_4 and concentrated in *vacuo*. The resulting residue was purified via column chromatography (90:10, Hexane: CH_2Cl_2). Pure product **11** was obtained (77 % yield). ^{1}H NMR ($CDCl_3$, δ, ppm); 6.03 (s, 2H), 3.24 (t, 2H, *J* = 6.8 Hz), 2.92 - 2.88 (m, 2H), 2.49 (s, 6H), 2.38 (s, 6H), 1.62 - 1.55 (m, 4H), 1.49 - 1.42 (m, 2H), 1.33 - 1.28 (m, 10H). FTIR cm^{-1} : 2091.

4.3.3. The Synthesis of BODIPY$Br_2(CH_2)_{10}N_3$ (12)

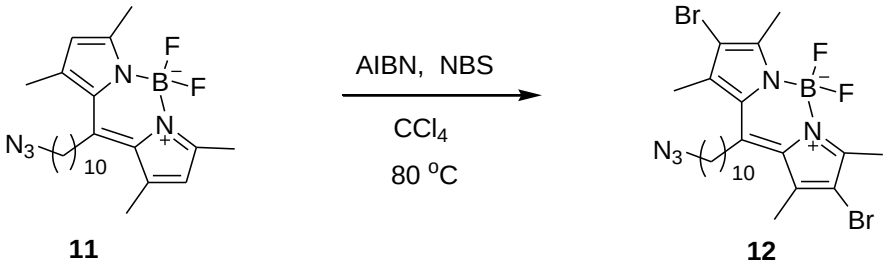

11 **12**

Figure 4.6. BODIPY$Br_2(CH_2)_{10}N_3$ synthesis

Bodipy$(CH_2)_{10}N_3$ **(11)** (0.2 g, 0.465 mmol), N-bromo succinimide (NBS) (0.166 g, 0.932 mmol) and Azobisisobutyronitrile (AIBN) (0.153 g, 0.932 mmol) were taken in a round bottom flask and dissolved in carbon tetrachloride (CCl_4). Mixture was refluxed at 80 ^oC for 40 min. with a stir bar. Resulting residue was concentrated and purified via column chromatography (100 % Hexane) to give product **12** with a yield of 75 %. ^1H NMR ($CDCl_3$, δ, ppm); 3.24 (t, 2H, *J* = 6.8 Hz), 2.94 - 2.99 (m, 2H), 2.55 (s, 6H), 2.43 (s, 6H), 1.56 - 1.62 (m, 4H), 1.44 - 1.50 (m, 2H), 1.29 - 1.35 (m, 10H). FTIR cm^{-1} : 2092.

4.3.4. The Synthesis of BODIPY$Br_2(C_6H_5OMe)_2(CH_2)_{10}N_3$ (14)

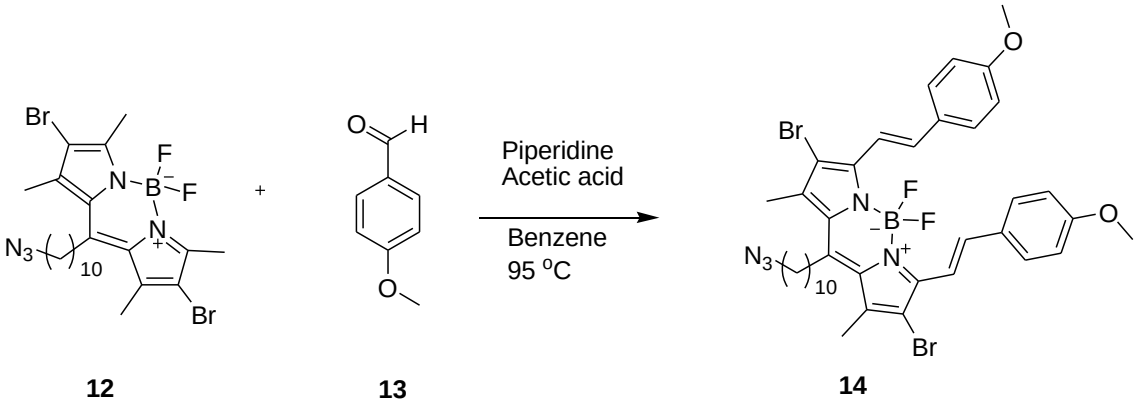

12 **13** **14**

Figure 4.7. BODIPY$Br_2(C_6H_5OMe)_2(CH_2)_{10}N_3$ synthesis

To a solution of piperidine (0.7 mL, 7 mmol) and acetic acid (0.7 mL, 7 mmol) in benzene (50 mL), Bodipy$Br_2(CH_2)_{10}N_3$ **(12)** (0.125 g, 0.213 mmol) and p-anisaldehyde (68 µL, 0.53 mmol) were added. By using Dean stark apparatus, the mixture was refluxed at 95 ^oC for 48 h. After evaporation of benzene, the resulting residue was dissolved in CH_2Cl_2, extracted with water (3 x 50 mL), dried with Na_2SO_4 and concentrated in *vacuo*. The product was purified by column chromatography with CH_2Cl_2:Hexane (40:60). The reactive dye as 25 mg was obtained with a 15 % yield. ^1H NMR ($CDCl_3$, δ, ppm); 8.03 (d, 2H, *J* = 7.6 Hz), 7.54 - 7.59 (m, 6H), 6.93 (d, 4H, *J* = 4.4 Hz), 3.84 (s, 6H), 3.24 (t, 2H, *J* = 6.8 Hz), 3.01 - 3.06 (m, 2H), 2.49 (s, 6H), 1.59 - 1.62 (m, 4H), 1.48 - 1.52 (m, 2H), 1.30 - 1.35 (m, 10H). ^{13}C-NMR ($CDCl_3$, ppm); 159.6, 146.4, 142.8, 137.7, 137.2, 131.0, 128.8, 128.5, 127.8, 115.5, 113.5, 113.0, 109.4, 54.5, 54.2, 50.5, 28.4, 14.7, 14.2. FTIR cm^{-1} : 2089.

4.4. Polymer Dye Conjugation

4.4.1. The Conjugation of $BODIPYBr_2(C_6H_5OMe)_2(CH_2)_{10}N_3$ 14 to Polymer 6

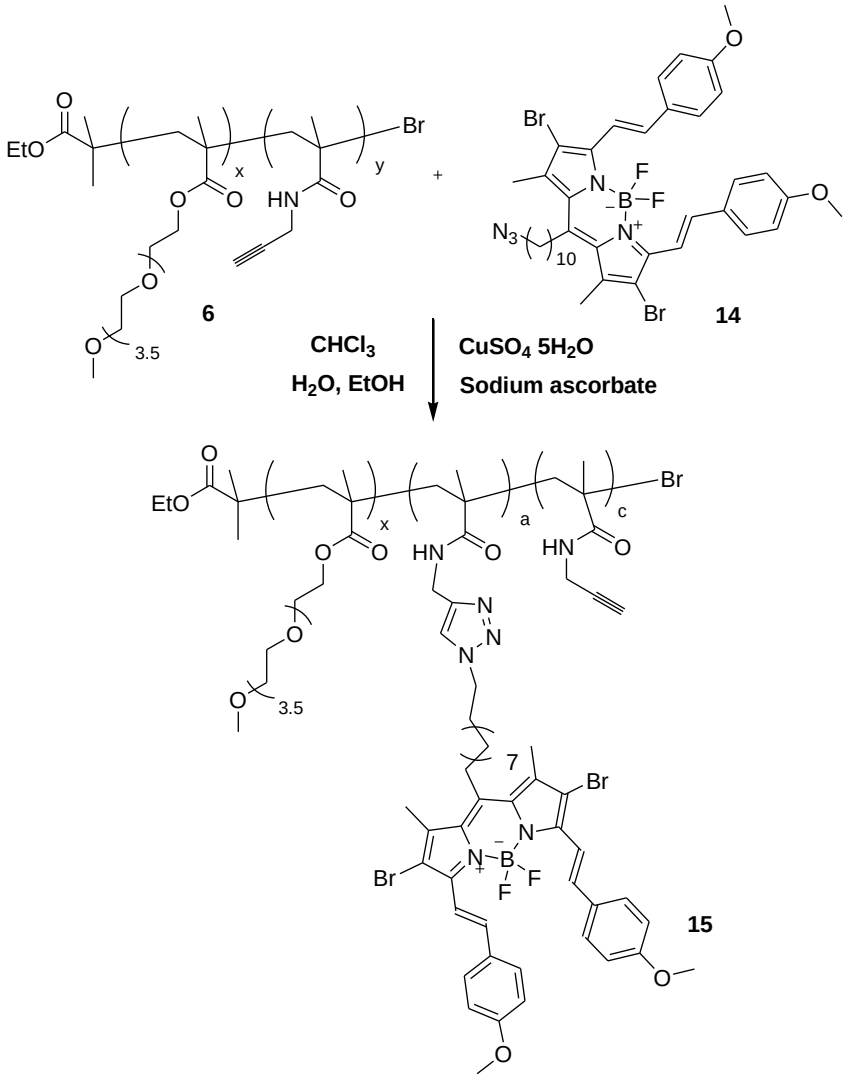

Figure 4.8. $BODIPYBr_2(C_6H_5OMe)_2(CH_2)_{10}N_3$ conjugation to Polymer **6**

A solution of the compound **14** (0.0098 mmol, 8 mg), the polymer **6** (0.0563 mmol, 100 mg), sodium ascorbate (0.00532 mmol, 1.05 mg), and $CuSO_4$ (0.0027 mmol, 0.7 mg) in a mixture of $CHCl_3$, EtOH and H_2O (1: 0.7: 0.8) (2.5 mL) was stirred at room temperature for 72 h. After voparization of organic solvents, water was lyophilized and polymer residue in THF was passed through aluminium oxide to ged rid of $CuSO_4$ and sodium ascorbate. After removing THF in *vacuo,* polymer was washed via cold diethyl

ether for many times until not seeing free dye in TLC almost. Then the same polymer was purified via sephhadex G-25 with H_2O as a mobile phase, to be sure of cleaning of the polymer from free unbound dye. Then polymer was lyophilized again and ^{1}H-NMR spectra of the polymer was taken in $CDCl_3$. ^{1}H NMR ($CDCl_3$, δ, ppm); 8.03 (d, 2H, *J* = 8.0 Hz), 7.58 (d, 4H, *J* = 4.0 Hz), 7.51 (d, 2H, *J* = 5.6 Hz), 6.92 (d, 4H, *J* = 4.0 Hz), 4.06 (br s, 4H, COO-CH_2), 3.64 (br s, 14H, -CH_2CH_2O-), 3.36 (s, 3H, O-CH_3), 2.48 (s, 6H), 2.28 - 0.84 (m, 6H, CH_2 and CH_3 along polymer backbone and CH_2 along alkane chain of dye, br s, 1H, ≡CH), (some peaks from dye overlaps with polymer peaks between 4.06 - 3.36 ppm).

4.4.2. The Conjugation of $BODIPYBr_2(C_6H_5OMe)_2(CH_2)_{10}N_3$ 14 to Polymer 7

The compound **14** (16 mg, 0.0194 mmol), the polymer **7** (0.2 g, 0.1256 mmol), sodium ascorbate (1.92 mg, 0.0097 mmol), and CuSO4 (1.2 mg, 0.00485 mmol) were disolved in a mixture of $CHCl_3$, EtOH and H_2O (1:0.75:0.75, 2.5 mL). The mixture was stirred at room temperature for 72 h. After voparization of organic solvents, water was lyophilized and polymer residue in THF was passed through aluminium oxide to ged rid of $CuSO_4$ and sodium ascorbate. After removing THF in *vacuo* polymer was washed via cold diethyl ether for many times until not seeing free dye in TLC almost. Furthermore, the polymer was purified also via sephhadex G-25 with H_2O as a mobile phase, to be sure of the cleaning of the polymer from unbound dye. Then polymer was lyophilized and ^{1}H-NMR spectra of the polymer was taken in $CDCl_3$. ^{1}H NMR ($CDCl_3$, δ, ppm); 8.03 (broad singlet, 2H), 7.51 (broad doublet, 4H, *J* = 4.2 Hz), 7.41 (d, 2H, *J* = 3.8 Hz), 6.97 (broad singlet, 4H), 4.06 (br s, 4H, COO-CH_2), 3.63 (br s, 14H, -CH_2CH_2O-), 3.35 (s, 3H, O-CH_3), 2.79 (br s, 4H, CH_2CH_2C=ON), 2.04 - 0.84 (m, 6H, CH_2 and CH_3 along polymer backbone and CH_2 along alkane chain of dye),(some peaks from dye overlaps with polymer peaks between 4.06 - 3.36 ppm).

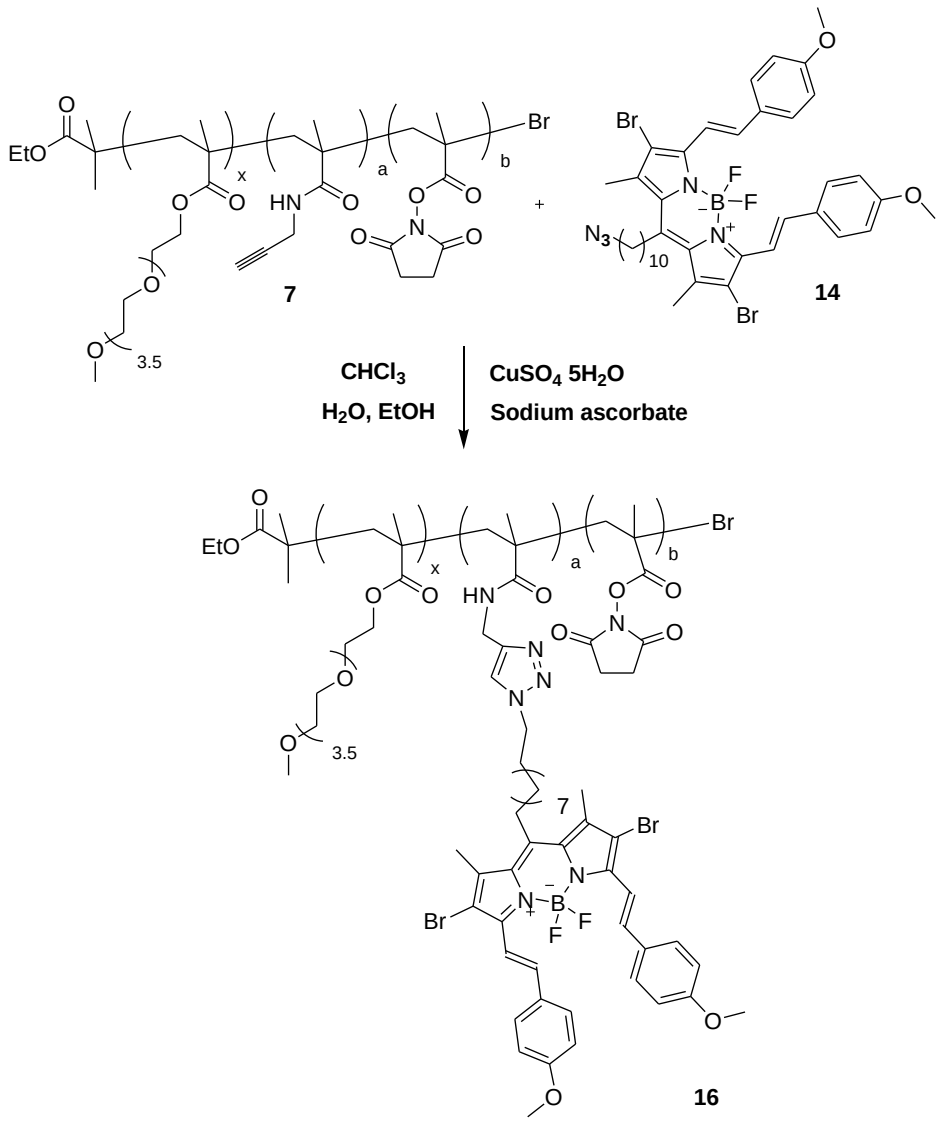

Figure 4.9. BODIPY$Br_2(C_6H_5OMe)_2(CH_2)_{10}N_3$ conjugation to Polymer **7**

4.4.3. The conjugation of Alendronate amine to polymer 16

The polymer conjugate **16** (0.528 g, 0.126 mmol NHS) was disssolved in THF (0.6 mL) and added to solution of alendronate amine (13.7 mg, 0.055 mmol) in water (0.4 mL). The solution mixture was stirred at ambient temperature for 48 h. The pH of solution was controlled by adding NaOH to the solution. The pH was increased from 7 to 9 through first one hour at the beginning of reaction by addition of 0.2M NaOH.

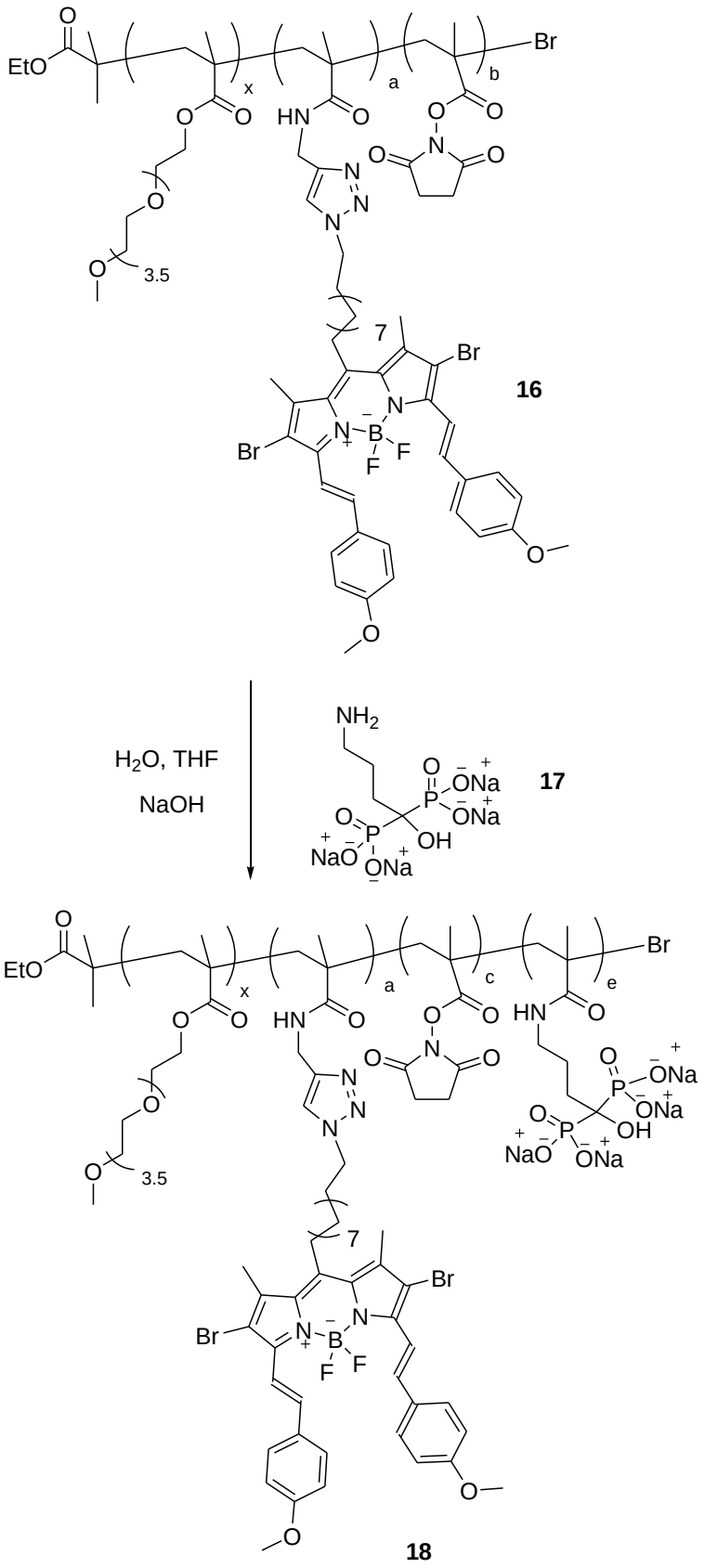

Figure 4.10. The synthesis of compound **18**

After reaction, THF was evaporated and polymer obtained was purified via sephhadex G-25 with H_2O as a mobile phase to remove unreacted alendronate amine. Proton NMR spectra of lyophilized polymer was taken in D_2O. Further purification and characterization via ^{31}P NMR is necessary to unequivocally ascertain the attachment of alendronate to the polymer construct. ^1H NMR ($CDCl_3$, δ, ppm); 7.50 (d, 4H), 7.27 (d, 2H), 6.97 (d, 4H), 4.12 (br s, 4H, COO-CH_2), 3.66 (br s, 14H, -CH_2CH_2O-), 3.34 (s, 3H, O-CH_3), 2.90 (br s, 4H, CH_2CH_2C=ON), 2.62-2.53 (m, 4H, -CH_2CH_2-), 1.94-0.86 (m, 6H, CH_2 and CH_3 along polymer backbone), (some peaks from dye and alendronate amine overlap with polymer peaks between 4.12- 3.34 ppm).

5. CONCLUSIONS

In this study, a polymer construct bearing a Bodipy dye was synthesized. This construct, aiming to accumulate in the tumor via enhanced permeation and retention effect can be used for photodynamic therapy. To improve on targeting, the construct was also ornamented with bisphosphonates for specific targeting to bone tissue.

APPENDIX

^{1}H NMR, ^{13}C NMR, UV and FTIR spectrums of the synthesized products are included.

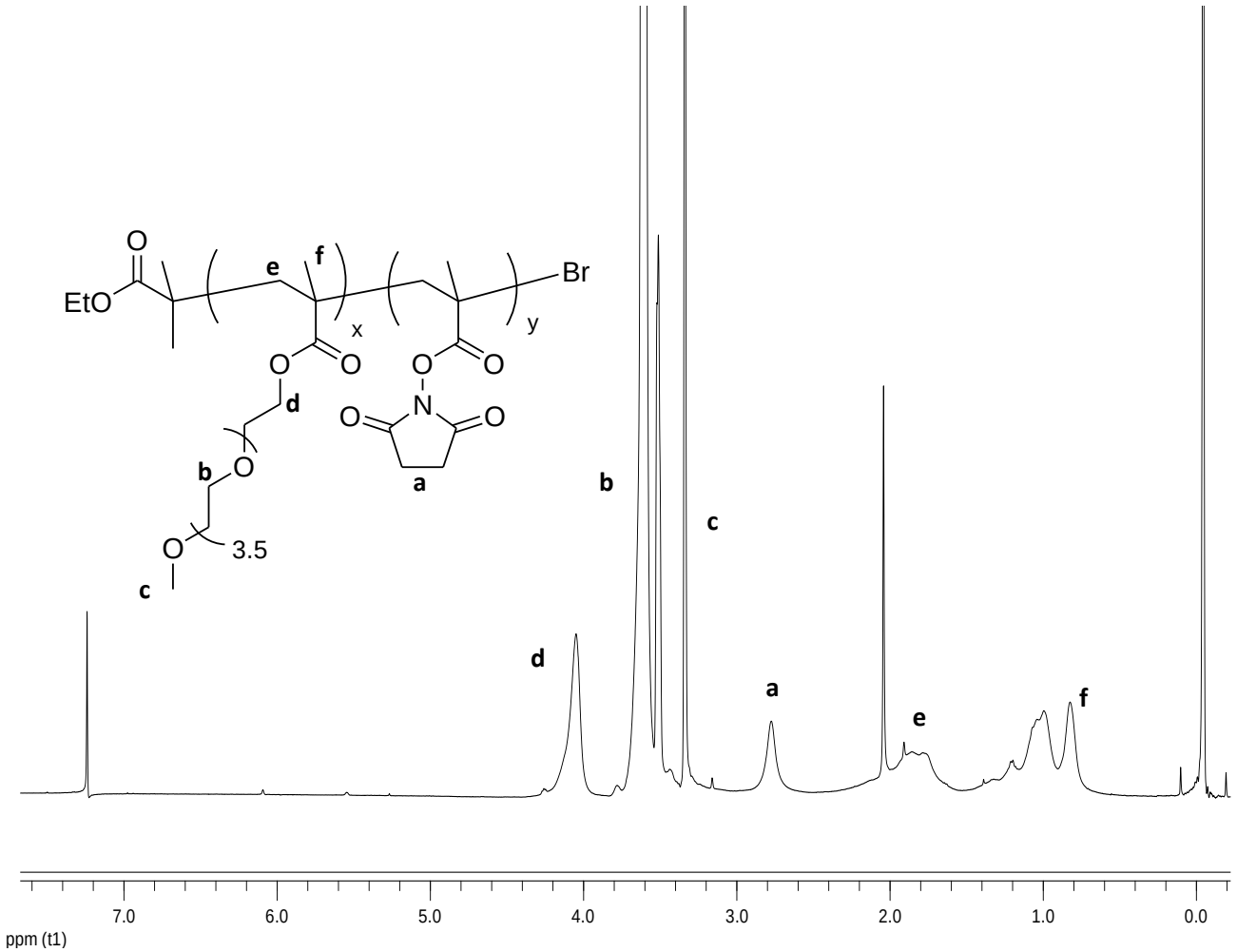

Figure A. 1. ^{1}H NMR spectra of PEG-NHS copolymer (**4**)

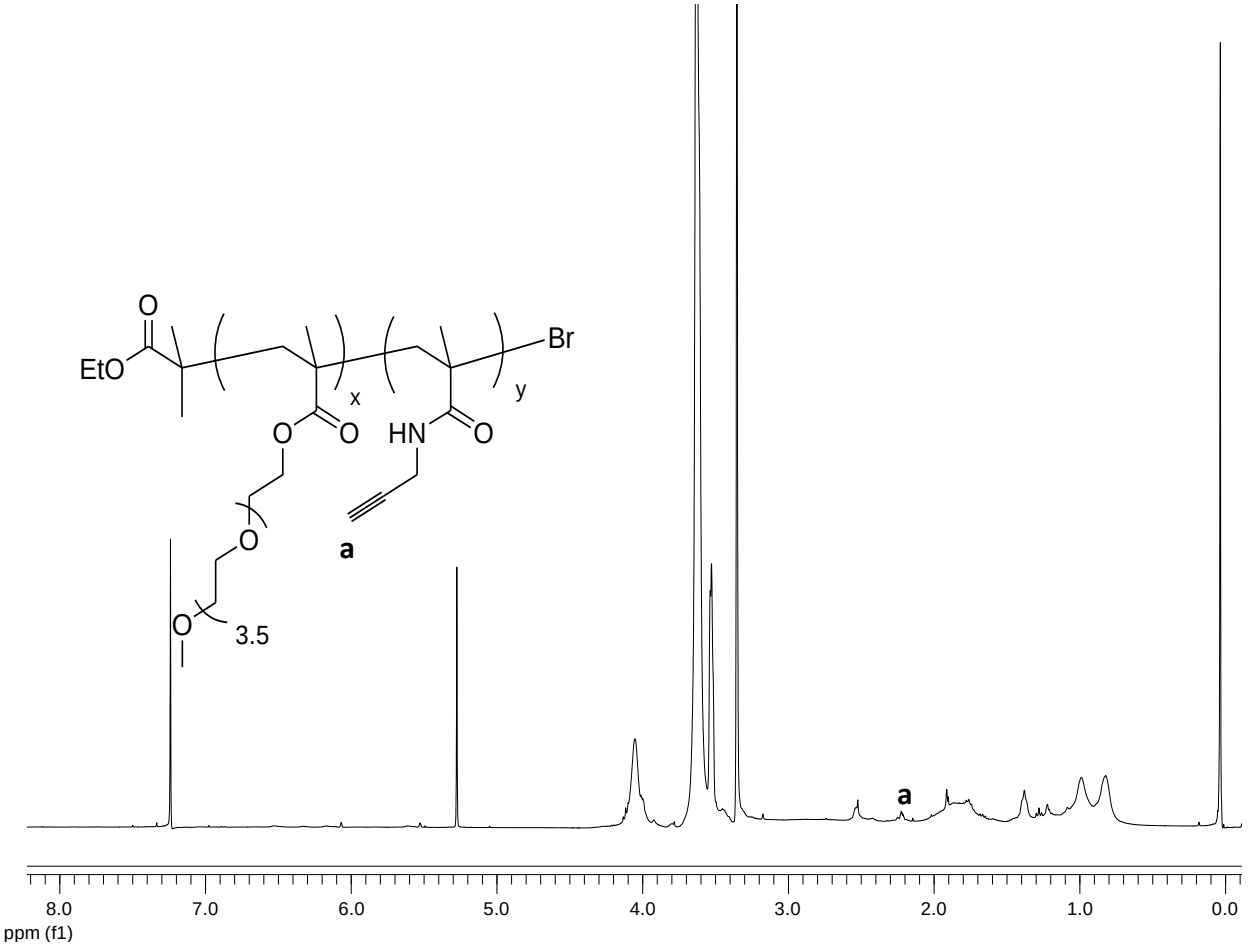

Figure A.2. ^{1}H NMR spectra of PEG-Alkyne copolymer (**6**)

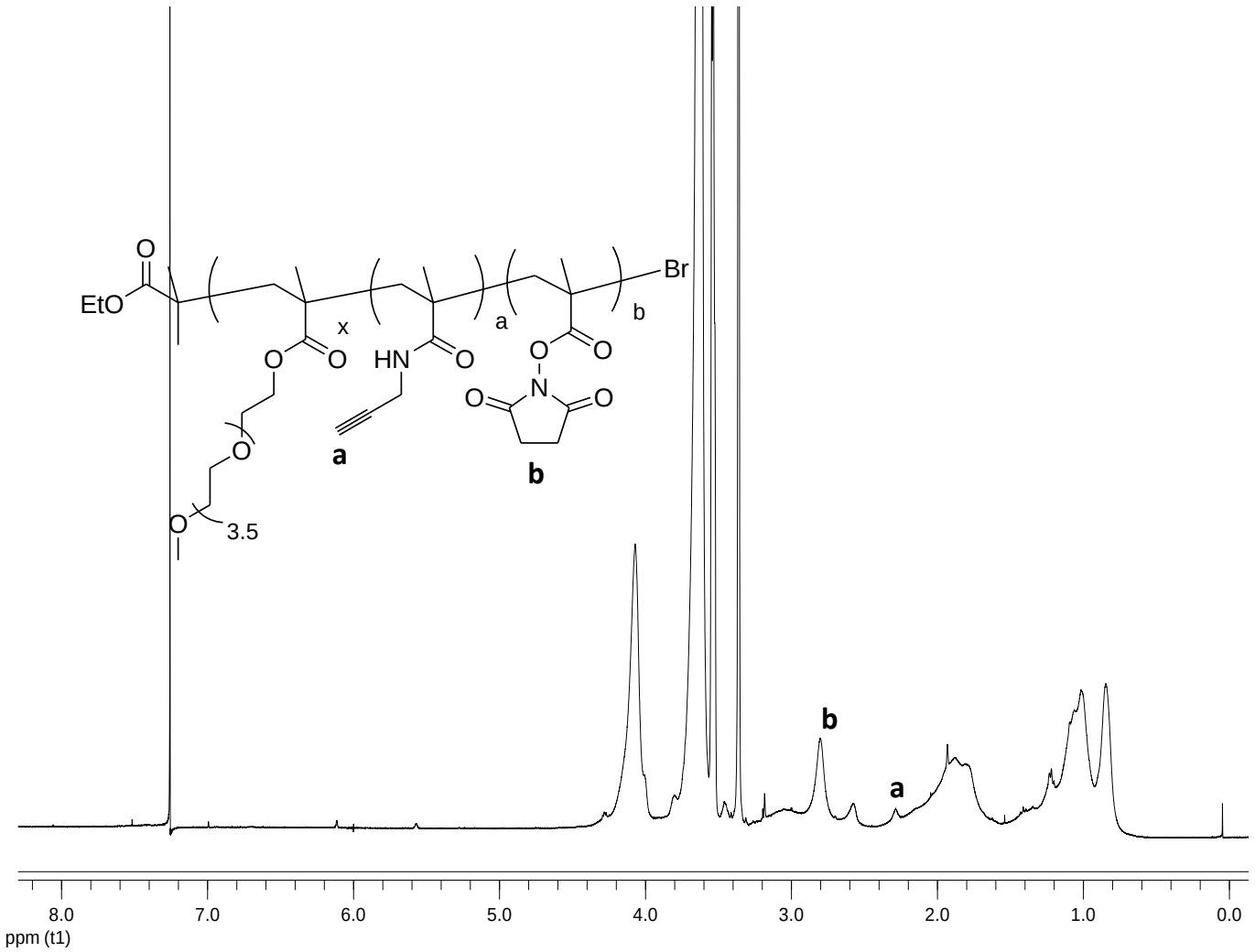

Figure A.3. ^{1}H NMR spectra of PEG-NHS-Alkyne copolymer (**7**)

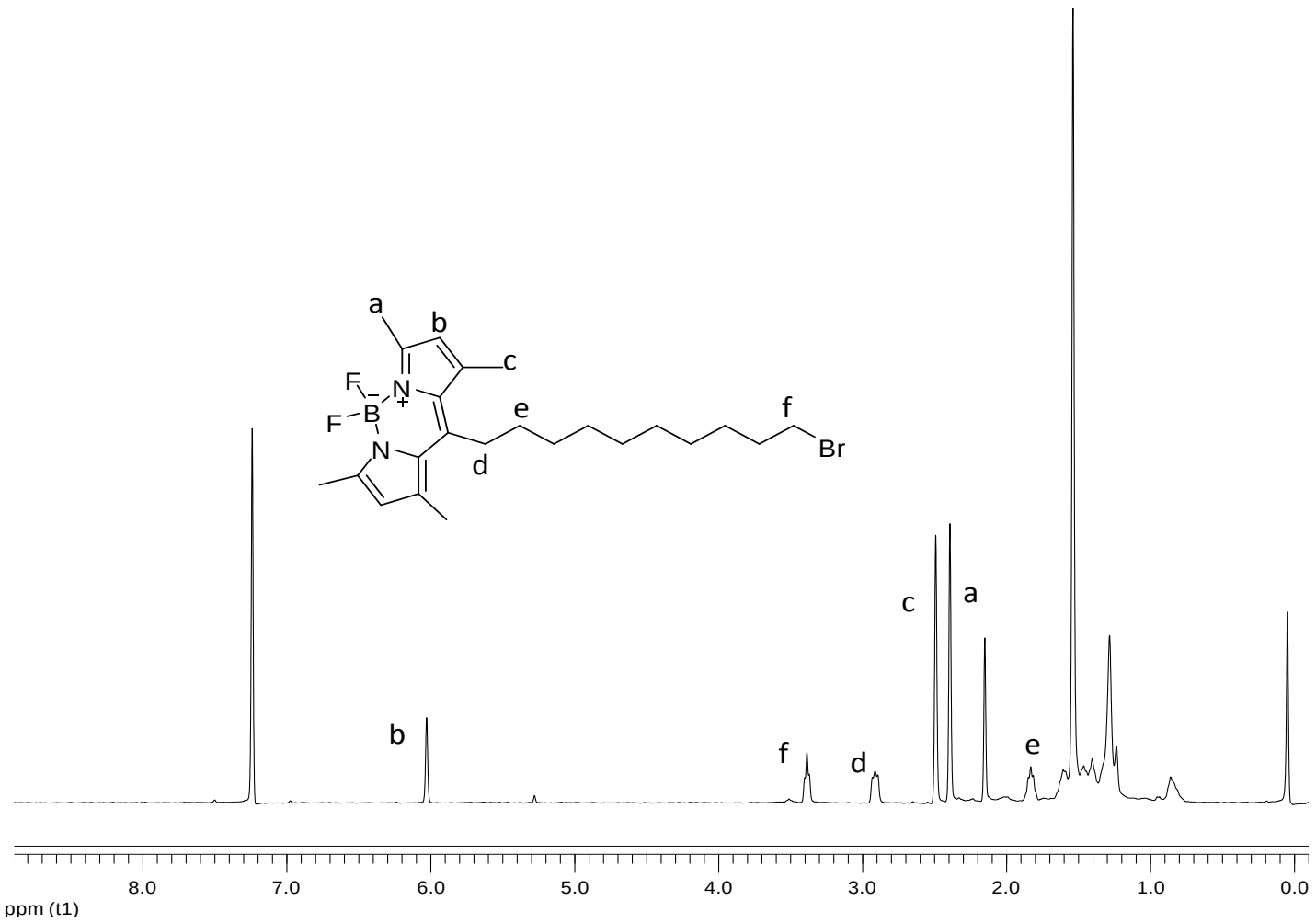

Figure A.4. ^{1}H NMR spectra of BODIPY$(CH_2)_{10}$Br **(10)**

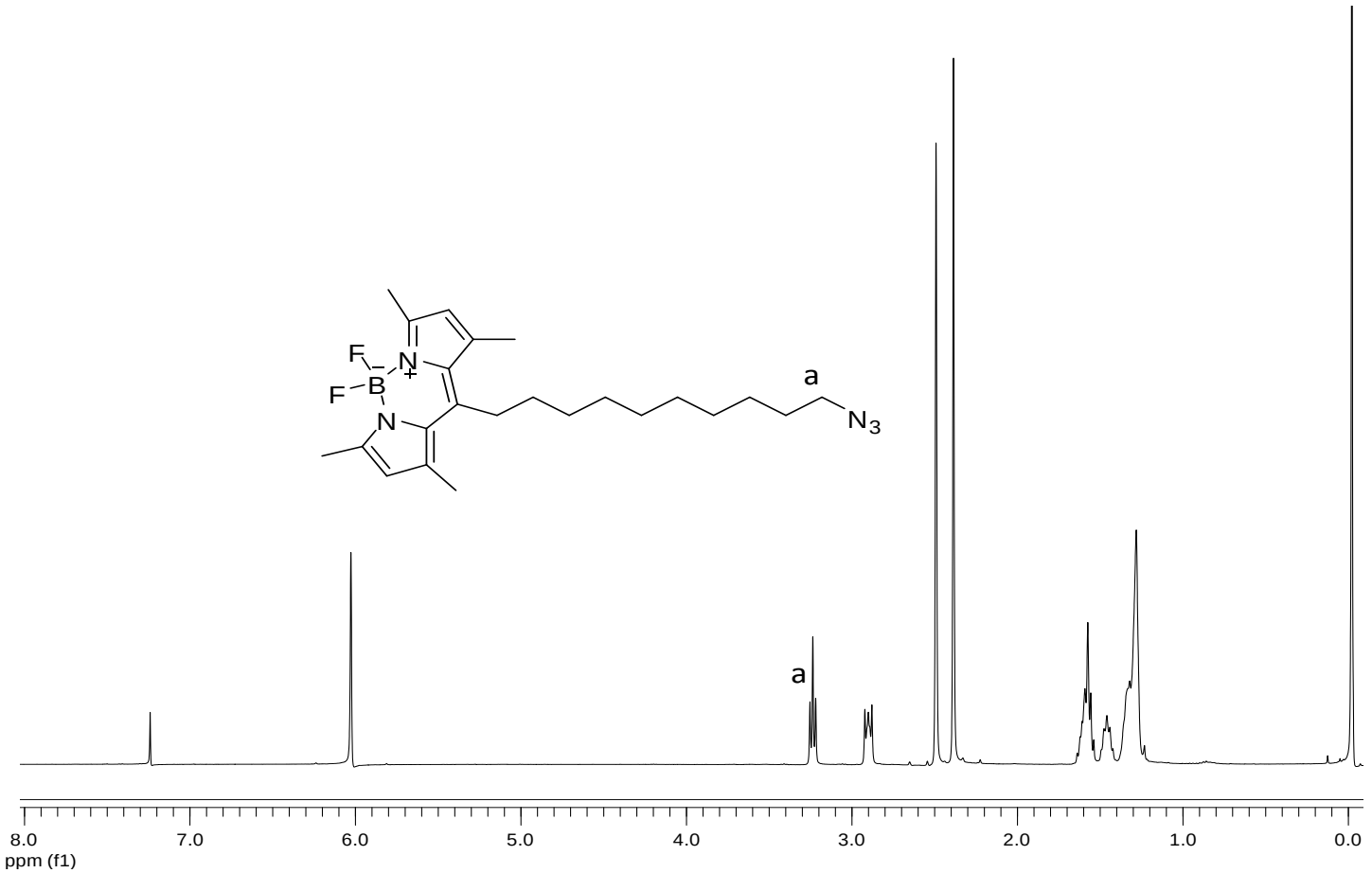

Figure A.5.^{1}H NMR spectra of BODIPY$(CH_2)_{10}N_3$ **(11)**

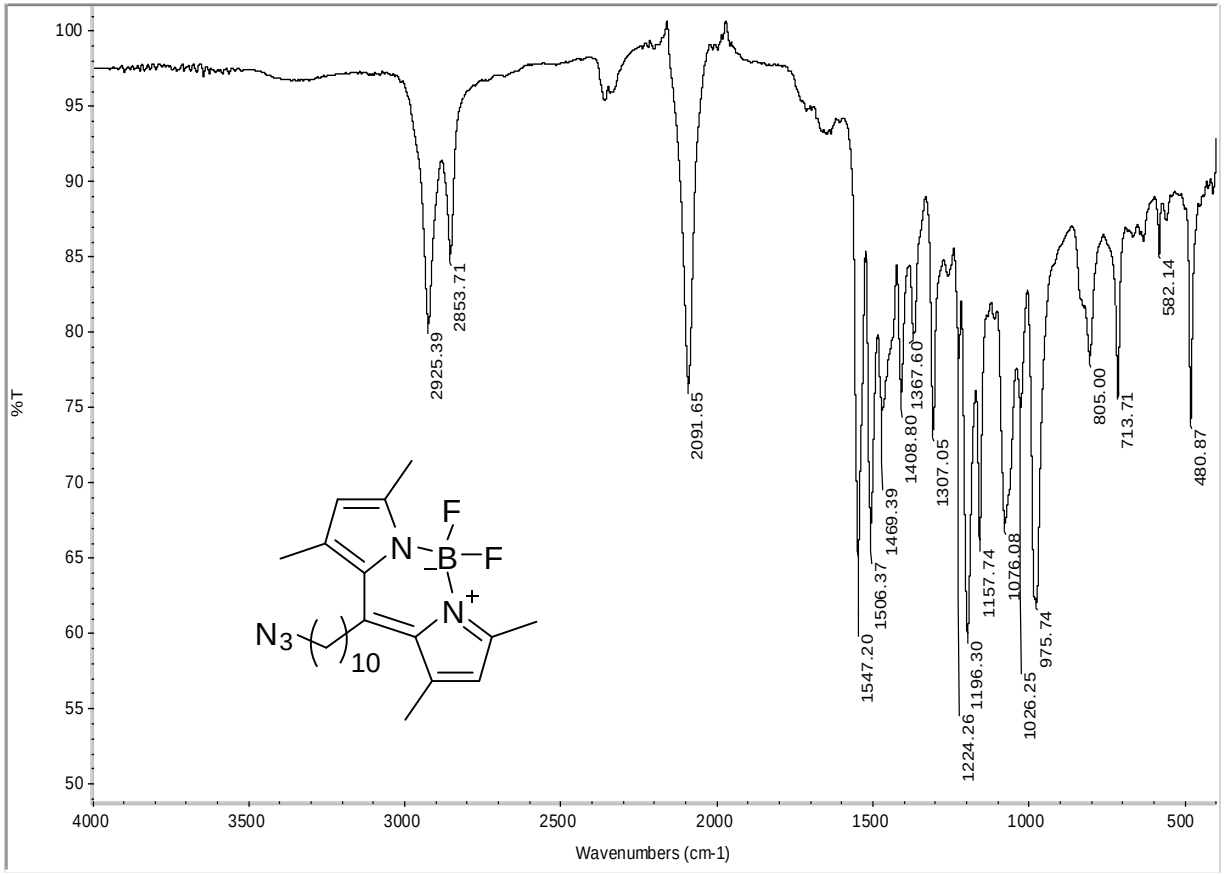

Figure A.6. IR spectrum of BODIPY$(CH_2)_{10}N_3$ **(11)**

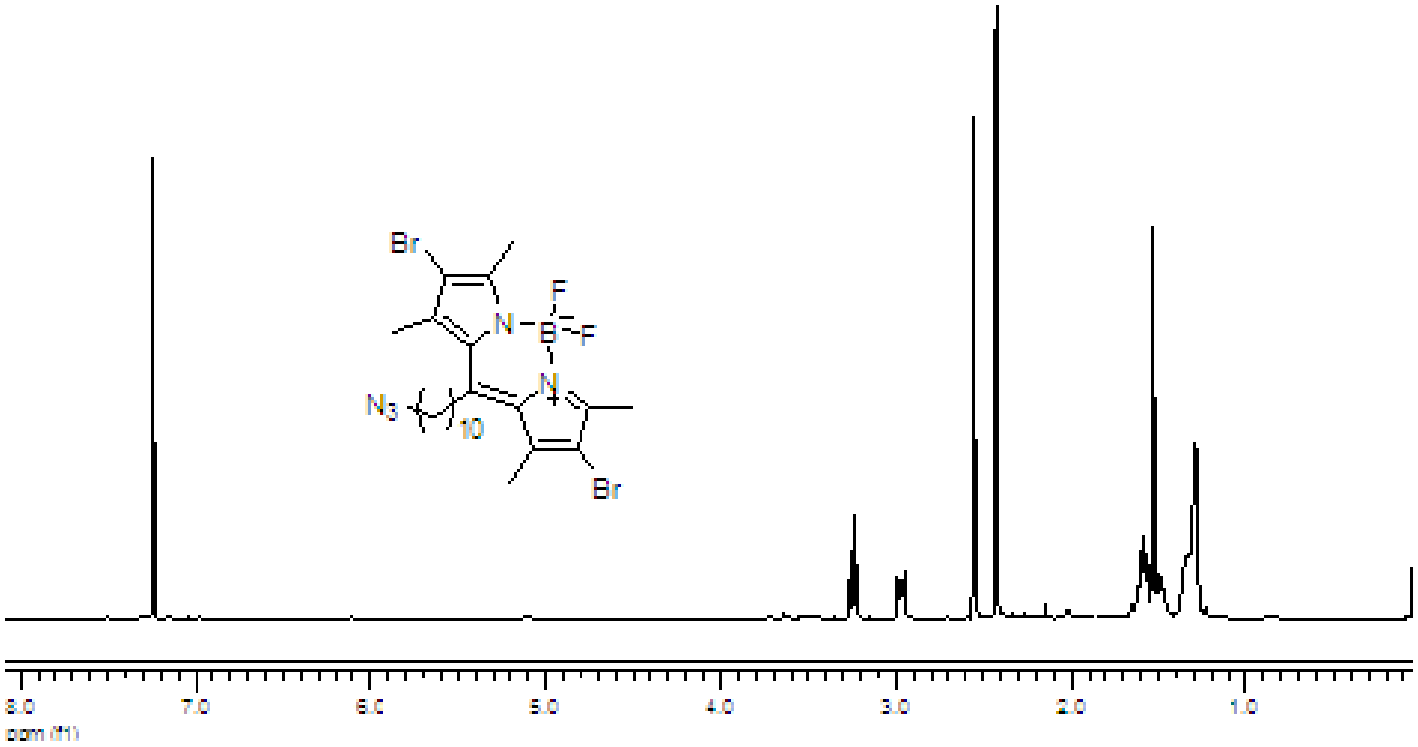

Figure A.7.^{1}H NMR spectra of BODIPY$Br_2(CH_2)_{10}N_3$ **(12)**

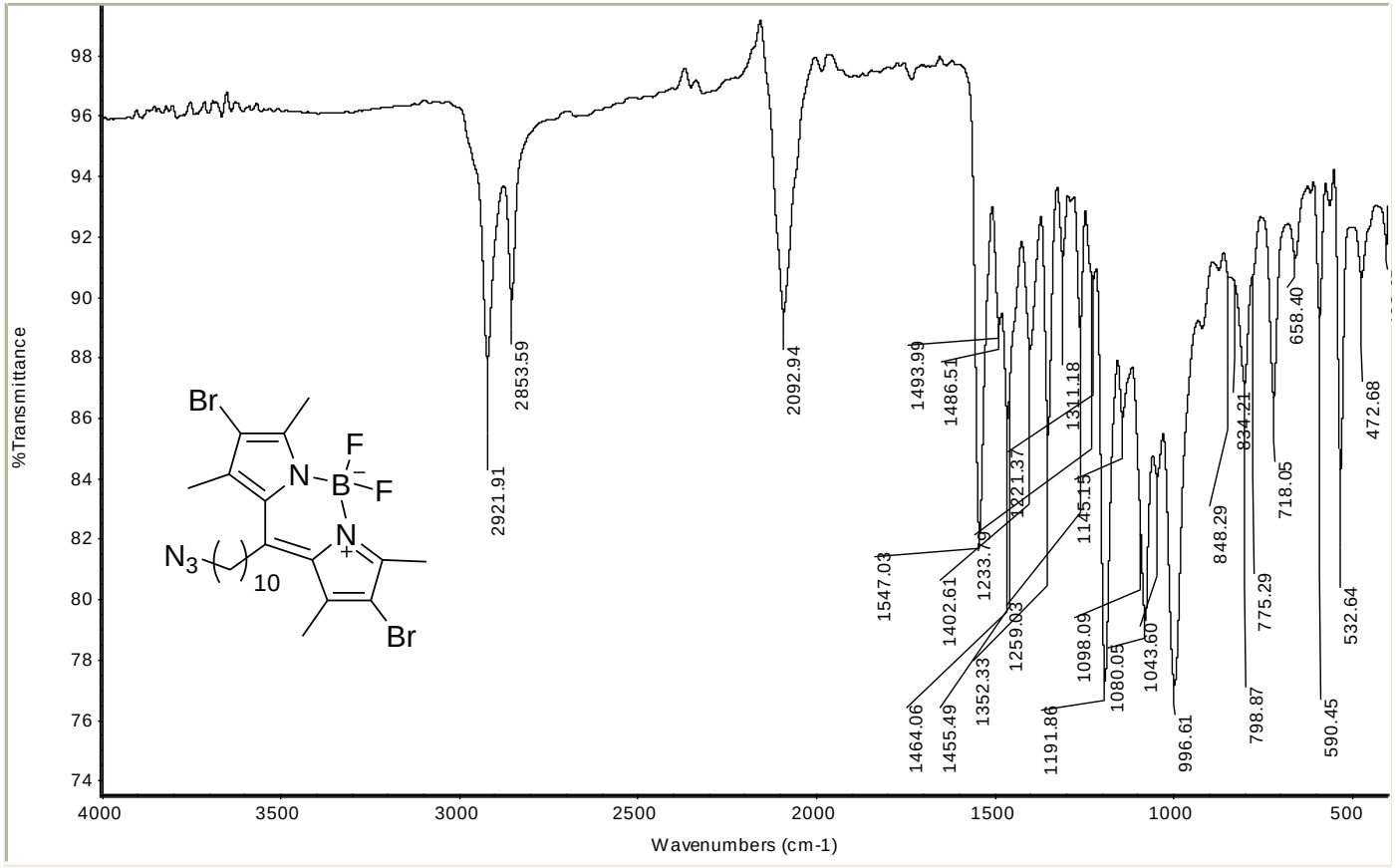

Figure A.8. IR spectra of BODIPY$Br_2(CH_2)_{10}N_3$ **(12)**

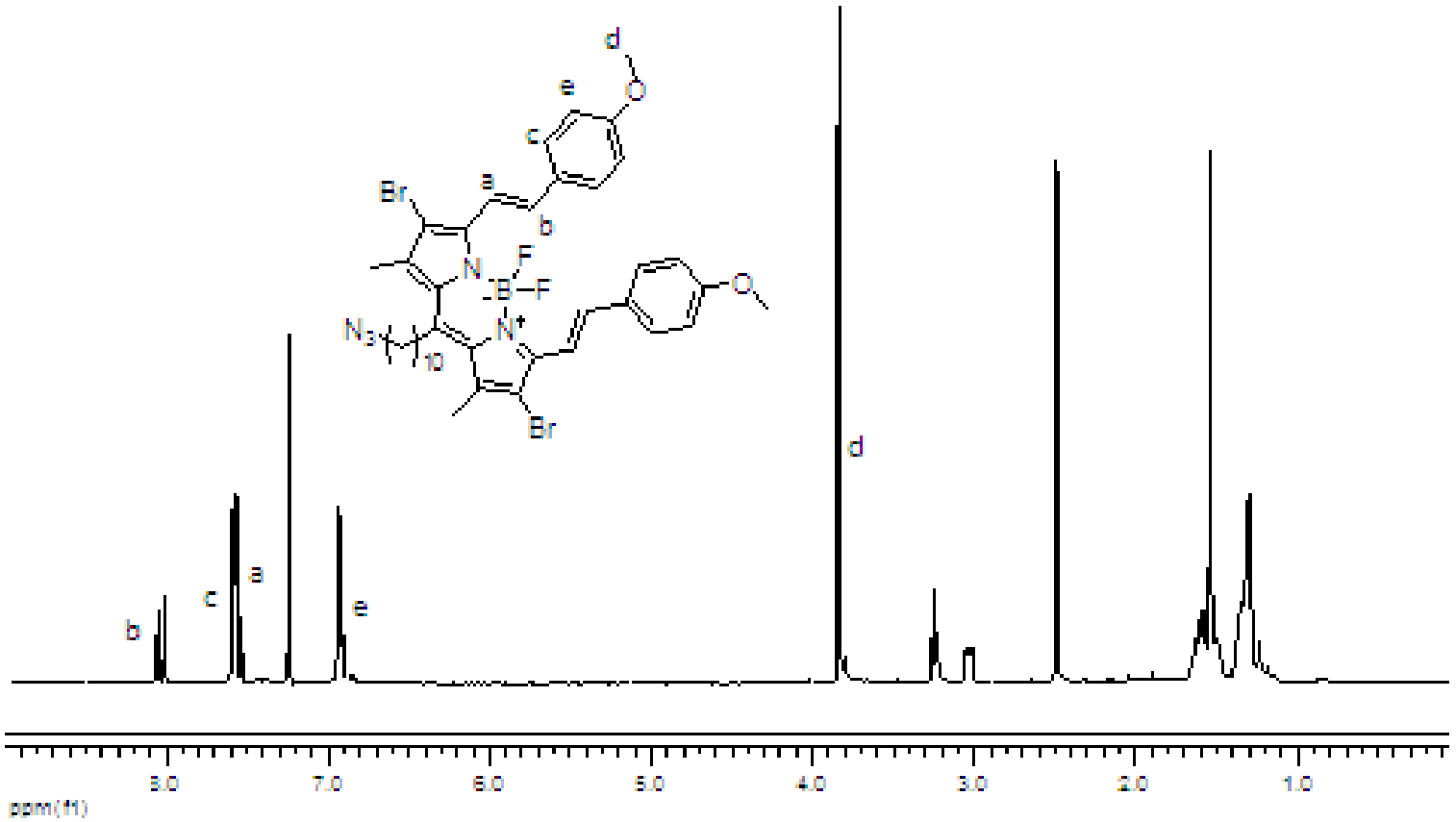

Figure A.9. ^{1}H NMR spectra of $BODIPYBr_2(C_6H_5OMe)_2(CH_2)_{10}N_3$ **(14)**

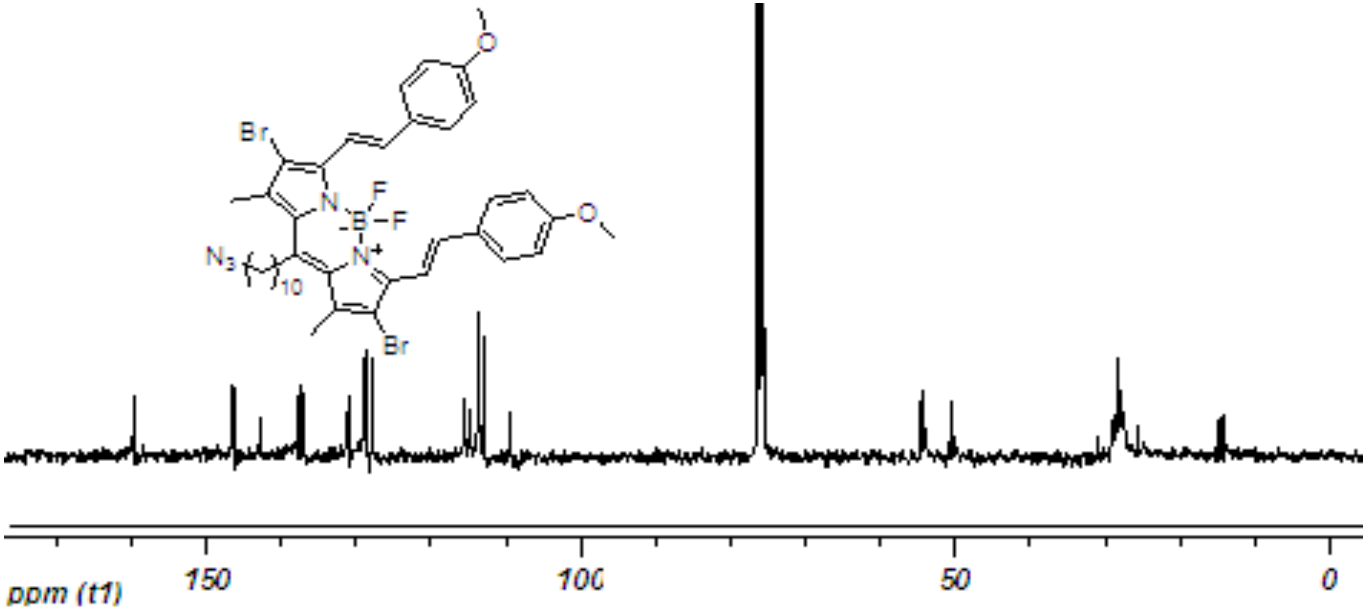

Figure A.10. ^{13}C-NMR spectra of BODIPY$Br_2(C_6H_5OMe)_2(CH_2)_{10}N_3$ **(14)**

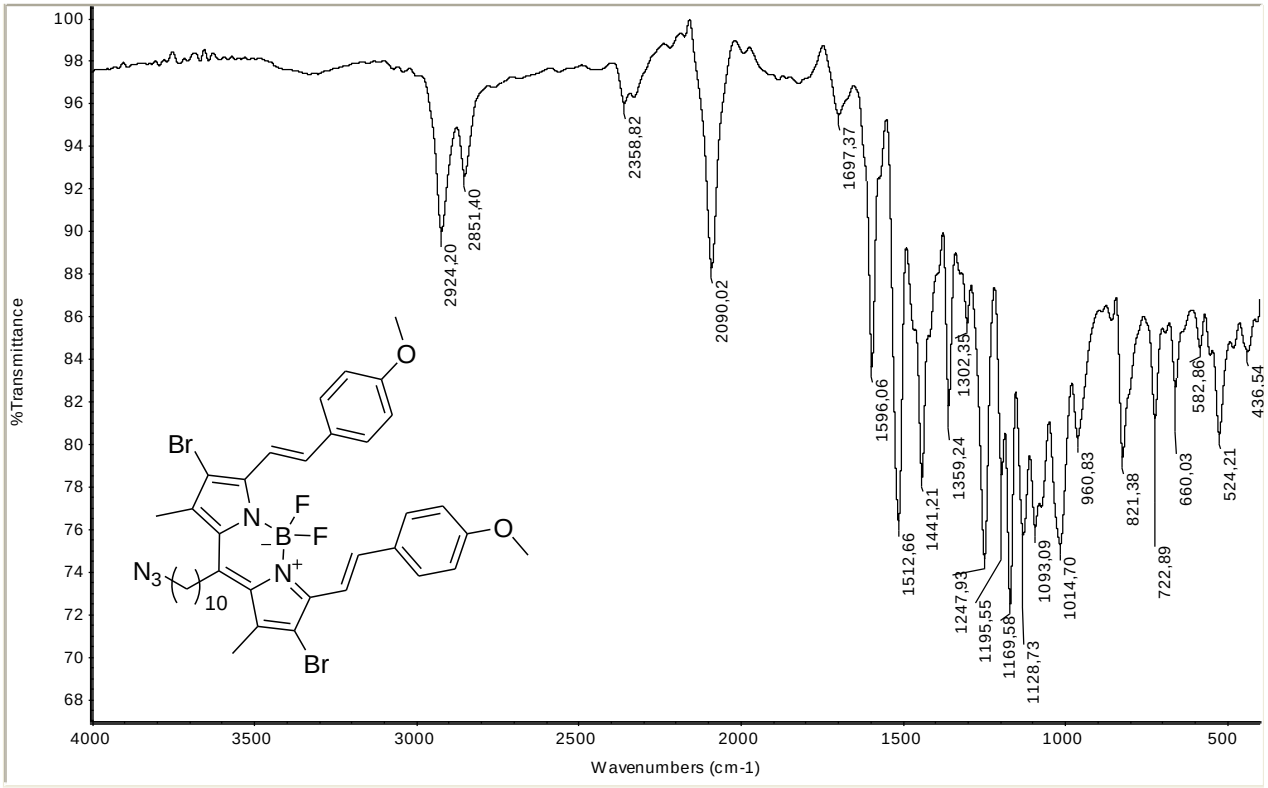

Figure A.11. IR spectra of $BODIPYBr_2(C_6H_5OMe)_2(CH_2)_{10}N_3$ **(14)**

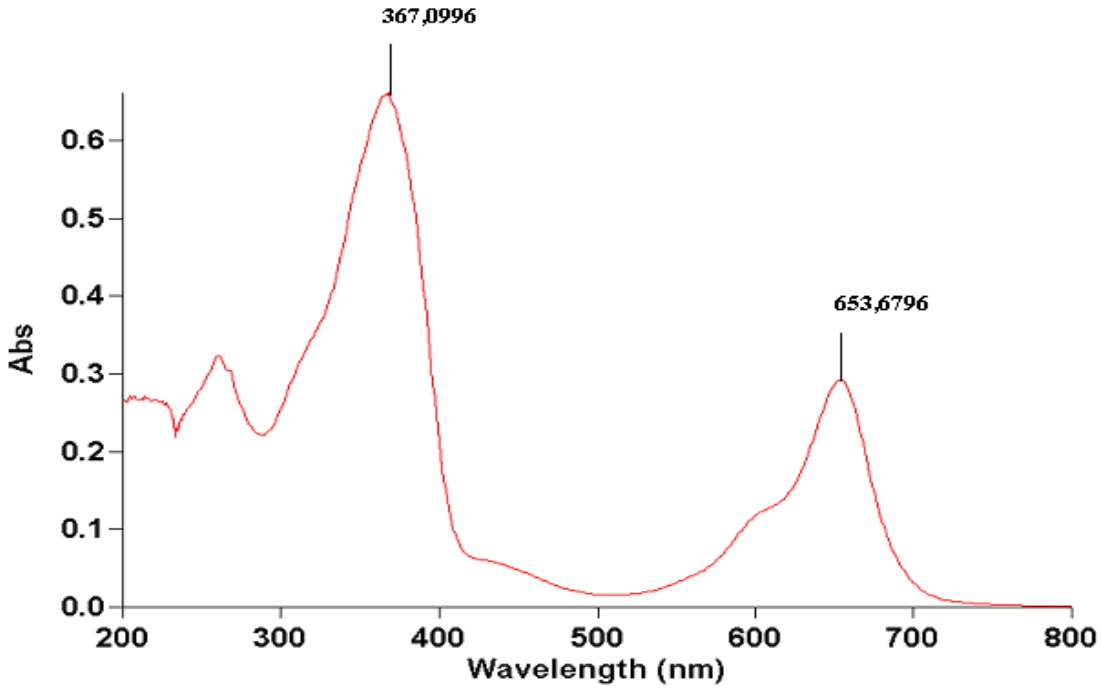

Figure A.12. UV spectra of $BODIPYBr_2(C_6H_5OMe)_2(CH_2)_{10}N_3$ **(14)**

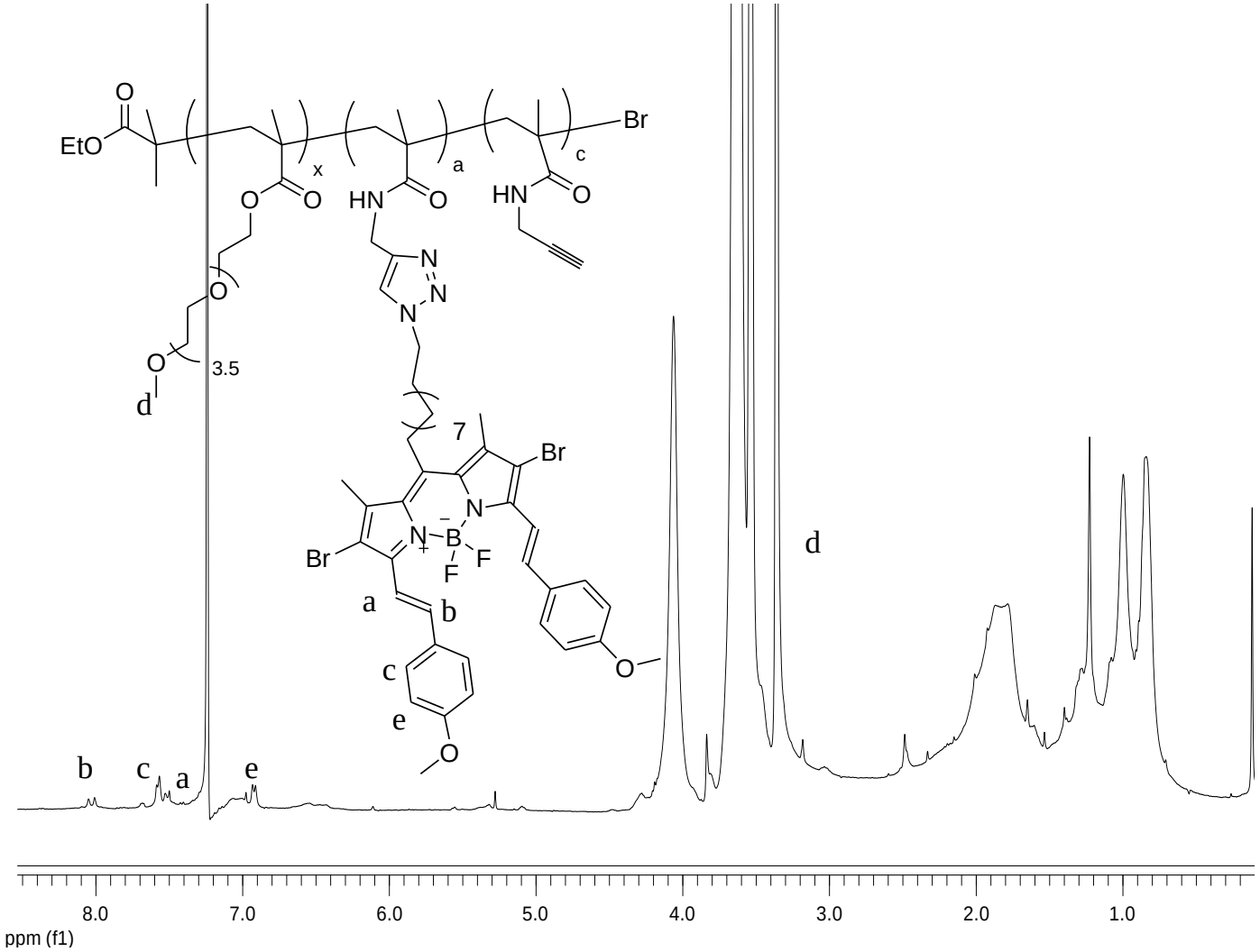

Figure A.13. ^{1}H NMR spectra of the polymer conjugate **15**

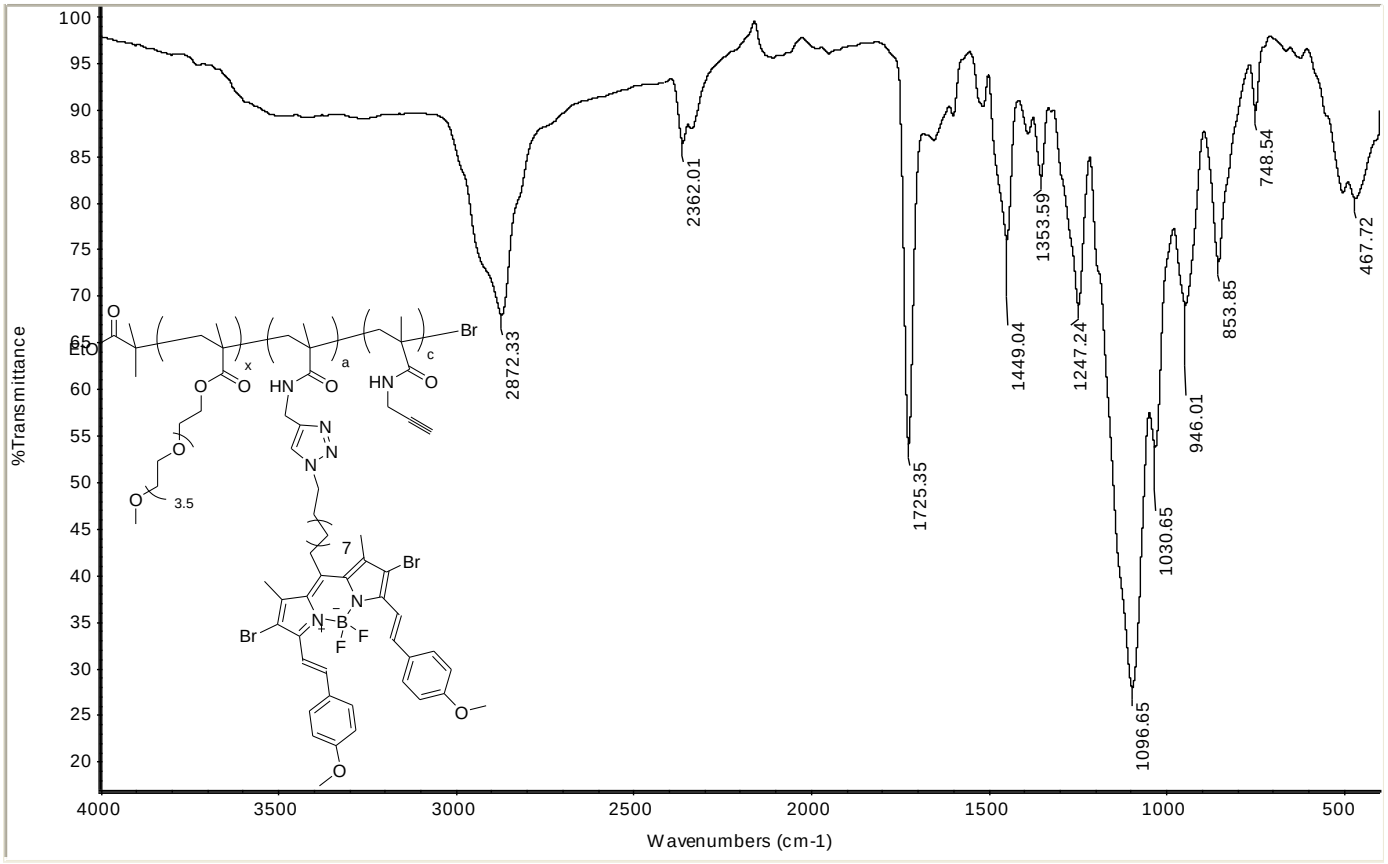

Figure A.14. IR spectra of the polymer conjugate **15**

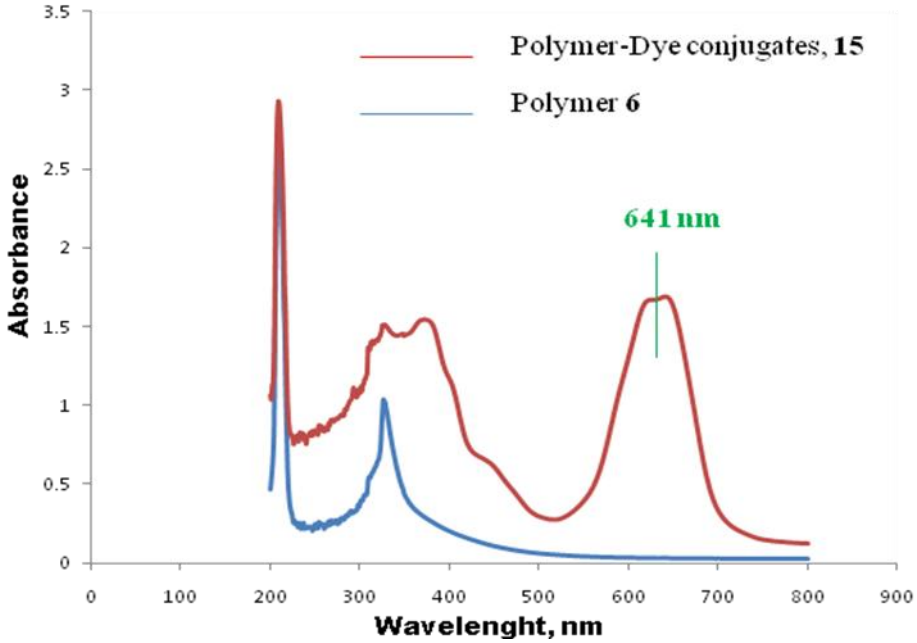

Figure A.15. UV spectrum of polymer **6** and polymer dye conjugate **15**

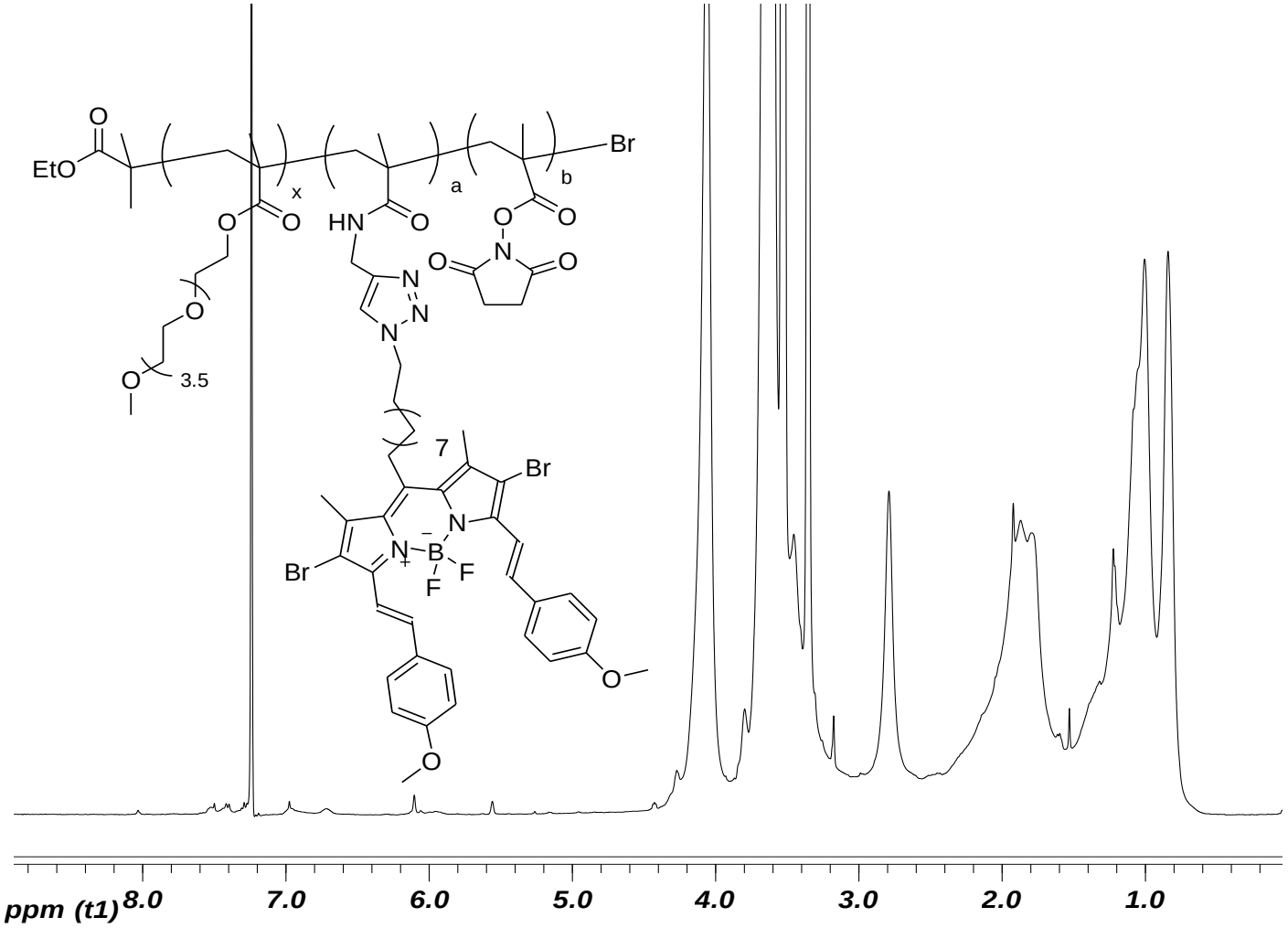

Figure A.16. [1] H NMR spectra of polymer conjugate **16**

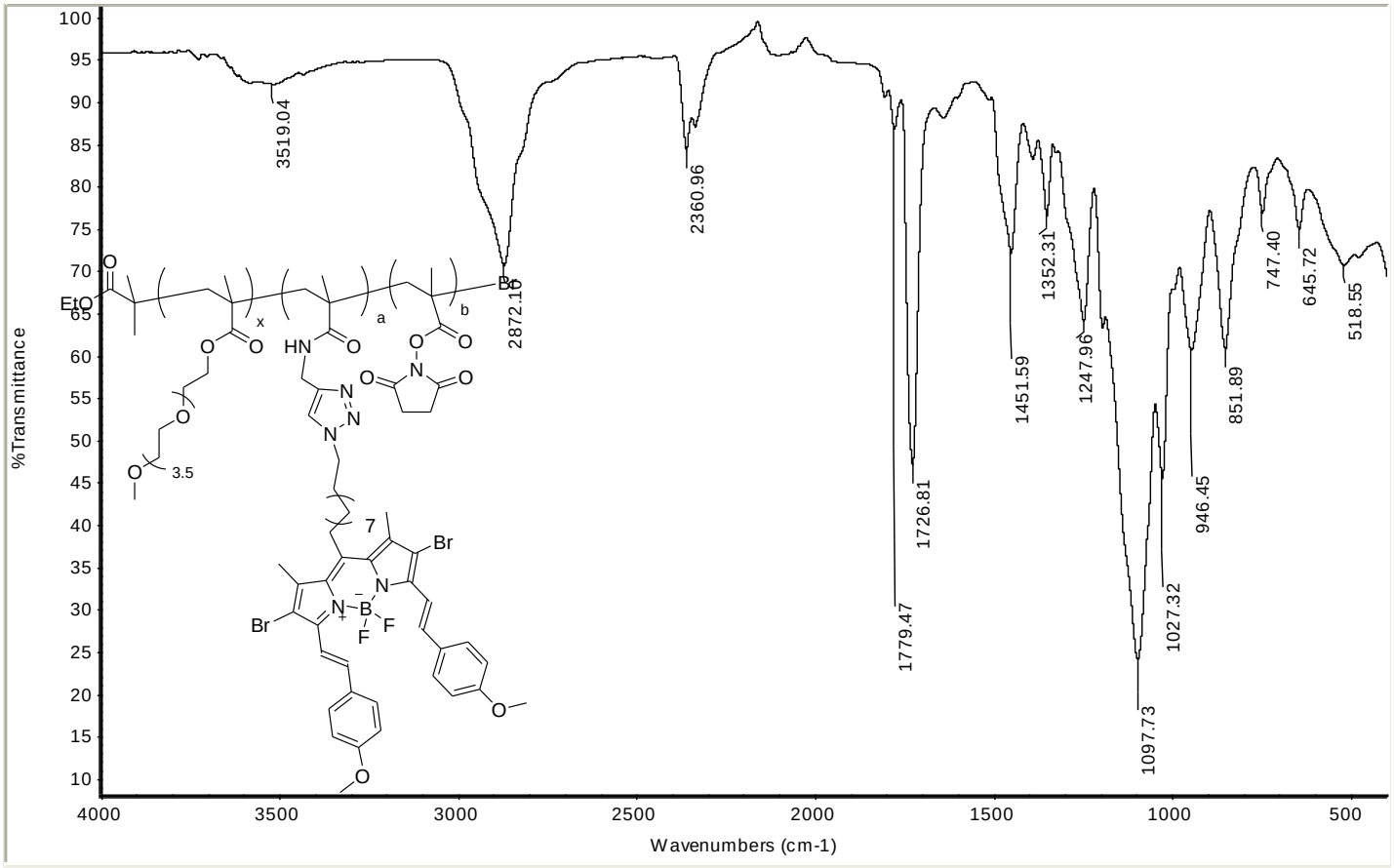

Figure A.17. IR spectra of the polymer conjugate **16**

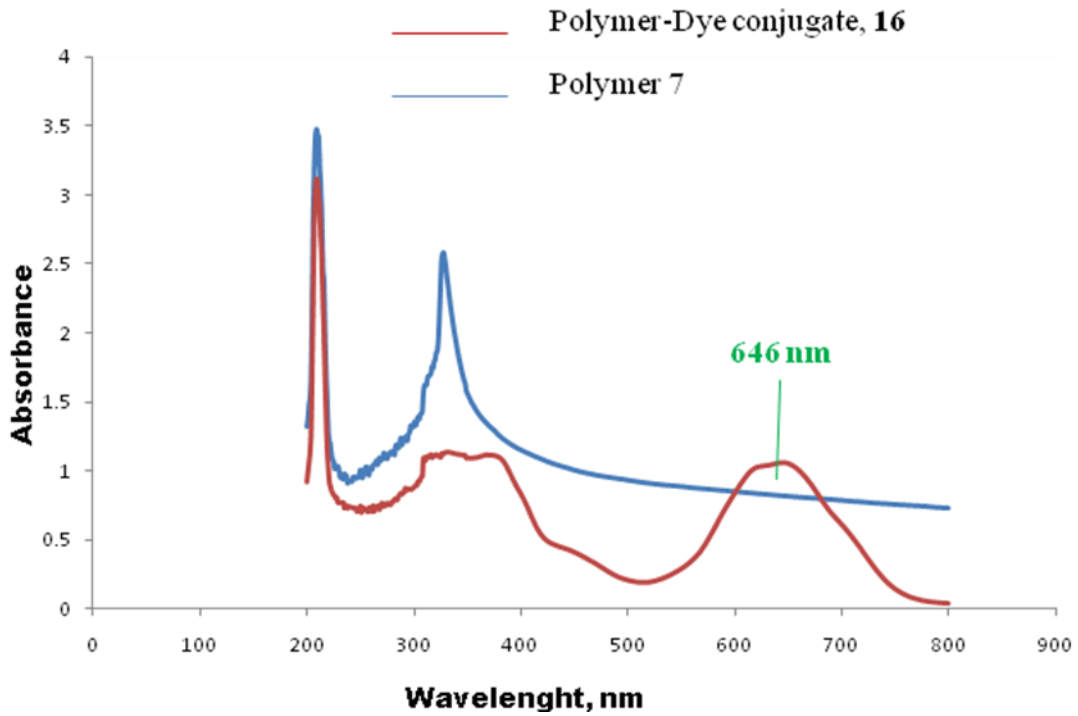

Figure A.18. UV specrum of polymer **7** and polymer dye conjugate **16**

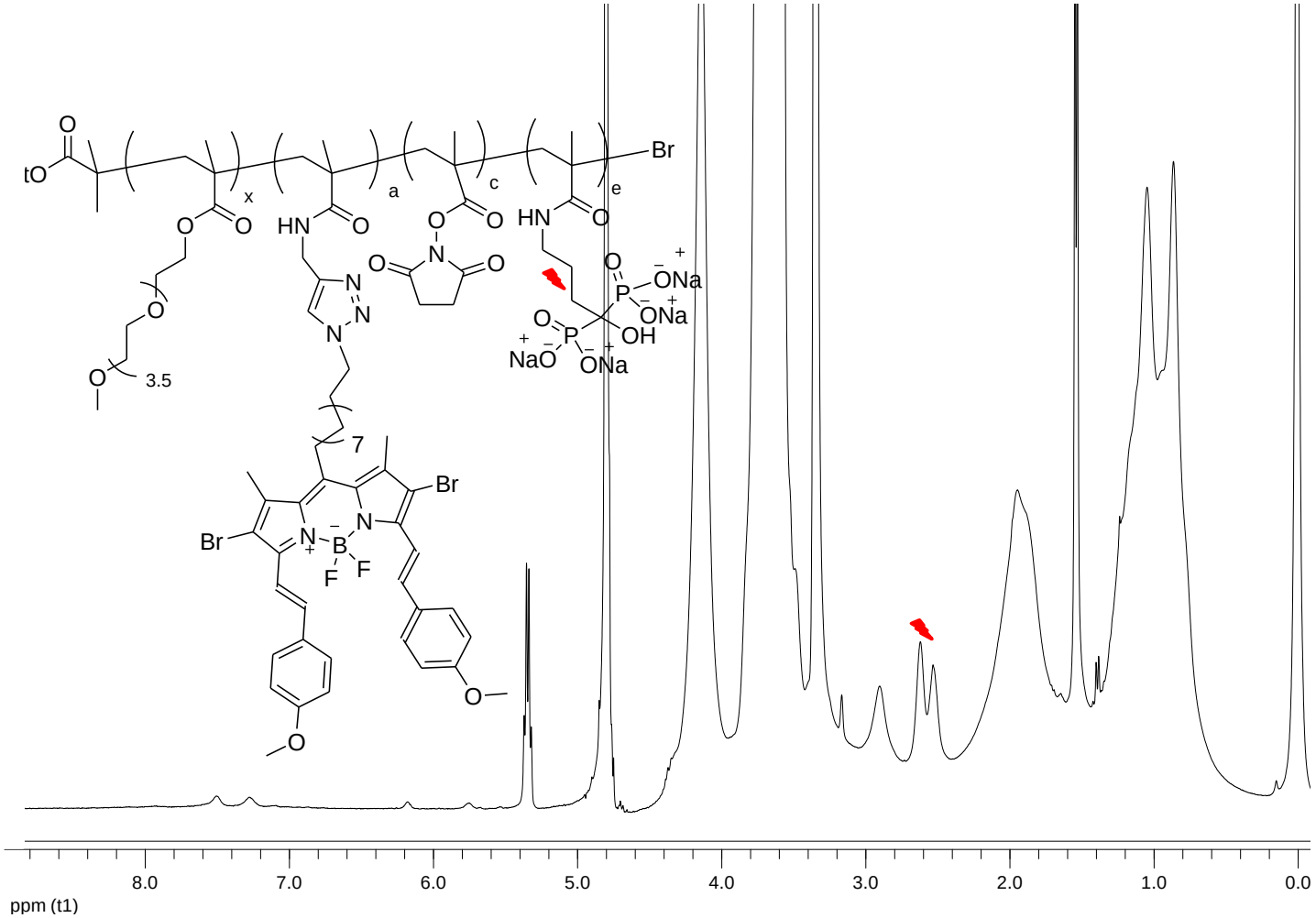

Figure A.19.[1]H NMR spectra of the polymer conjugate **18**

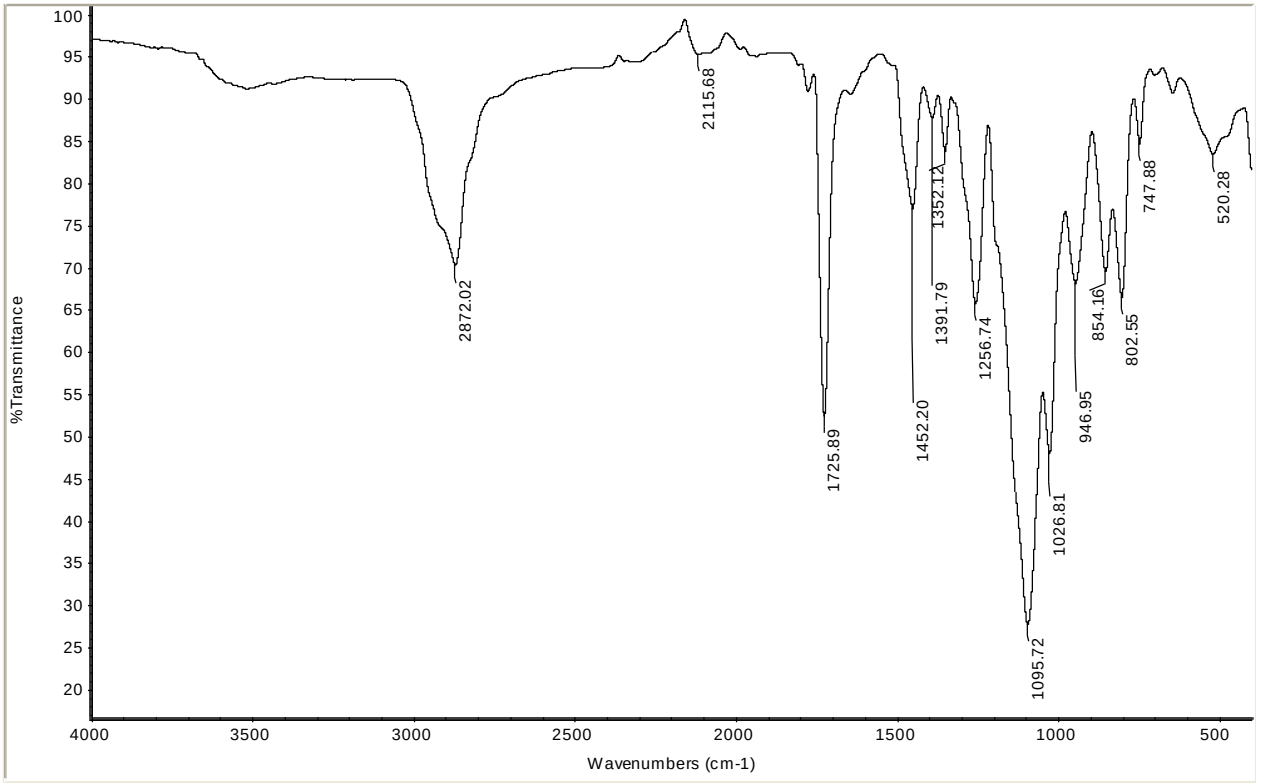

Figure A.20. IR spectra of the polymer conjugate **18**

REFERENCES

1. Bonnett, R., Advanced Chemistry Texts, *Gordon and Breach Science Publishers*, vol 1, 2000.

2. Bonnet, R. and G. Martinez, *Tetrahedron*, 57, 9513-9547, 2001.

3. Regehly, M., Photoinduced transfer processes in complex carrier systems for photodynamic therapy, Phd Thesis, Humboldt University of Berlin, 2008.

4. McDonnell, S. O., M. J. Hall, L. T. Allen, A. Byrne, W. M. Gallagher and D.F. O'Shea, *Journal of the American Chemical Society*, 127, 16360-1636, 2005.

5. Atilgan, S., Z. Ekmekçi, A. L. Doğan, D. Güç and E. U. Akkaya, *Chemical Communications*, 4398-4400, 2006.

6. Lovell, J. F., T. W. B. Liu, J. Chen and G. Zheng, *Chemical Reviews*, 110, 2839-2857, 2010.

7. Allison, R. R., G. H. Downie, R. Cuenca, X. H. Hu, C. J. H. Childs and C. H. Sibata, *Photodiagosis and Photodyamic Therapy*, 1, 27-42, 2004.

8. Nyman E. S. and P. H. Hynninen, *Journal of Photochemistry and Photobiology B: Biology*, 73, 1-28, 2004.

9. Yokoyama M., *Journal of Artificial Organs*, 8, 77-84, 2005.

10. Bisland S. K., D. Singh and J. Garie, *Journal of Bioconjugate Chemistry*, 10, 982-992, 1999.

11. Ogura S., K. Yazaki, K. Yamaguchi, T. Kamachi and I. Okura, *Journal of Controlled Release*, 103, 1, 2005.

12. Zhang M., Z. Zhang, D. Blessington, H. Li, T. M. Busch, V. Madrak, J. Miles, B. Chance, J. D. Glickson and G. Zheng, *Journal of Bioconjugate Chemistry,* 14, 709-714, 2003.

13. Vrouenraets, M. B., G. W. M. Visser, F. A. Stewart, M. Stigter, H. Oppelaar, P. E. Postmus, G. B. Snow and G. A. M. S. Van Dongen, *Cancer Research,* 59, 1505-1513, 1999.

14. Savellano, M. D. and H. Tayyaba, *Photochemistry and Photobiology,* 77, 431-439, 2003.

15. Van Dongen G. A. M. S., G. W. M. Visser and M. B. Vrouenraets, *Advanced Drug Delivery Reviews,* 56, 31-52, 2004.

16. Matsumura, Y. and H. Maeda, *Cancer Research,* 46, 6387-6392, 1986.

17. Derycke A. S., A. Kamuhabwa, A. Gijsens, T. Roskams, D. De Vos, A. Kasran, J. Huwyler, L. Missiaen and P. A. de Witte, *Journal of the National Cancer Institute*, 96, 1620-1630, 2004.

18. Polo, L., G. Valduga, G. Jori and E. Reddi, *The International Journal of Biochemistry & Cell Biology*, 34, 10-23, 2002.

19. Roby A., S. Erdogan and V. P. Torchilin, *European Journal of Pharmaceutics and Biopharmaceutics*, 62, 235-240, 2006.

20. Kim, S., J.H. Kim, O. Jeo, I. C. Kwon and K. Park, *European Journal of Pharmaceutics and Biopharmaceutics,* 71, 420-430, 2009.

21. Nather, A., Bone Grafts and Bone Substitutes, *World Scientific Publishing Co Pte Ltd*, 2005.

22. Winzenberg, T. and G. Jones, *Reviews on Recent Clinical Trials*, 3, 139-149, 2008.

23. Fleisch,H., *Breast Cancer Research*, 4, 30-34, 2002.

24. Russell, R and G. Graham, *New York Academy of Sciences*, 1068, 367-401, 2006.

25. Petal, M., T. Shah and A. Amin, *Begell House Inc.*, 24,2, 147-202, 2007.

26. Cha R.T., T. Du, J. H. Li and Z. Yuan, *Polymer International*, 55, 1057-1062, 2006.

27. Lee, T.Y., C.T. Lin, S.Y. Kuo, D.K. Chang and H.C. Wu, Cancer Research, 67, 10958-10965, 2007.

28. Chandrasekar, D., R. Sistla, F.J. Ahmad, R. K. Khar and P. V. Diwan, *Biomaterials*, 28, 504-512, 2007.

29. Couvreur, P. and C. Vauthier, *Pharmaceutical Research*, 23, 1417-1450, 2006.

30. Cuchelkar, V., P. Kopeckova and J. Kopecek, *Macromolecular Bioscience*, 8, 5, 375-383, 2008.

31. Cuchelkar, V., P. Kopeckova and J. Kopecek, *Molecular Pharmaceutics*, 5, 5, 776-786, 2008.

32. Erbas, S., A. Gorgulu, M. Kocakusakogullari and E. U. Akkaya, *Chemical Communications*, 4956-4958, 2009.

33. Yogo, T., Y. Urano, A. Mizushima, H. Sunahara, T. Inoue, K. Hirose, M. Iino, K. Kikuchi and T. Nagano, *Proc. Natl. Acad. Sci. U S A*, 105, 1, 28-32, 2008.

34. Ozlem, S. and E. U. Akkaya, *Journal of American Chemical Soceity*, 131, 48-49, 2009.

35. El-Mabhouh, A. A., C. A. Angelov, R. Cavell and J. R. Mercer, *Nuclear Medicine and Biology*, 33, 715-722, 2006.

36. Zaheer, A., R. E. Lenkinski, A. Mahmood, A. G. Jones, L. G. Cantley and J. V. Frangioni, *Nature Biotechnology*, 19, 1148-1154, 2001.

37. Wang, D., S. Miller, M. Sima, P. Kopeckova, J. Kopecek, *Bioconjugate Chemistry*, 14, 853-859, 2003.

38. Hamblin, M. R., J. L. Miller, I. Rizvi, B. Ortel, E. V. Maytin and T. Hassan, *Cancer Research*, 61, 7155-7162, 2001.

39. Hamblin, M. R., J. L. Miller, I. Rizvi, H. G. Loew, T. Hasan, *British Journal of Cancer*, 89, 937-943, 2003.

40. Canham, S. M., J. Y. Bass, O. Navarro, S. G. Lim, N. Das and S. A. Blum, *Organometallics*, 27, 10, 2172-2175, 2008.

41. Deniz, E., G. C. Isbasar, A. Bozdemir, L. T. Yildirim, A. Siemiarczuk and E. U. Akkaya, *Organic Letters*, 10, 16, 2008.

42. Yilmaz, M. D., O. A. Bozdemir, and E. U. Akkaya, *Organic Letters*, 8, 13, 2871-2873, 2006.